

3GPP TR 38.901 V16.0.0 (2019-10)

Technical Report

**3rd Generation Partnership Project;
Technical Specification Group Radio Access Network;
Study on channel model for frequencies from 0.5 to 100 GHz
(Release 16)**



Keywords

New Radio

3GPP

Postal address

3GPP support office address

650 Route des Lucioles - Sophia Antipolis
Valbonne - FRANCE
Tel.: +33 4 92 94 42 00 Fax: +33 4 93 65 47 16

Internet

<http://www.3gpp.org>

Copyright Notification

No part may be reproduced except as authorized by written permission.
The copyright and the foregoing restriction extend to reproduction in all media.

© 2019, 3GPP Organizational Partners (ARIB, ATIS, CCSA, ETSI, TSDSI, TTA, TTC).
All rights reserved.

UMTS™ is a Trade Mark of ETSI registered for the benefit of its members

3GPP™ is a Trade Mark of ETSI registered for the benefit of its Members and of the 3GPP Organizational Partners

LTE™ is a Trade Mark of ETSI registered for the benefit of its Members and of the 3GPP Organizational Partners

GSM® and the GSM logo are registered and owned by the GSM Association

3GPP

Contents

Foreword.....	5
1 Scope.....	6
2 References.....	6
3 Definitions, symbols and abbreviations.....	7
3.1 Definitions.....	7
3.2 Symbols.....	7
3.3 Abbreviations.....	8
4 Introduction.....	9
5 General.....	10
6 Status/expectation of existing information on high frequencies.....	10
6.1 Channel modelling works outside of 3GPP.....	10
6.2 Scenarios of interest.....	12
6.3 Channel measurement capabilities.....	13
6.4 Modelling objectives.....	13
7 Channel model(s) for 0.5-100 GHz.....	14
7.1 Coordinate system.....	14
7.1.1 Definition.....	14
7.1.2 Local and global coordinate systems.....	15
7.1.3 Transformation from a LCS to a GCS.....	15
7.1.4 Transformation from an LCS to a GCS for downtilt angle only.....	18
7.2 Scenarios.....	19
7.3 Antenna modelling.....	22
7.3.1 Antenna port mapping.....	23
7.3.2 Polarized antenna modelling.....	23
7.4 Pathloss, LOS probability and penetration modelling.....	24
7.4.1 Pathloss.....	24
7.4.2 LOS probability.....	30
7.4.3 O2I penetration loss.....	31
7.4.3.1 O2I building penetration loss.....	31
7.4.3.2 O2I car penetration loss.....	32

7.4.4	Autocorrelation of shadow fading.....	32
7.5	Fast fading model.....	33
7.6	Additional modelling components.....	51
7.6.1	Oxygen absorption.....	51
7.6.2	Large bandwidth and large antenna array.....	52
7.6.2.1	Modelling of the propagation delay.....	52
7.6.2.2	Modelling of intra-cluster angular and delay spreads.....	52
7.6.3	Spatial consistency.....	54
7.6.3.1	Spatial consistency procedure.....	54
7.6.3.2	Spatially-consistent UT/BS mobility modelling.....	54
7.6.3.3	LOS/NLOS, indoor states and O2I parameters.....	58
7.6.3.4	Applicability of spatial consistency.....	59
7.6.4	Blockage.....	60
7.6.4.1	Blockage model A.....	61
7.6.4.2	Blockage model B.....	63
7.6.5	Correlation modelling for multi-frequency simulations.....	65
7.6.5.1	Alternative channel generation method.....	66
7.6.6	Time-varying Doppler shift.....	68
7.6.7	UT rotation.....	68
7.6.8	Explicit ground reflection model.....	68
7.6.9	Absolute time of arrival.....	71
7.6.10	Dual mobility.....	72
7.6.11	Sources of EM interference.....	72
7.6.12	Embedded devices.....	72
7.7	Channel models for link-level evaluations.....	73
7.7.1	Clustered Delay Line (CDL) models.....	73
7.7.2	Tapped Delay Line (TDL) models.....	76
7.7.3	Scaling of delays.....	79
7.7.4	Spatial filter for generating TDL channel model.....	80
7.7.4.1	Exemplary filters/antenna patterns.....	80
7.7.4.2	Generation procedure.....	81
7.7.5	Extension for MIMO simulations.....	81
7.7.5.1	CDL extension: Scaling of angles.....	81
7.7.5.2	TDL extension: Applying a correlation matrix.....	82
7.7.6	K-factor for LOS channel models.....	83

7.8	Channel model calibration.....	83
7.8.1	Large scale calibration.....	83
7.8.2	Full calibration.....	84
7.8.3	Calibration of additional features.....	85
7.8.4	Calibration of the indoor factory scenario.....	87
8	Map-based hybrid channel model (Alternative channel model methodology).....	88
8.1	Coordinate system.....	89
8.2	Scenarios.....	89
8.3	Antenna modelling.....	89
8.4	Channel generation.....	89
Annex A: Further parameter definitions.....		100
A.1	Calculation of angular spread.....	100
A.2	Calculation of mean angle.....	100
Annex B: Change history.....		101

Foreword

This Technical Report has been produced by the 3rd Generation Partnership Project (3GPP).

The contents of the present document are subject to continuing work within the TSG and may change following formal TSG approval. Should the TSG modify the contents of the present document, it will be re-released by the TSG with an identifying change of release date and an increase in version number as follows:

Version x.y.z

where:

- x the first digit:
 - 1 presented to TSG for information;
 - 2 presented to TSG for approval;
 - 3 or greater indicates TSG approved document under change control.
- y the second digit is incremented for all changes of substance, i.e. technical enhancements, corrections, updates, etc.
- z the third digit is incremented when editorial only changes have been incorporated in the document.

1 Scope

The present document captures the findings of the study item, "Study on channel model for frequency spectrum above 6 GHz" [2] and from further findings of the study item, "Study on New Radio Access Technology [22]" and the study item "Study on Channel Modeling for Indoor Industrial Scenarios [23]". The channel models in the present document address the frequency range 0.5-100 GHz. The purpose of this TR is to help TSG RAN WG1 to properly model and evaluate the performance of physical layer techniques using the appropriate channel model(s). Therefore, the TR will be kept up-to-date via CRs in the future.

This document relates to the 3GPP evaluation methodology and covers the modelling of the physical layer of both Mobile Equipment and Access Network of 3GPP systems.

This document is intended to capture the channel model(s) for frequencies from 0.5GHz up to 100GHz.

2 References

The following documents contain provisions which, through reference in this text, constitute provisions of the present document.

- References are either specific (identified by date of publication, edition number, version number, etc.) or non-specific.
- For a specific reference, subsequent revisions do not apply.
- For a non-specific reference, the latest version applies. In the case of a reference to a 3GPP document (including a GSM document), a non-specific reference implicitly refers to the latest version of that document *in the same Release as the present document*.

- [1] 3GPP TR 21.905: "Vocabulary for 3GPP Specifications".
- [2] 3GPP TD RP-151606: "Study on channel model for frequency spectrum above 6 GHz".
- [3] 3GPP TR 36.873 (V12.2.0): "Study on 3D channel model for LTE".
- [4] 3GPP RP-151847: "Report of RAN email discussion about >6GHz channel modelling", Samsung.
- [5] 3GPP TD R1-163408: "Additional Considerations on Building Penetration Loss Modelling for 5G System Performance Evaluation", Straight Path Communications.
- [6] ICT-317669-METIS/D1.4: "METIS channel model, METIS 2020, Feb, 2015".
- [7] Glassner, A S: "An introduction to ray tracing. Elsevier, 1989".
- [8] McKown, J. W., Hamilton, R. L.: "Ray tracing as a design tool for radio networks, Network, IEEE, 1991(6): 27-30".
- [9] Kurner, T., Cichon, D. J., Wiesbeck, W.: "Concepts and results for 3D digital terrain-based wave propagation models: An overview", IEEE J.Select. Areas Commun., vol. 11, pp. 1002–1012, 1993.
- [10] Born, M., Wolf, E.: "Principles of optics: electromagnetic theory of propagation, interference and diffraction of light", CUP Archive, 2000.
- [11] Friis, H.: "A note on a simple transmission formula", proc. IRE, vol. 34, no. 5, pp. 254–256, 1946.
- [12] Kouyoumjian, R.G., Pathak, P.H.: "A uniform geometrical theory of diffraction for an edge in a perfectly conducting surface" Proc. IEEE, vol. 62, pp. 1448–1461, Nov. 1974.
- [13] Pathak, P.H., Burnside, W., Marhefka, R.: "A Uniform GTD Analysis of the Diffraction of Electromagnetic Waves by a Smooth Convex Surface", IEEE Transactions on Antennas and Propagation, vol. 28, no. 5, pp. 631–642, 1980.

- [14] IST-WINNER II Deliverable 1.1.2 v.1.2, "WINNER II Channel Models", IST-WINNER2, Tech. Rep., 2007 (<http://www.ist-winner.org/deliverables.html>).
- [15] 3GPP TR36.101: "User Equipment (UE) radio transmission and reception".
- [16] 3GPP TR36.104: "Base Station (BS) radio transmission and reception".
- [17] Asplund, H., Medbo, J., Göransson, B., Karlsson, J., Sköld, J.: "A simplified approach to applying the 3GPP spatial channel model", in Proc. of PIMRC 2006.
- [18] ITU-R Rec. P.1816: "The prediction of the time and the spatial profile for broadband land mobile services using UHF and SHF bands".
- [19] ITU-R Rec. P.2040-1: "Effects of building materials and structures on radiowave propagation above about 100 MHz", International Telecommunication Union Radiocommunication Sector ITU-R, 07/2015.
- [20] ITU-R Rec. P.527-3: "Electrical characteristics of the surface of the earth", International Telecommunication Union Radiocommunication Sector ITU-R, 03/1992.
- [21] Jordan, E.C., Balmain, K.G.: "Electromagnetic Waves and Radiating Systems", Prentice-Hall Inc., 1968.
- [22] 3GPP TD RP-162469: "Study on New Radio (NR) Access Technology".
- [23] 3GPP TD RP-182138: "SID on Channel Modeling for Indoor Industrial Scenarios".

3 Definitions, symbols and abbreviations

3.1 Definitions

For the purposes of the present document, the terms and definitions given in TR 21.905 [1] apply.

3.2 Symbols

For the purposes of the present document, the following symbols apply:

A	antenna radiation power pattern
A_{\max}	maximum attenuation
d_{2D}	2D distance between Tx and Rx
d_{3D}	3D distance between Tx and Rx
d_H	antenna element spacing in horizontal direction
d_V	antenna element spacing in vertical direction
f	frequency
f_c	center frequency / carrier frequency
$F_{rx,u,\theta}$	Receive antenna element u field pattern in the direction of the spherical basis vector $\hat{\theta}$
$F_{rx,u,\phi}$	Receive antenna element u field pattern in the direction of the spherical basis vector $\hat{\phi}$
$F_{tx,s,\theta}$	Transmit antenna element s field pattern in the direction of the spherical basis vector $\hat{\theta}$
$F_{tx,s,\phi}$	Transmit antenna element s field pattern in the direction of the spherical basis vector $\hat{\phi}$
h_{BS}	antenna height for BS
h_{UT}	antenna height for UT
$\hat{r}_{rx,n,m}$	spherical unit vector of cluster n , ray m , for receiver
$\hat{r}_{tx,n,m}$	spherical unit vector of cluster n , ray m , for transmitter

α	bearing angle
β	downtilt angle
γ	slant angle
λ	wavelength
κ	cross-polarization power ratio in linear scale
μ_{lgASA}	mean value of 10-base logarithm of azimuth angle spread of arrival
μ_{lgASD}	mean value of 10-base logarithm of azimuth angle spread of departure
μ_{lgDS}	mean value of 10-base logarithm of delay spread
μ_{lgZSA}	mean value of 10-base logarithm of zenith angle spread of arrival
μ_{lgZSD}	mean value of 10-base logarithm of zenith angle spread of departure
Pr_{LOS}	LOS probability
SLA_V	side-lobe attenuation in vertical direction
σ_{lgASA}	standard deviation of 10-base logarithm of azimuth angle spread of arrival
σ_{lgASD}	standard deviation of 10-base logarithm of azimuth angle spread of departure
σ_{lgDS}	standard deviation value of 10-base logarithm of delay spread
σ_{lgZSA}	standard deviation of 10-base logarithm of zenith angle spread of arrival
σ_{lgZSD}	standard deviation of 10-base logarithm of zenith angle spread of departure
σ_{SF}	standard deviation of SF
ϕ	azimuth angle
θ	zenith angle
$\hat{\phi}$	spherical basis vector (unit vector) for GCS
$\hat{\phi}'$	spherical basis vector (unit vector) for LCS
$\phi_{3\text{dB}}$	horizontal 3 dB beamwidth of an antenna
$\hat{\theta}$	spherical basis vector (unit vector), orthogonal to $\hat{\phi}$, for GCS
$\hat{\theta}'$	spherical basis vector (unit vector), orthogonal to $\hat{\phi}'$, for LCS
θ_{etilt}	electrical steering angle in vertical direction
$\theta_{3\text{dB}}$	vertical 3 dB beamwidth of an antenna
ψ	Angular displacement between two pairs of unit vectors

3.3 Abbreviations

For the purposes of the present document, the abbreviations given in TR 21.905 [1] and the following apply. An abbreviation defined in the present document takes precedence over the definition of the same abbreviation, if any, in TR 21.905 [1].

2D	two-dimensional
3D	three-dimensional
AOA	Azimuth angle Of Arrival
AOD	Azimuth angle Of Departure
AS	Angular Spread
ASA	Azimuth angle Spread of Arrival
ASD	Azimuth angle Spread of Departure
BF	Beamforming
BS	Base Station
BP	Breakpoint
BW	Beamwidth
CDF	Cumulative Distribution Function
CDL	Clustered Delay Line
CRS	Common Reference Signal

D2D	Device-to-Device
DFT	Discrete Fourier Transform
DS	Delay Spread
GCS	Global Coordinate System
IID	Independent and identically distributed
InF	Indoor Factory
InF-SL	Indoor Factory with Sparse clutter and Low base station height (both Tx and Rx are below the average height of the clutter)
InF-DL	Indoor Factory with Dense clutter and Low base station height (both Tx and Rx are below the average height of the clutter)
InF-SH	Indoor Factory with Sparse clutter and High base station height (Tx or Rx elevated above the clutter)
InF-DH	Indoor Factory with Dense clutter and High base station height (Tx or Rx elevated above the clutter)
InF-HH	Indoor Factory with High Tx and High Rx (both elevated above the clutter)
InH	Indoor Hotspot
IRR	Infrared Reflecting
ISD	Intersite Distance
K	Ricean K factor
LCS	Local Coordinate System
LOS	Line Of Sight
MIMO	Multiple-Input-Multiple-Output
MPC	Multipath Component
NLOS	Non-LOS
O2I	Outdoor-to-Indoor
O2O	Outdoor-to-Outdoor
OFDM	Orthogonal Frequency-Division Multiplexing
PAS	Power angular spectrum
PL	Path Loss
PRB	Physical Resource Block
RCS	Radar cross-section
RMa	Rural Macro
RMS	Root Mean Square
RSRP	Reference Signal Received Power
Rx	Receiver
SCM	Spatial Channel Model
SINR	Signal-to-Interference-plus-Noise Ratio
SIR	Signal-to-Interference Ratio
SSCM	Statistical Spatial Channel Model
SF	Shadow Fading
SLA	Sidelobe Attenuation
TDL	Tapped Delay Line
TOA	Time Of Arrival
TRP	Transmission Reception Point
Tx	Transmitter
UMa	Urban Macro
UMi	Urban Micro
UT	User Terminal
UTD	Uniform Theory of Diffraction
V2V	Vehicle-to-Vehicle
XPR	Cross-Polarization Ratio
ZOA	Zenith angle Of Arrival
ZOD	Zenith angle Of Departure
ZSA	Zenith angle Spread of Arrival
ZSD	Zenith angle Spread of Departure

4 Introduction

At 3GPP TSG RAN #69 meeting the Study Item Description on "Study on channel model for frequency spectrum above 6 GHz" was approved [2]. This study item covers the identification of the status/expectation of existing information on high frequencies (e.g. spectrum allocation, scenarios of interest, measurements, etc), and the channel model(s) for frequencies up to 100 GHz. This technical report documents the channel model(s). The new channel model has to a large degree been aligned with earlier channel models for <6 GHz such as the 3D SCM model (3GPP TR 36.873) or IMT-Advanced (ITU-R M.2135). The new model supports comparisons across frequency bands over the range 0.5-100 GHz. The modelling methods defined in this technical report are generally applicable over the range 0.5-100 GHz, unless explicitly mentioned otherwise in this technical report for specific modelling method, involved parameters and/or scenario.

Subsequently, at the 3GPP TSG RAN #81 meeting the Study Item Description "Study on Channel Modeling for Indoor Industrial Scenarios" was approved [23]. The findings from this study item is also captured in the present technical report. The Industrial channel model was developed by considering new measurements and information in the literature. An overview list of all such contributions and sources is available in tdoc R1-1909706.

The channel model is applicable for link and system level simulations in the following conditions:

- For system level simulations, supported scenarios are urban microcell street canyon, urban macrocell, indoor office, rural macrocell, and indoor factory.
- Bandwidth is supported up to 10% of the center frequency but no larger than 2GHz.
- Mobility of either one end of the link or both ends of the link is supported
- For the stochastic model, spatial consistency is supported by correlation of LSPs and SSPs as well as LOS/NLOS state.
- Large array support is based on far field assumption and stationary channel over the size of the array.

5 General

6 Status/expectation of existing information on high frequencies

6.1 Channel modelling works outside of 3GPP

This subclause summarizes the channel modelling work outside of 3GPP based on the input from companies.

Groups and projects with channel models:

- METIS (Mobile and wireless communications Enablers for the Twenty-twenty Information Society)
- MiWEBA (Millimetre-Wave Evolution for Backhaul and Access)
- ITU-R M
- COST2100
- IEEE 802.11
- NYU WIRELESS: interdisciplinary academic research center

- Fraunhofer HHI has developed the QuaDRiGa channel model, Matlab implementation is available at <http://quadrige-channel-model.de>

Groups and projects which intend to develop channel models:

- 5G mmWave Channel Model Alliance: NIST initiated, North America based
- mmMAGIC (Millimetre-Wave Based Mobile Radio Access Network for Fifth Generation Integrated Communications): Europe based
- IMT-2020 5G promotion association: China based

METIS Channel Models:

- Identified 5G requirements (e.g., wide frequency range, high bandwidth, massive MIMO, 3-D and accurate polarization modelling)
- Performed channel measurements at various bands between 2GHz and 60 GHz
- Provided different channel model methodologies (map-based model, stochastic model or hybrid model). For stochastic model, the proposed channel is focused on outdoor square, Indoor cafeteria and indoor shopping mall scenarios.

MiWEBA Channel Models:

- Addressed various challenges: Shadowing, spatial consistency, environment dynamics, spherical wave modelling, dual mobility Doppler model, ratio between diffuse and specular reflections, polarization
- Proposed Quasi-deterministic channel model
- Performed channel measurements at 60 GHz
- Focused on university campus, street canyon, hotel lobby, backhaul, and D2D scenarios.

ITU-R M Channel Models:

- Addressed the propagation loss and atmospheric loss on mmW
- Introduced enabling antenna array technology and semiconductor technology
- Proposed deployment scenarios, focused on dense urban environment for high data rate service: indoor shopping mall, indoor enterprise, in home, urban hotspot in a square/street, mobility in city.

COST2100 and COST IC1004 Channel Models:

- Geometry-based stochastic channel model that reproduce the stochastic properties of MIMO channels over time, frequency and space. It is a cluster-level model where the statistics of the large scale parameters are always guaranteed in each series of channel instances.

NYU WIRELESS Channel Models:

- Conducted many urban propagation measurements on 28/38/60/73 GHz bands for both outdoor and indoor channels, measurements are continuing.
- Proposed 3 areas for 5G mmWave channel modelling which are small modifications or extensions from 3GPP's current below 6GHz channel models
- 1) LOS/NLOS/blockage modelling (a squared exponential term); 2). Wideband power delay profiles (time clusters and spatial lobes for a simple extension to the existing 3GPP SSCM model); 3). Physics-based path loss model (using the existing 3GPP path loss equations, but simply replacing the "floating" optimization parameter with a deterministic 1 m "close-in" free space reference term in order to provide a standard and stable definition of "path loss exponent" across all different parties, scenarios, and frequencies).

802.11 ad/ay Channel Models:

- Conducted ray-tracing methodology on 60 GHz band indoor channels, including conference room, cubicle, living room scenarios
- Intra cluster parameters were proposed in terms of ray excess delay and ray power distribution

- Human blockage models were proposed in terms of blockage probability and blockage attenuation

5G mmWave Channel Model Alliance:

- Will provide a venue to promote fundamental research into measurement, analysis, identification of physical parameters, and statistical representations of mmWave propagation channels.
- Divided into six collaborative working groups that include a Steering Committee; Modelling Methodology Group; Measurement Methodology Group; and groups that focus on defining and parameterizing Indoor, Outdoor, and Emerging Usage Scenarios.
- Sponsored by Communications Technology Research Laboratory within the NIST.

mmMAGIC:

- Brings together major infrastructure vendors, major European operators, leading research institutes and universities, measurement equipment vendors and one SME.
- Will undertake extensive radio channel measurements in the 6-100 GHz range.
- Will develop and validate advanced channel models that will be used for rigorous validation and feasibility analysis of the proposed concepts and system, as well as for usage in regulatory and standards fora.

IMT-2020 5G promotion association

- Jointly established by three ministries of China based on the original IMT-Advanced promotion group
- Members including the main operators, vendors, universities and research institutes in China
- The major platform to promote 5G technology research in China and to facilitate international communication and cooperation

QuaDRiGa (Fraunhofer HHI)

- QuaDRiGa (QUasi Deterministic RadIo channel GenerAtor) was developed at the Fraunhofer Heinrich Hertz Institute within the [Wireless Communications and Networks Department](#) to enable the modelling of MIMO radio channels for specific network configurations, such as indoor, satellite or heterogeneous configurations.
- Besides being a fully-fledged 3D geometry-based stochastic channel model (well aligned with TR36.873), QuaDRiGa contains a collection of features created in SCM(e) and WINNER channel models along with novel modelling approaches which provide features to enable quasi-deterministic multi-link tracking of users (receiver) movements in changing environments. QuaDRiGa supports Massive MIMO modelling enabled through a new multi-bounce scattering approach and spherical wave propagation. It will be continuously extended with features required by 5G and frequencies beyond 6 GHz. The QuaDRiGa model is supported by data from extensive channel measurement campaigns at 10 / 28 / 43 / 60 / 82 GHz performed by the same group.

6.2 Scenarios of interest

Brief description of the key scenarios of interest identified (see note):

- (1) UMi (Street canyon, open area) with O2O and O2I: This is similar to 3D-UMi scenario, where the BSs are mounted below rooftop levels of surrounding buildings. UMi open area is intended to capture real-life scenarios such as a city or station square. The width of the typical open area is in the order of 50 to 100 m.

Example: [Tx height:10m, Rx height: 1.5-2.5 m, ISD: 200m]

- (2) UMa with O2O and O2I: This is similar to 3D-UMa scenario, where the BSs are mounted above rooftop levels of surrounding buildings.

Example: [Tx height:25m, Rx height: 1.5-2.5 m, ISD: 500m]

- (3) Indoor: This scenario is intended to capture various typical indoor deployment scenarios, including office environments, and shopping malls. The typical office environment is comprised of open cubicle areas, walled offices, open areas, corridors etc. The BSs are mounted at a height of 2-3 m either on the ceilings or walls. The shopping malls are often 1-5 stories high and may include an open area (or "atrium") shared by several floors. The BSs are mounted at a height of approximately 3 m on the walls or ceilings of the corridors and shops.

Example: [Tx height: 2-3m, Rx height: 1.5m, area: 500 square meters]

- (4) Backhaul, including outdoor above roof top backhaul in urban area and street canyon scenario where small cell BSs are placed at lamp posts.
- (5) D2D/V2V. Device-to-device access in open area, street canyon, and indoor scenarios. V2V is a special case where the devices are mobile.
- (6) Other scenarios such as Stadium (open-roof) and Gym (close-roof).
- (7) Indoor industrial scenarios

Note: The scenarios of interest are based on the plenary email discussion and different from the supported scenarios in clause 7. The indoor industrial scenarios were identified at a later stage in the 3GPP TSG RAN #81 meeting.

6.3 Channel measurement capabilities

The measurement capability as reported by each company is summarized in the following table.

Table 6.3-1: Channel measurement capabilities

	6 - 20 GHz	20 - 30 GHz	30 - 60 GHz	>60 GHz
Urban macro	CMCC Nokia/Aalborg	Nokia/Aalborg	NYU	
Urban micro	Aalto University CMCC Ericsson Intel/Fraunhofer HHI Nokia/Aalborg NTT DOCOMO Orange	AT&T Aalto University CMCC Huawei Intel/Fraunhofer HHI Nokia/Aalborg NTT DOCOMO NYU Qualcomm Samsung CATT KT ETRI ITRI/CCU ZTE	AT&T Huawei Intel/Fraunhofer HHI NTT DOCOMO Qualcomm CATT ETRI ITRI/CCU ZTE	AT&T Aalto University Huawei Intel/Fraunhofer HHI NYU
Indoor	Aalto University CMCC Ericsson Huawei Intel/Fraunhofer HHI Nokia/Aalborg NTT DOCOMO Orange	AT&T Alcatel-Lucent Aalto University BUPT CMCC Huawei Intel/Fraunhofer HHI Nokia/Aalborg NTT DOCOMO NYU Qualcomm Samsung CATT KT ETRI ITRI/CCU ZTE	AT&T Ericsson Huawei Intel/Fraunhofer HHI NTT DOCOMO NYU Qualcomm CATT ETRI ITRI/CCU ZTE	AT&T Aalto University Huawei Intel/Fraunhofer HHI NYU
O2I	Ericsson Huawei Intel/Fraunhofer HHI Nokia/Aalborg NTT DOCOMO Orange	AT&T Alcatel-Lucent Ericsson Huawei Intel/Fraunhofer HHI NTT DOCOMO NYU Samsung KT	AT&T Ericsson Huawei Intel/Fraunhofer HHI NTT DOCOMO	AT&T Huawei Intel/Fraunhofer HHI

6.4 Modelling objectives

The requirements for channel modelling are as follows.

- Channel model SI should take into account the outcome of RAN-level discussion in the '5G' requirement study item
- Complexity in terms of Description, Generating channel coefficients, development complexity and Simulation time should be considered.
- Support frequency range up to 100 GHz.
 - The critical path of the SI is 6 – 100 GHz
 - Take care of mmW propagation aspects such as blocking and atmosphere attenuation.

- The model should be consistent in space, time and frequency
- Support large channel bandwidths (up to 10% of carrier frequency)
- Aim for the channel model to cover a range of coupling loss considering current typical cell sizes, e.g. up to km-range macro cells. Note: This is to enable investigation of the relevance of the 5G system using higher frequency bands to existing deployments.
- Accommodate UT mobility
 - Mobile speed up to 500 km/h.
 - Develop a methodology considering that model extensions to D2D and V2V may be developed in future SI.
- Support large antenna arrays

7 Channel model(s) for 0.5-100 GHz

7.1 Coordinate system

7.1.1 Definition

A coordinate system is defined by the x, y, z axes, the spherical angles and the spherical unit vectors as shown in Figure 7.1.1. Figure 7.1.1 defines the zenith angle θ and the azimuth angle ϕ in a Cartesian coordinate system. Note that $\theta=0$ points to the zenith and $\theta=90^\circ$ points to the horizon. The field component in the direction of $\hat{\theta}$ is given by F_θ and the field component in the direction of $\hat{\phi}$ is given by F_ϕ .

Figure 7.1.1: Definition of spherical angles and spherical unit vectors in a Cartesian coordinate system, where \hat{n} is the given direction, $\hat{\theta}$ and $\hat{\phi}$ are the spherical basis vectors

7.1.2 Local and global coordinate systems

A Global Coordinate System (GCS) is defined for a system comprising multiple BSs and UTs. An array antenna for a BS or a UT can be defined in a Local Coordinate System (LCS). An LCS is used as a reference to define the vector far-field that is pattern and polarization, of each antenna element in an array. It is assumed that the far-field is known in the

LCS by formulae. The placement of an array within the GCS is defined by the translation between the GCS and a LCS. The orientation of the array with respect to the GCS is defined in general by a sequence of rotations (described in subclause 7.1.3). Since this orientation is in general different from the GCS orientation, it is necessary to map the vector fields of the array elements from the LCS to the GCS. This mapping depends only on the orientation of the array and is given by the equations in subclause 7.1.3. Note that any arbitrary mechanical orientation of the array can be achieved by rotating the LCS with respect to the GCS.

7.1.3 Transformation from a LCS to a GCS

A GCS with coordinates (x, y, z, θ, ϕ) and unit vectors $(\hat{\theta}, \hat{\phi})$ and an LCS with "primed" coordinates $(x', y', z', \theta', \phi')$ and "primed" unit vectors $(\hat{\theta}', \hat{\phi}')$ are defined with a common origins in Figures 7.1.3-1 and 7.1.3-2. Figure 7.1.3-1 illustrates the sequence of rotations that relate the GCS (gray) and the LCS (blue). Figure 7.1.3-2 shows the coordinate direction and unit vectors of the GCS (gray) and the LCS (blue). Note that the vector fields of the array antenna elements are defined in the LCS. In Figure 7.1.3-1 we consider an arbitrary 3D-rotation of the LCS with respect to the GCS given by the angles α, β, γ . The set of angles α, β, γ can also be termed as the orientation of the array antenna with respect to the GCS.

Note that the transformation from a LCS to a GCS depends only on the angles α, β, γ . The angle α is called the bearing angle, β is called the downtilt angle and γ is called the slant angle.

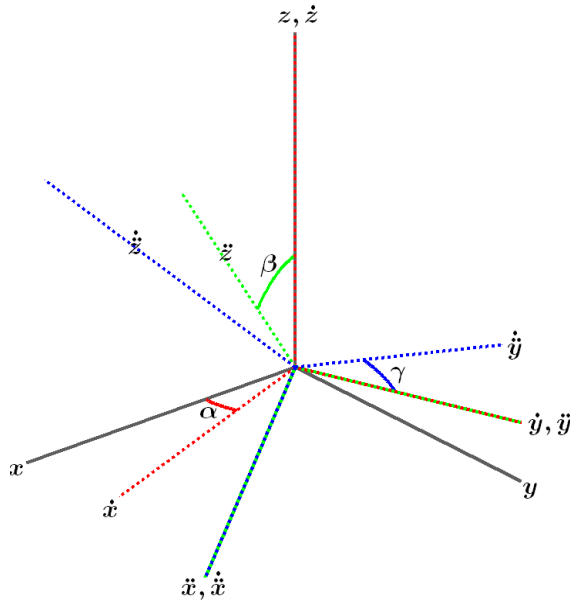


Figure 7.1.3-1: Orienting the LCS (blue) with respect to the GCS (gray) by a sequence of 3 rotations: α, β, γ .

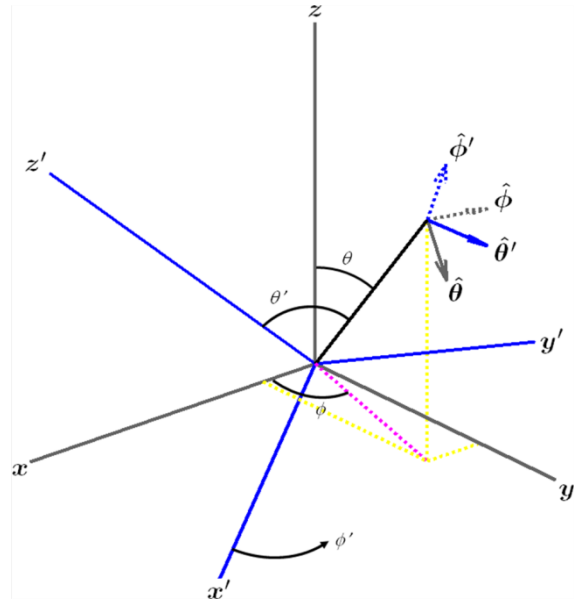


Figure 7.1.3-2: Definition of spherical coordinates and unit vectors in both the GCS and LCS.

Let $A'(\theta', \phi')$ denote an antenna element pattern in the LCS and $A(\theta, \phi)$ denote the same antenna element pattern in the GCS. Then the two are related simply by

$$A(\theta, \phi) = A'(\theta', \phi') \quad (7.1-1)$$

with θ' and ϕ' given by (7.1-7) and (7.1-8).

Let us denote the polarized field components in the LCS by $F_{\theta'}'(\theta', \phi')$, $F_{\phi'}'(\theta', \phi')$ and in the GCS by $F_{\theta}(\theta, \phi)$, $F_{\phi}(\theta, \phi)$. Then they are related by equation (7.1-11).

Any arbitrary 3D rotation can be specified by at most 3 elemental rotations, and following the framework of

Figure 7.1.3-1, a series of rotations about the z , \dot{y} and \ddot{x} axes are assumed here, in that order. The dotted and double-dotted marks indicate that the rotations are intrinsic, which means that they are the result of one (\cdot) or two ($\cdot\cdot$) intermediate rotations. In other words, the \dot{y} axis is the original y axis after the first rotation about z , and the \ddot{x} axis is the original x axis after the first rotation about z and the second rotation about \dot{y} . A first rotation of α about z sets the antenna bearing angle (i.e. the sector pointing direction for a BS antenna element). The second rotation of β about \dot{y} sets the antenna downtilt angle. Finally, the third rotation of γ about \ddot{x} sets the antenna slant angle. The orientation of the x , y and z axes after all three rotations can be denoted as \ddot{x} , \ddot{y} and \ddot{z} . These triple-dotted axes represents the final orientation of the LCS, and for notational purposes denoted as the x' , y' and z' axes (local or "primed" coordinate system).

In order to establish the equations for transformation of the coordinate system and the polarized antenna field patterns between the GCS and the LCS, it is necessary to determine the composite rotation matrix that describes the transformation of point (x, y, z) in the GCS into point (x', y', z') in the LCS. This rotation matrix is computed as the product of three elemental rotation matrices. The matrix to describe rotations about the z , \dot{y} and \ddot{x} axes by the angles α , β and γ respectively and in that order is defined as

$$R = R_z(\alpha) R_y(\beta) R_x(\gamma) = \begin{pmatrix} +\cos\alpha & -\sin\alpha & 0 \\ +\sin\alpha & +\cos\alpha & 0 \\ 0 & 0 & 1 \end{pmatrix} \begin{pmatrix} +\cos\beta & 0 & +\sin\beta \\ 0 & 1 & 0 \\ -\sin\beta & 0 & +\cos\beta \end{pmatrix} \begin{pmatrix} 1 & 0 & 0 \\ 0 & +\cos\gamma & -\sin\gamma \\ 0 & +\sin\gamma & +\cos\gamma \end{pmatrix} \quad (7.1-2)$$

The reverse transformation is given by the inverse of R , which is also equal to the transpose of R since it is orthogonal.

$$R^{-1} = R_x(-\gamma) R_y(-\beta) R_z(-\alpha) = R^T \quad (7.1-3)$$

The simplified forward and reverse composite rotation matrices are given by

$$R = \begin{pmatrix} \cos\alpha \cos\beta & \cos\alpha \sin\beta \sin\gamma - \sin\alpha \cos\gamma & \cos\alpha \sin\beta \cos\gamma + \sin\alpha \sin\gamma \\ \sin\alpha \cos\beta & \sin\alpha \sin\beta \sin\gamma + \cos\alpha \cos\gamma & \sin\alpha \sin\beta \cos\gamma - \cos\alpha \sin\gamma \\ -\sin\beta & \cos\beta \sin\gamma & \cos\beta \cos\gamma \end{pmatrix} \quad (7.1-4)$$

and

$$R^{-1} = \begin{pmatrix} \cos\alpha \cos\beta & \sin\alpha \cos\beta & -\sin\beta \\ \cos\alpha \sin\beta \sin\gamma - \sin\alpha \cos\gamma & \sin\alpha \sin\beta \sin\gamma + \cos\alpha \cos\gamma & \cos\beta \sin\gamma \\ \cos\alpha \sin\beta \cos\gamma + \sin\alpha \sin\gamma & \sin\alpha \sin\beta \cos\gamma - \cos\alpha \sin\gamma & \cos\beta \cos\gamma \end{pmatrix} \quad (7.1-5)$$

These transformations can be used to derive the angular and polarization relationships between the two coordinate systems.

In order to establish the angular relationships, consider a point (x, y, z) on the unit sphere defined by the spherical coordinates $(\rho=1, \theta, \phi)$, where ρ is the unit radius, θ is the zenith angle measured from the $+z$ -axis, and ϕ is the azimuth angle measured from the $+x$ -axis in the x - y plane. The Cartesian representation of that point is given by

$$\begin{pmatrix} x \\ y \\ z \end{pmatrix} = \begin{pmatrix} \sin\theta \cos\phi \\ \sin\theta \sin\phi \\ \cos\theta \end{pmatrix} \quad (7.1-6)$$

The zenith angle is computed as $\arccos(\hat{p} \cdot \hat{z})$ and the azimuth angle as $\arg(\hat{x} \cdot \hat{p} + j \hat{y} \cdot \hat{p})$, where \hat{x} , \hat{y} and \hat{z} are the Cartesian unit vectors. If this point represents a location in the GCS defined by θ and ϕ , the

corresponding position in the LCS is given by $R^{-1}\hat{\rho}$, from which local angles θ' and ϕ' can be computed. The results are given in equations (7.1-7) and (7.1-8).

$$\begin{aligned} \begin{bmatrix} \hat{\rho} \\ \hat{\rho} \\ \hat{\rho} \end{bmatrix} \begin{bmatrix} \hat{\rho} \\ \hat{\rho} \\ \hat{\rho} \end{bmatrix}^T R^{-1} \hat{\rho} = \arccos(\cos \beta \cos \gamma \cos \theta + (\sin \beta \cos \gamma \cos(\varphi - \alpha) - \sin \gamma \sin(\varphi - \alpha)) \sin \theta) \\ \theta'(\alpha, \beta, \gamma; \theta, \varphi) = \arccos \hat{\rho} \end{aligned} \quad (7.1-7)$$

$$\begin{aligned} \phi'(\alpha, \beta, \gamma; \theta, \varphi) = \arg \left(\begin{bmatrix} 1 \\ j \\ 0 \end{bmatrix}^T R^{-1} \hat{\rho} \right) = \arg \\ (\cos \beta \sin \theta \cos(\varphi - \alpha) - \sin \beta \cos \theta) + \\ j(\cos \beta \sin \gamma \cos \theta + (\sin \beta \sin \gamma \cos(\varphi - \alpha) + \cos \gamma \sin(\varphi - \alpha)) \sin \theta) \end{aligned} \quad (7.1-8)$$

These formulae relate the spherical angles (θ, ϕ) of the GCS to the spherical angles (θ', ϕ') of the LCS given the rotation operation defined by the angles (α, β, γ) .

Let us denote the polarized field components $F_\theta(\theta, \varphi)$, $F_\phi(\theta, \varphi)$ in the GCS and $F_{\theta'}(\theta', \varphi')$, $F_{\phi'}(\theta', \varphi')$ in the LCS. These are related by

$$\begin{pmatrix} F_\theta(\theta, \varphi) \\ F_\phi(\theta, \varphi) \end{pmatrix} = \begin{pmatrix} \hat{\theta}(\theta, \varphi)^T R \hat{\theta}'(\theta', \varphi') & \hat{\theta}(\theta, \varphi)^T R \hat{\phi}'(\theta', \varphi') \\ \hat{\phi}(\theta, \varphi)^T R \hat{\theta}'(\theta', \varphi') & \hat{\phi}(\theta, \varphi)^T R \hat{\phi}'(\theta', \varphi') \end{pmatrix} \begin{pmatrix} F_{\theta'}(\theta', \varphi') \\ F_{\phi'}(\theta', \varphi') \end{pmatrix} \quad (7.1-9)$$

In this equation, $\hat{\theta}$ and $\hat{\phi}$ represent the spherical unit vectors of the GCS, and $\hat{\theta}'$ and $\hat{\phi}'$ are the representations in the LCS. The forward rotation matrix R transforms the LCS unit vectors into the GCS frame of reference. These pairs of unit vectors are orthogonal and can be represented as shown in Figure 7.1.3-3.

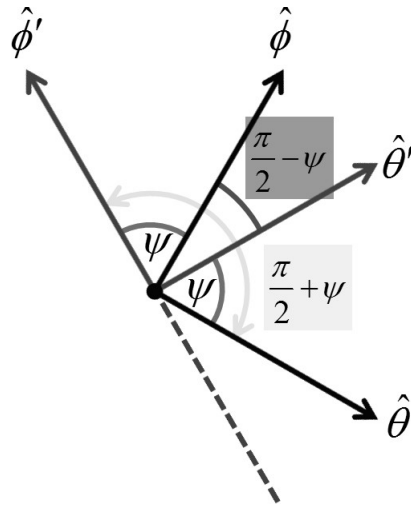


Figure 7.1.3-3: Rotation of the spherical basis vectors by an angle ψ due to the orientation of the LCS with respect to the GCS

Assuming an angular displacement of ψ between the two pairs of unit vectors, the rotation matrix of equation (7.1-9) can be further simplified as:

$$\begin{pmatrix} \hat{\theta}(\theta, \varphi)^T R \hat{\theta}'(\theta', \varphi') & \hat{\theta}(\theta, \varphi)^T R \hat{\phi}'(\theta', \varphi') \\ \hat{\phi}(\theta, \varphi)^T R \hat{\theta}'(\theta', \varphi') & \hat{\phi}(\theta, \varphi)^T R \hat{\phi}'(\theta', \varphi') \end{pmatrix} = \begin{pmatrix} \cos \psi & \cos(\pi/2 + \psi) \\ \cos(\pi/2 - \psi) & \cos \psi \end{pmatrix} = \begin{pmatrix} +\cos \psi & -\sin \psi \\ +\sin \psi & +\cos \psi \end{pmatrix} \quad (7.1-10)$$

and equation (7.1-9) can be written as:

$$\begin{pmatrix} F_{\theta}(\theta, \varphi) \\ F_{\varphi}(\theta, \varphi) \end{pmatrix} = \begin{pmatrix} +\cos \psi & -\sin \psi \\ +\sin \psi & +\cos \psi \end{pmatrix} \begin{pmatrix} F_{\theta'}(\theta', \varphi') \\ F_{\varphi'}(\theta', \varphi') \end{pmatrix} \quad (7.1-11)$$

The angle ψ can be computed in numerous ways from equation (7.1-10), with one such way approach being

$$\psi = \arg(\hat{\theta}(\theta, \varphi)^T R \hat{\theta}'(\theta', \varphi') + j \hat{\varphi}(\theta, \varphi)^T R \hat{\theta}'(\theta', \varphi')) \quad (7.1-12)$$

The dot products are readily computed using the Cartesian representation of the spherical unit vectors. The general expressions for these unit vectors are given by

$$\hat{\theta} = \begin{pmatrix} \cos \theta \cos \varphi \\ \cos \theta \sin \varphi \\ -\sin \theta \end{pmatrix} \quad (7.1-13)$$

and

$$\hat{\varphi} = \begin{pmatrix} -\sin \varphi \\ +\cos \varphi \\ 0 \end{pmatrix} \quad (7.1-14)$$

The angle ψ can be expressed as a function of mechanical orientation (α, β, γ) and spherical position (θ, ϕ), and is given by

$$\psi = \arg \left(\frac{(\sin \gamma \cos \theta \sin(\varphi - \alpha) + \cos \gamma (\cos \beta \sin \theta - \sin \beta \cos \theta \cos(\varphi - \alpha))) + j(\sin \gamma \cos(\varphi - \alpha) + \sin \beta \cos \gamma \sin(\varphi - \alpha))}{\sin \theta} \right) \quad (7.1-15)$$

It can be shown that $\cos \psi$ and $\sin \psi$ can be expressed as:

$$\cos \psi = \frac{\cos \beta \cos \gamma \sin \theta - (\sin \beta \cos \gamma \cos(\varphi - \alpha) - \sin \gamma \sin(\varphi - \alpha)) \cos \theta}{\sqrt{1 - (\cos \beta \cos \gamma \cos \theta + (\sin \beta \cos \gamma \cos(\varphi - \alpha) - \sin \gamma \sin(\varphi - \alpha)) \sin \theta)^2}} \quad (7.1-16)$$

$$\sin \psi = \frac{\sin \beta \cos \gamma \sin(\varphi - \alpha) + \sin \gamma \cos(\varphi - \alpha)}{\sqrt{1 - (\cos \beta \cos \gamma \cos \theta + (\sin \beta \cos \gamma \cos(\varphi - \alpha) - \sin \gamma \sin(\varphi - \alpha)) \sin \theta)^2}} \quad (7.1-17)$$

7.1.4 Transformation from an LCS to a GCS for downtilt angle only

In this subclause equations are provided for the transformation from LCS to GCS assuming that the orientation of the LCS (with respect to the GCS) is such that the bearing angle $\alpha=0$, the downtilt angle β is non-zero and the slant angle $\gamma=0$. In other words the y' -axis of the LCS is parallel to the y -axis of the GCS. Considering a BS antenna element the x -axis of the GCS is aligned with the pointing direction of the sector. Mechanical downtilt is modelled as a rotation of the LCS around the y -axis. For zero mechanical downtilt the LCS coincides with the GCS.

This transformation relates the spherical angles (θ, φ) in the global coordinate system to spherical angles (θ', φ') in the local (antenna-fixed) coordinate system and is defined as follows:

$$\theta' = \arccos(\cos \varphi \sin \theta \sin \beta + \cos \theta \cos \beta) \quad (7.1-18)$$


$$\varphi' = \arg(\cos \varphi \sin \theta \cos \beta - \cos \theta \sin \beta + j \sin \varphi \sin \theta) \quad (7.1-19)$$

where β is the mechanical tilt angle around the y -axis as defined in Figure 7.1.4. Note that the equations (7.1-7), (7.1-8) reduce to equations (7.1-18), (7.1-19) if both α and γ are zero.

The antenna element pattern $A(\theta, \varphi)$ in the GCS is related to the antenna element pattern $A'(\theta', \varphi')$ in the LCS by the relation

$$A(\theta, \varphi) = A'(\theta', \varphi') \quad (7.1-20)$$

with θ' and φ' given by (7.1-18) and (7.1-19).


Figure 7.1.4: Definition of angles and unit vectors when the LCS has been rotated an angle β around the y -axis of the GCS

For a mechanical tilt angle β , the global coordinate system field components $F_\theta(\theta, \varphi)$ and $F_\varphi(\theta, \varphi)$, are calculated from the field components $F'_{\theta'}(\theta', \varphi')$ and $F'_{\varphi'}(\theta', \varphi')$ of the radiation pattern in the local (antenna-fixed) coordinate system as:

$$F_\theta(\theta, \varphi) = F'_{\theta'}(\theta', \varphi') \cos \psi - F'_{\varphi'}(\theta', \varphi') \sin \psi \quad (7.1-21)$$

$$F_\varphi(\theta, \varphi) = F'_{\theta'}(\theta', \varphi') \sin \psi + F'_{\varphi'}(\theta', \varphi') \cos \psi \quad (7.1-22)$$

where θ' and φ' are defined as in (7.1-18) and (7.1-19), and ψ is defined as:

$$\psi = \arg(\sin \theta \cos \beta - \cos \varphi \cos \theta \sin \beta + j \sin \varphi \sin \beta) \quad (7.1-23)$$

Note that the equation (7.1-15) is reduced to equation (7.1-23) if both α and γ are zero.

As an example, in the horizontal cut, i.e., for $\theta = 90^\circ$, equations (7.1-18), (7.1-19) and (7.1-23) become

$$\theta' = \arccos(\cos \varphi \sin \beta) \quad (7.1-24)$$

$$\varphi' = \arg(\cos \varphi \cos \beta + j \sin \varphi) \quad (7.1-25)$$

$$\psi = \arg(\cos \beta + j \sin \varphi \sin \beta) \quad (7.1-26)$$

7.2 Scenarios

The detailed scenario description in this subclause can be used for channel model calibration.

UMi-street canyon and UMa

Details on UMi-street canyon and UMa scenarios are listed in Table 7.2-1.

Table 7.2-1: Evaluation parameters for UMi-street canyon and UMa scenarios

Parameters		UMi - street canyon	UMa
Cell layout		Hexagonal grid, 19 micro sites, 3 sectors per site (ISD = 200m)	Hexagonal grid, 19 macro sites, 3 sectors per site (ISD = 500m)
BS antenna height h_{BS}		10m	25m
UT location	Outdoor/indoor	Outdoor and indoor	Outdoor and indoor
	LOS/NLOS	LOS and NLOS	LOS and NLOS
	Height h_{UT}	Same as 3D-UMi in TR36.873	Same as 3D-UMa in TR36.873
Indoor UT ratio		80%	80%
UT mobility (horizontal plane only)		3km/h	3km/h
Min. BS - UT distance (2D)		10m	35m
UT distribution (horizontal)		Uniform	Uniform

Indoor-office

Details on indoor-office scenarios are listed in Table 7.2-2 and presented in Figure 7.2-1. More details, if necessary, can be added to Figure 7.2-1.

Table 7.2-2: Evaluation parameters for indoor-office scenarios

Parameters		Indoor - office open office	Indoor - office mixed office
Layout	Room size (WxLxH)	120mx50mx3m	
	ISD	20m	
BS antenna height h_{BS}		3 m (ceiling)	
UT location	LOS/NLOS	LOS and NLOS	
	Height h_{UT}	1 m	
UT mobility (horizontal plane only)		3 km/h	
Min. BS - UT distance (2D)		0	
UT distribution (horizontal)		Uniform	

Note: The only difference between the open office and mixed office models in this TR is the line of sight probability.

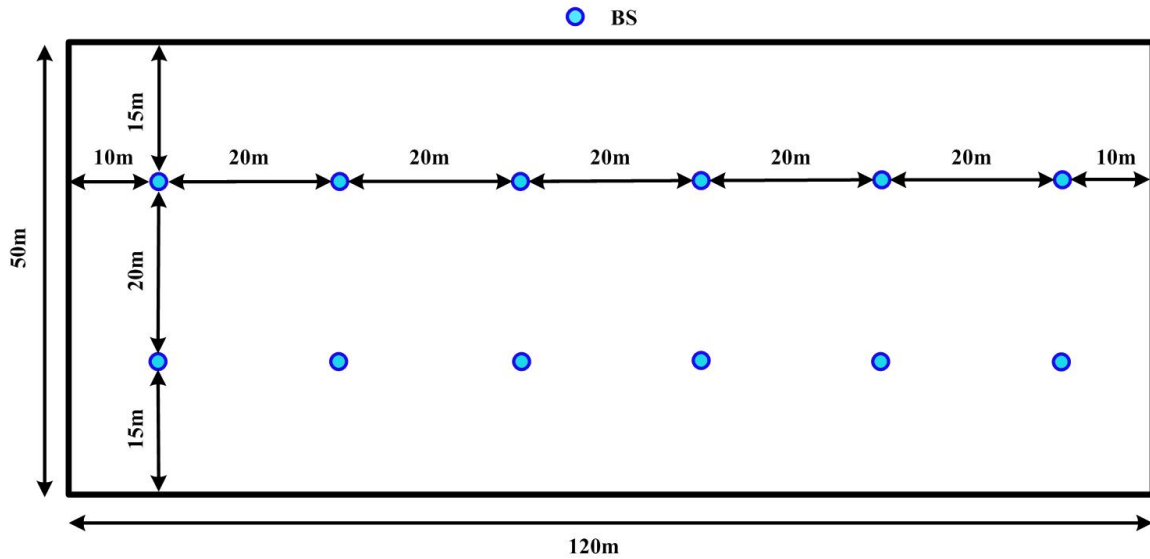


Figure 7.2-1: Layout of indoor office scenarios.

RMa

The rural deployment scenario focuses on larger and continuous coverage. The key characteristics of this scenario are continuous wide area coverage supporting high speed vehicles. This scenario will be noise-limited and/or interference-limited, using macro TRPs. Details of RMa scenario is described in Table 7.2-3.

Table 7.2-3: Evaluation parameters for RMa

Parameters	RMa
Carrier Frequency	Up to 7Ghz
BS height h_{BS}	35m
Layout	Hexagonal grid, 19 Macro sites, 3sectors per site, ISD = 1732m or 5000m
UT height h_{UT}	1.5m
UT distribution	Uniform
Indoor/Outdoor	50% indoor and 50% in car
LOS/NLOS	LOS and NLOS
Min BS - UT distance(2D)	35m

Indoor Factory (InF)

The indoor factory (InF) scenario focuses on factory halls of varying sizes and with varying levels of density of "clutter", e.g. machinery, assembly lines, storage shelves, etc. Details of the InF scenario are listed in Table 7.2-4.

Table 7.2-4: Evaluation parameters for InF

		InF				
Parameters		InF-SL (sparse clutter, low BS)	InF-DL (dense clutter, low BS)	InF-SH (sparse clutter, high BS)	InF-DH (dense clutter, high BS)	InF-HH (high Tx, high Rx)
Layout	Room size	Rectangular: 20-160000 m ²				
	Ceiling height	5-25 m	5-15 m	5-25 m	5-15 m	5-25 m

		Effective clutter height h_c	< Ceiling height, 0-10 m			
		External wall and ceiling type	Concrete or metal walls and ceiling with metal-coated windows			
Clutter type		Big machineries composed of regular metallic surfaces. For example: several mixed production areas with open spaces and storage/commis- sioning areas	Small to medium metallic machinery and objects with irregular structure. For example: assembly and production lines surrounded by mixed small-sized machineries.	Big machineries composed of regular metallic surfaces. For example: several mixed production areas with open spaces and storage/commis- sioning areas	Small to medium metallic machinery and objects with irregular structure. For example: assembly and production lines surrounded by mixed small-sized machineries.	Any
Typical clutter size, $d_{clutter}$		10 m	2 m	10 m	2 m	Any
Clutter density r (percentage of surface area occupied by clutter)		Low clutter density (<40%)	High clutter density ($\geq 40\%$)	Low clutter density (<40%)	High clutter density ($\geq 40\%$)	Any
BS antenna height h_{BS}		Clutter-embedded, i.e. the BS antenna height is below the average clutter height		Above clutter		Above clutter
UT location	LOS/NLOS	LOS and NLOS				100% LOS
	Height h_{UT}	Clutter-embedded				Above clutter

7.3 Antenna modelling

This subclause captures the antenna array structures considered in this SI for calibration.

The BS antenna is modelled by a uniform rectangular panel array, comprising $M_g N_g$ panels, as illustrated in Figure 7.3-1 with M_g being the number of panels in a column and N_g being the number of panels in a row. Furthermore the following properties apply:

- Antenna panels are uniformly spaced in the horizontal direction with a spacing of $d_{g,H}$ and in the vertical direction with a spacing of $d_{g,V}$.
- On each antenna panel, antenna elements are placed in the vertical and horizontal direction, where N is the number of columns, M is the number of antenna elements with the same polarization in each column.
 - Antenna numbering on the panel illustrated in Figure 7.3-1 assumes observation of the antenna array from the front (with x-axis pointing towards broad-side and increasing y-coordinate for increasing column number).
- The antenna elements are uniformly spaced in the horizontal direction with a spacing of d_H and in the vertical direction with a spacing of d_V .
- The antenna panel is either single polarized ($P=1$) or dual polarized ($P=2$).

The rectangular panel array antenna can be described by the following tuple (M_g, N_g, M, N, P) .

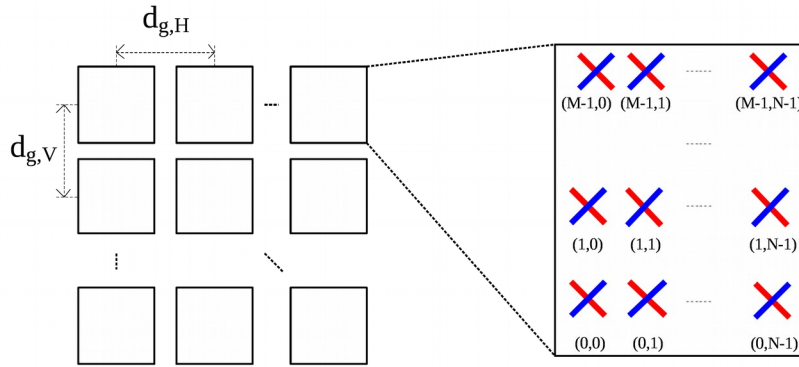


Figure 7.3-1: Cross-polarized panel array antenna model

The antenna radiation power pattern of each antenna element is generated according to Table 7.3-1.

Table 7.3-1: Radiation power pattern of a single antenna element

Parameter	Values
Vertical cut of the radiation power pattern (dB)	$A''_{dB}(\theta'', \varphi''=0^\circ) = -\min \left[12 \left(\frac{\theta'' - 90^\circ}{\theta_{3dB}} \right)^2, SLA_V \right]'' \in [0^\circ, 180^\circ] \hat{i}$ <p>with $\theta_{3dB} = 65^\circ, SLA_V = 30$ dB and $\{\theta\}$</p>
Horizontal cut of the radiation power pattern (dB)	$A''_{dB}(\theta''=90^\circ, \varphi'') = -\min \left[12 \left(\frac{\varphi''}{\varphi_{3dB}} \right)^2, A_{max} \right]'' \in [-180^\circ, 180^\circ] \hat{i}$ <p>with $\varphi_{3dB} = 65^\circ, A_{max} = 30$ dB and $\{\varphi\}$</p>
3D radiation power pattern (dB)	$A''_{dB}(\theta'', \varphi'') = -\min \left[-\left(A''_{dB}(\theta'', \varphi''=0^\circ) + A''_{dB}(\theta''=90^\circ, \varphi'') \right), A_{max} \right]$
Maximum directional gain of an antenna element $G_{E,max}$	8 dBi

7.3.1 Antenna port mapping

Legacy BS array antennas, i.e. uniform linear arrays with fix phase shifts between its M elements to obtain a beamtilt in vertical direction are modelled using complex weights

$$w_m = \frac{1}{\sqrt{M}} \exp \left(-j \frac{2\pi}{\lambda} (m-1) d_v \cos \theta_{etilt} \right) \quad (7.3-1)$$

where $m=1, \dots, M$, θ_{etilt} is the electrical vertical steering angle defined between 0° and 180° (90° represents perpendicular to the array). λ denotes the wavelength and d_v the vertical element spacing.

7.3.2 Polarized antenna modelling

In general the relationship between radiation field and power pattern is given by:

$$A''(\theta'', \varphi'') = |F''_{\theta}(\theta'', \varphi'')|^2 + |F''_{\varphi}(\theta'', \varphi'')|^2 \quad (7.3-2)$$

The following two models represent two options on how to determine the radiation field patterns based on a defined radiation power pattern.

Model-1:

In case of polarized antenna elements assume ζ is the polarization slant angle where $\zeta = 0$ degrees corresponds to a purely vertically polarized antenna element and $\zeta = \pm 45$ degrees correspond to a pair of cross-polarized antenna elements. Then the antenna element field components in θ' and φ' direction are given by

$$\begin{pmatrix} F'_{\theta}(\theta', \varphi') \\ F'_{\varphi}(\theta', \varphi') \end{pmatrix} = \begin{pmatrix} +\cos \psi & -\sin \psi \\ +\sin \psi & +\cos \psi \end{pmatrix} \begin{pmatrix} F''_{\theta}(\theta'', \varphi'') \\ F''_{\varphi}(\theta'', \varphi'') \end{pmatrix} \quad (7.3-3)$$

where
$$\cos \psi = \frac{\cos \zeta \sin \theta'' + \sin \zeta \sin \phi'' \cos \theta''}{\sqrt{1 - (\cos \zeta \cos \theta'' - \sin \zeta \sin \phi'' \sin \theta'')^2}}, \quad \sin \psi = \frac{\sin \zeta \cos \phi''}{\sqrt{1 - (\cos \zeta \cos \theta'' - \sin \zeta \sin \phi'' \sin \theta'')^2}}.$$

Note that the zenith and the azimuth field components $F'_{\theta}(\theta', \varphi')$, $F'_{\varphi}(\theta', \varphi')$, $F''_{\theta}(\theta'', \varphi'')$ and $F''_{\varphi}(\theta'', \varphi'')$ are defined in terms of the spherical basis vectors of an LCS as defined in Subclause 7.1. The difference between the single-primed and the double-primed components is that the single-primed field components account for the polarization slant and the double-primed field components do not. For a single polarized antenna (purely vertically polarized antenna) we can write $F''_{\theta}(\theta'', \varphi'') = \sqrt{A''(\theta'', \varphi'')}$ and $F''_{\varphi}(\theta'', \varphi'') = 0$ where $A''(\theta'', \varphi'')$ is the 3D antenna radiation power pattern as a function of azimuth angle ϕ'' and zenith angle θ'' in the LCS as defined in Table 7.3-1 converted into linear scale.

Model-2:

In case of polarized antennas, the polarization is modelled as angle-independent in both azimuth and elevation, in an LCS. For a linearly polarized antenna, the antenna element field pattern, in the vertical polarization and in the horizontal polarization, are given by

$$F'_{\theta}(\theta', \varphi') = \sqrt{A'(\theta', \varphi')} \cos(\zeta) \quad (7.3-4)$$

and

$$F'_{\varphi}(\theta', \varphi') = \sqrt{A'(\theta', \varphi')} \sin(\zeta), \quad (7.3-5)$$

respectively, where ζ is the polarization slant angle and $A'(\theta', \varphi')$ is the 3D antenna element power pattern as a function of azimuth angle, φ' and elevation angle, θ' in the LCS. Note that $\zeta = 0$ degrees correspond to a purely vertically polarized antenna element. The vertical and horizontal field directions are defined in terms of the spherical basis vectors, $\hat{\theta}'$ and $\hat{\phi}'$ respectively in the LCS as defined in Subclause 7.1.2. Also $A'(\theta', \varphi') = A'''(\theta''', \phi''')$, $\theta' = \theta'''$ and $\varphi' = \phi'''$ as defined in Table 7.1-1.

7.4 Pathloss, LOS probability and penetration modelling

7.4.1 Pathloss

The pathloss models are summarized in Table 7.4.1-1 and the distance definitions are indicated in Figure 7.4.1-1 and Figure 7.4.1-2. Note that the distribution of the shadow fading is log-normal, and its standard deviation for each scenario is given in Table 7.4.1-1.

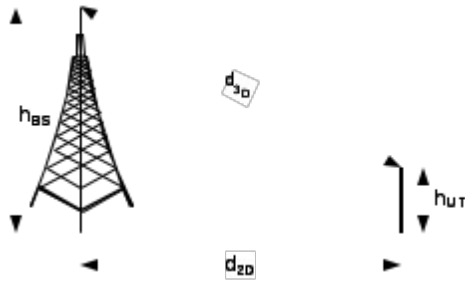


Figure 7.4.1-1: Definition of d_{2D} and d_{3D} for outdoor UTs

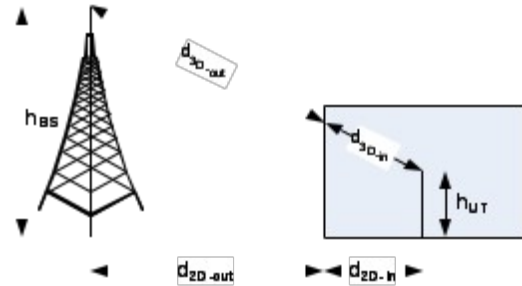


Figure 7.4.1-2: Definition of d_{2D-out} , d_{2D-in} and d_{3D-out} , d_{3D-in} for indoor UTs.

Note that

$$d_{3D-out} + d_{3D-in} = \sqrt{(d_{2D-out} + d_{2D-in})^2 + (h_{BS} - h_{UT})^2} \quad (7.4-1)$$

Table 7.4.1-1: Pathloss models

Scenario	LOS/NLOS	Pathloss [dB], f_c is in GHz and d is in meters, see note 6	Shadow fading std [dB]	Applicability range, antenna height default values
RMa	LOS	$PL_{RMa-LOS} = \begin{cases} PL_1 & 10\text{ m} \leq d_{2D} \leq d_{BP} \\ PL_2 & d_{BP} \leq d_{2D} \leq 10\text{ km} \end{cases}, \text{ see note 5}$ $PL_1 = 20 \log_{10}(40\pi d_{3D} f_c / 3) + \min(0.03 h^{1.72}, 10) \log_{10}(d_{3D}) - \min(0.044 h^{1.72}, 14.77) + 0.002 \log_{10}(h) d_{3D}$ $PL_2 = PL_1(d_{BP}) + 40 \log_{10}(d_{3D} / d_{BP})$	$\sigma_{SF} = 4$ $\sigma_{SF} = 6$	$h_{BS} = 35\text{ m}$ $h_{UT} = 1.5\text{ m}$ $W = 20\text{ m}$ $h = 5\text{ m}$ h = avg. building height W = avg. street width The applicability ranges:
	NLOS	$PL_{RMa-NLOS} = \max(PL_{RMa-LOS}, PL'_{RMa-NLOS})$ for $10\text{ m} \leq d_{2D} \leq 5\text{ km}$ $PL'_{RMa-NLOS} = 161.04 - 7.1 \log_{10}(W) + 7.5 \log_{10}(h) - (24.37 - 3.7(h/h_{BS})^2) \log_{10}(h_{BS}) + (43.42 - 3.1 \log_{10}(h_{BS}))(\log_{10}(d_{3D}) - 3) + 20 \log_{10}(f_c) - (3.2(\log_{10}(11.75 h_{UT}))^2 - 4.97)$	$\sigma_{SF} = 8$	$5\text{ m} \leq h \leq 50\text{ m}$ $5\text{ m} \leq W \leq 50\text{ m}$ $10\text{ m} \leq h_{BS} \leq 150\text{ m}$ $1\text{ m} \leq h_{UT} \leq 10\text{ m}$
UMa	LOS	$PL_{UMa-LOS} = \begin{cases} PL_1 & 10\text{ m} \leq d_{2D} \leq d'_{BP} \\ PL_2 & d'_{BP} \leq d_{2D} \leq 5\text{ km} \end{cases}, \text{ see note 1}$ $PL_1 = 28.0 + 22 \log_{10}(d_{3D}) + 20 \log_{10}(f_c)$ $PL_2 = 28.0 + 40 \log_{10}(d_{3D}) + 20 \log_{10}(f_c) - 9 \log_{10}((d'_{BP})^2 + (h_{BS} - h_{UT})^2)$	$\sigma_{SF} = 4$	$1.5\text{ m} \leq h_{UT} \leq 22.5\text{ m}$ $h_{BS} = 25\text{ m}$
	NLOS	$PL_{UMa-NLOS} = \max(PL_{UMa-LOS}, PL'_{UMa-NLOS})$ for $10\text{ m} \leq d_{2D} \leq 5\text{ km}$ $PL'_{UMa-NLOS} = 13.54 + 39.08 \log_{10}(d_{3D}) + 20 \log_{10}(f_c) - 0.6(h_{UT} - 1.5)$	$\sigma_{SF} = 6$	$1.5\text{ m} \leq h_{UT} \leq 22.5\text{ m}$ $h_{BS} = 25\text{ m}$ Explanations: see note 3
	Optional	$PL = 32.4 + 20 \log_{10}(f_c) + 30 \log_{10}(d_{3D})$	$\sigma_{SF} = 7.8$	
UMi - Street Canyon	LOS	$PL_{UMi-LOS} = \begin{cases} PL_1 & 10\text{ m} \leq d_{2D} \leq d'_{BP} \\ PL_2 & d'_{BP} \leq d_{2D} \leq 5\text{ km} \end{cases}, \text{ see note 1}$ $PL_1 = 32.4 + 21 \log_{10}(d_{3D}) + 20 \log_{10}(f_c)$ $PL_2 = 32.4 + 40 \log_{10}(d_{3D}) + 20 \log_{10}(f_c) - 9.5 \log_{10}((d'_{BP})^2 + (h_{BS} - h_{UT})^2)$	$\sigma_{SF} = 4$	$1.5\text{ m} \leq h_{UT} \leq 22.5\text{ m}$ $h_{BS} = 10\text{ m}$

	NLOS	$PL_{UMi-NLOS} = \max(PL_{UMi-LOS}, PL'_{UMi-NLOS})$ <p style="text-align: center;">for $10\text{ m} \leq d_{2D} \leq 5\text{ km}$</p> $PL'_{UMi-NLOS} = 35.3 \log_{10}(d_{3D}) + 22.4 + 21.3 \log_{10}(f_c) - 0.3(h_{UT} - 1.5)$	$\sigma_{SF} = 7.82$	$1.5\text{ m} \leq h_{UT} \leq 22.5\text{ m}$ $h_{BS} = 10\text{ m}$ Explanations: see note 4
		Optional $PL = 32.4 + 20 \log_{10}(f_c) + 31.9 \log_{10}(d_{3D})$	$\sigma_{SF} = 8.2$	
InH - Office	LOS	$PL_{InH-LOS} = 32.4 + 17.3 \log_{10}(d_{3D}) + 20 \log_{10}(f_c)$	$\sigma_{SF} = 3$	$1\text{ m} \leq d_{3D} \leq 150\text{ m}$
	NLOS	$PL_{InH-NLOS} = \max(PL_{InH-LOS}, PL'_{InH-NLOS})$ $PL'_{InH-NLOS} = 38.3 \log_{10}(d_{3D}) + 17.30 + 24.9 \log_{10}(f_c)$	$\sigma_{SF} = 8.03$	$1\text{ m} \leq d_{3D} \leq 150\text{ m}$
		Optional $PL'_{InH-NLOS} = 32.4 + 20 \log_{10}(f_c) + 31.9 \log_{10}(d_{3D})$	$\sigma_{SF} = 8.29$	$1\text{ m} \leq d_{3D} \leq 150\text{ m}$
InF	LOS	$PL_{LOS} = 31.84 + 21.50 \log_{10}(d_{3D}) + 19.00 \log_{10}(f_c)$	$\sigma_{SF} = 4$	$1 \leq d_{3D} \leq 600\text{ m}$
	NLOS	InF-SL: $PL = 33 + 25.5 \log_{10}(d_{3D}) + 20 \log_{10}(f_c)$ $PL_{NLOS} = \max(PL, PL_{LOS})$	$\sigma_{SF} = 5.7$	
		InF-DL: $PL = 18.6 + 35.7 \log_{10}(d_{3D}) + 20 \log_{10}(f_c)$ $PL_{NLOS} = \max(PL, PL_{LOS}, PL_{InF-SL})$	$\sigma_{SF} = 7.2$	
		InF-SH: $PL = 32.4 + 23.0 \log_{10}(d_{3D}) + 20 \log_{10}(f_c)$ $PL_{NLOS} = \max(PL, PL_{LOS})$	$\sigma_{SF} = 5.9$	
		InF-DH: $PL = 33.63 + 21.9 \log_{10}(d_{3D}) + 20 \log_{10}(f_c)$ $PL_{NLOS} = \max(PL, PL_{LOS})$	$\sigma_{SF} = 4.0$	

Note 1: Breakpoint distance $d'_{BP} = 4 h'_{BS} h'_{UT} f_c / c$, where f_c is the centre frequency in Hz, $c = 3.0 \times 10^8$ m/s is the propagation velocity in free space, and h'_{BS} and h'_{UT} are the effective antenna heights at the BS and the UT, respectively. The effective antenna heights h'_{BS} and h'_{UT} are computed as follows: $h'_{BS} = h_{BS} - h_E$, $h'_{UT} = h_{UT} - h_E$, where h_{BS} and h_{UT} are the actual antenna heights, and h_E is the effective environment height. For UMi $h_E = 1.0$ m. For UMa $h_E = 1$ m with a probability equal to $1/(1+C(d_{2D}, h_{UT}))$ and chosen from a discrete uniform distribution $\text{uniform}(12, 15, \dots, (h_{UT}-1.5))$ otherwise. With $C(d_{2D}, h_{UT})$ given by

$$C(d_{2D}, h_{UT}) = \begin{cases} 0 & , h_{UT} < 13 \text{ m} \\ \left(\frac{h_{UT} - 13}{10} \right)^{1.5} g(d_{2D}) & , 13 \text{ m} \leq h_{UT} \leq 23 \text{ m} \end{cases}$$

where

$$g(d_{2D}) = \begin{cases} 0 & , d_{2D} \leq 18 \text{ m} \\ \frac{5}{4} \left(\frac{d_{2D}}{100} \right)^3 \exp\left(\frac{-d_{2D}}{150}\right) & , 18 \text{ m} < d_{2D} \end{cases}$$

Note that h_E depends on d_{2D} and h_{UT} and thus needs to be independently determined for every link between BS sites and UTs. A BS site may be a single BS or multiple co-located BSs.

Note 2: The applicable frequency range of the PL formula in this table is $0.5 < f_c < f_H$ GHz, where $f_H = 30$ GHz for RMa and $f_H = 100$ GHz for all the other scenarios. It is noted that RMa pathloss model for >7 GHz is validated based on a single measurement campaign conducted at 24 GHz.

Note 3: UMa NLOS pathloss is from TR36.873 with simplified format and $PL_{UMa-LOS}$ = Pathloss of UMa LOS outdoor scenario.

Note 4: $PL_{UMi-LOS}$ = Pathloss of UMi-Street Canyon LOS outdoor scenario.

Note 5: Break point distance $d_{BP} = 2\pi h_{BS} h_{UT} f_c / c$, where f_c is the centre frequency in Hz, $c = 3.0 \times 10^8$ m/s is the propagation velocity in free space, and h_{BS} and h_{UT} are the antenna heights at the BS and the UT, respectively.

Note 6: f_c denotes the center frequency normalized by 1GHz, all distance related values are normalized by 1m, unless it is stated otherwise.

7.4.2 LOS probability

The Line-Of-Sight (LOS) probabilities are given in Table 7.4.2-1.

Table 7.4.2-1 LOS probability

Scenario	LOS probability (distance is in meters)
RMa	$\Pr_{\text{LOS}} = \begin{cases} 1 & , d_{2\text{D-out}} \leq 10 \text{ m} \\ \exp\left(-\frac{d_{2\text{D-out}} - 10}{1000}\right) & , 10 \text{ m} < d_{2\text{D-out}} \end{cases}$
UMi - Street canyon	$\Pr_{\text{LOS}} = \begin{cases} 1 & , d_{2\text{D-out}} \leq 18 \text{ m} \\ \frac{18}{d_{2\text{D-out}}} + \exp\left(-\frac{d_{2\text{D-out}}}{36}\right) \left(1 - \frac{18}{d_{2\text{D-out}}}\right) & , 18 \text{ m} < d_{2\text{D-out}} \end{cases}$
UMa	$\Pr_{\text{LOS}} = \begin{cases} 1 & , d_{2\text{D-out}} \leq 18 \text{ m} \\ \left[\frac{18}{d_{2\text{D-out}}} + \exp\left(-\frac{d_{2\text{D-out}}}{63}\right) \left(1 - \frac{18}{d_{2\text{D-out}}}\right) \right] \left[1 + C'(h_{\text{UT}}) \frac{5}{4} \left(\frac{d_{2\text{D-out}}}{100}\right)^3 \exp\left(-\frac{d_{2\text{D-out}}}{150}\right) \right] & , 18 \text{ m} < d_{2\text{D-out}} \end{cases}$ <p>where</p> $C'(h_{\text{UT}}) = \begin{cases} 0 & , h_{\text{UT}} \leq 13 \text{ m} \\ \left(\frac{h_{\text{UT}} - 13}{10}\right)^{1.5} & , 13 \text{ m} < h_{\text{UT}} \leq 23 \text{ m} \end{cases}$
Indoor - Mixed office	$\Pr_{\text{LOS}} = \begin{cases} 1 & , d_{2\text{D-in}} \leq 1.2 \text{ m} \\ \exp\left(-\frac{d_{2\text{D-in}} - 1.2}{4.7}\right) & , 1.2 \text{ m} < d_{2\text{D-in}} < 6.5 \text{ m} \\ \exp\left(-\frac{d_{2\text{D-in}} - 6.5}{32.6}\right) \cdot 0.32 & , 6.5 \text{ m} \leq d_{2\text{D-in}} \end{cases}$
Indoor - Open office	$\Pr_{\text{LOS}} = \begin{cases} 1 & , d_{2\text{D-in}} \leq 5 \text{ m} \\ \exp\left(-\frac{d_{2\text{D-in}} - 5}{70.8}\right) & , 5 \text{ m} < d_{2\text{D-in}} \leq 49 \text{ m} \\ \exp\left(-\frac{d_{2\text{D-in}} - 49}{211.7}\right) \cdot 0.54 & , 49 \text{ m} < d_{2\text{D-in}} \end{cases}$
InF-SL InF-SH InF-DL InF-DH	$Pr_{\text{LOS}, \text{subsc}}(d_{2\text{D}}) = \exp\left(\frac{-d_{2\text{D}}}{k_{\text{subsc}}}\right)$ <p>where</p> $k_{\text{subsc}} = \begin{cases} \frac{-d_{\text{clutter}}}{\ln(1-r)} & \text{for InF-SL and InF-DL} \\ \frac{-d_{\text{clutter}}}{\ln(1-r)} \cdot \frac{h_{\text{BS}} - h_{\text{UT}}}{h_{\text{c}} - h_{\text{UT}}} & \text{for InF-SH and InF-DH} \end{cases}$ <p>The parameters d_{clutter} , r , and h_{c} are defined in Table 7.2-4</p>
InF-HH	$Pr_{\text{LOS}} = 1$
Note:	The LOS probability is derived with assuming antenna heights of 3m for indoor, 10m for UMi, and 25m for UMa

7.4.3 O2I penetration loss

7.4.3.1 O2I building penetration loss

The pathloss incorporating O2I building penetration loss is modelled as in the following:

$$PL = PL_b + PL_{tw} + PL_{in} + N(0, \sigma_P^2) \quad (7.4-2)$$

where PL_b is the basic outdoor path loss given in Subclause 7.4.1, where d_{3D} is replaced by $d_{3D-out} + d_{3D-in}$. PL_{tw} is the building penetration loss through the external wall, PL_{in} is the inside loss dependent on the depth into the building, and σ_P is the standard deviation for the penetration loss.

PL_{tw} is characterized as:

$$PL_{tw} = PL_{npi} - 10 \log_{10} \sum_{i=1}^N \left(p_i \times 10^{\frac{L_{material_i}}{-10}} \right) \quad (7.4-3)$$

PL_{npi} is an additional loss is added to the external wall loss to account for non-perpendicular incidence;

$L_{material_i} = a_{material_i} + b_{material_i} \cdot f$, is the penetration loss of material i , example values of which can be found

in Table 7.4.3-1; p_i is proportion of i -th materials, where $\sum_{i=1}^N p_i = 1$; and N is the number of materials.

Table 7.4.3-1: Material penetration losses

Material	Penetration loss [dB]
Standard multi-pane glass	$L_{glass} = 2 + 0.2f$
IRR glass	$L_{IRRglass} = 23 + 0.3f$
Concrete	$L_{concrete} = 5 + 4f$
Wood	$L_{wood} = 4.85 + 0.12f$
Note: f is in GHz	

Table 7.4.3-2 gives PL_{tw} , PL_{in} and σ_P for two O2I penetration loss models. The O2I penetration is UT-specifically generated, and is added to the SF realization in the log domain.

Table 7.4.3-2: O2I building penetration loss model

	Path loss through external wall: PL_{tw} in [dB]	Indoor loss: PL_{in} in [dB]	Standard deviation: σ_P in [dB]
Low-loss model	$5 - 10 \log_{10} \left(0.3 \cdot 10^{\frac{-L_{glass}}{10}} + 0.7 \cdot 10^{\frac{-L_{concrete}}{10}} \right)$	$0.5 d_{2D-in}$	4.4
High-loss model	$5 - 10 \log_{10} \left(0.7 \cdot 10^{\frac{-L_{IRRglass}}{10}} + 0.3 \cdot 10^{\frac{-L_{concrete}}{10}} \right)$	$0.5 d_{2D-in}$	6.5

d_{2D-in} is minimum of two independently generated uniformly distributed variables between 0 and 25 m for UMa and UMi-Street Canyon, and between 0 and 10 m for RMa. d_{2D-in} shall be UT-specifically generated.

Both low-loss and high-loss models are applicable to UMa and UMi-Street Canyon.

Only the low-loss model is applicable to RMa.

Only the high-loss model is applicable to InF.

The composition of low and high loss is a simulation parameter that should be determined by the user of the channel models, and is dependent on the use of metal-coated glass in buildings and the deployment scenarios. Such use is expected to differ in different markets and regions of the world and also may increase over years to new regulations and energy saving initiatives. Furthermore, the use of such high-loss glass currently appears to be more predominant in commercial buildings than in residential buildings in some regions of the world (see note).

Note: One example survey for the US market can be found in [5]. The survey does not necessarily be representative for all the scenarios. Other ratios outside of the survey should not be precluded.

For backwards compatibility with TR 36.873 [3], the following building penetration model should be used for UMa and UMi single-frequency simulations at frequencies below 6 GHz.

Table 7.4.3-3. O2I building penetration loss model for single-frequency simulations <6 GHz

Parameter	Value
PL_{tw}	20 dB
PL_{in}	$0.5 d_{2D-in}$ with d_{2D-in} being a <i>single, link-specific</i> , uniformly distributed variable between 0 and 25 m
σ_p	0 dB
σ_{SF}	7 dB (note: replacing the respective value in Table 7.4.1-1)

7.4.3.2 O2I car penetration loss

The pathloss incorporating O2I car penetration loss is modelled as in the following:

$$PL = PL_b + N(\mu, \sigma_p^2) \quad (7.4-4)$$

where PL_b is the basic outdoor path loss given in Subclause 7.4.1. $\mu = 9$, and $\sigma_p = 5$. The car penetration loss shall be UT-specifically generated. Optionally, for metallized car windows, $\mu = 20$ can be used. The O2I car penetration loss models are applicable for at least 0.6-60 GHz.

7.4.4 Autocorrelation of shadow fading

The long-term (log-normal) fading in the logarithmic scale around the mean path loss PL (dB) is characterized by a Gaussian distribution with zero mean and standard deviation. Due to the slow fading process versus distance Δx (Δx is in the horizontal plane), adjacent fading values are correlated. Its normalized autocorrelation function $R(\Delta x)$ can be described with sufficient accuracy by the exponential function ITU-R Rec. P.1816 [18]

$$R(\Delta x) = e^{-\frac{|\Delta x|}{d_{cor}}} \quad (7.4-5)$$

with the correlation length d_{cor} being dependent on the environment, see the correlation parameters for shadowing and other large scale parameters in Table 7.5-6 (Channel model parameters). In a spatial consistency procedure in Subclause

7.6.3, the cluster specific random variables are also correlated following the exponential function with respect to correlation distances in the two dimensional horizontal plane.

7.5 Fast fading model

The radio channel realizations are created using the parameters listed in Table 7.5-1. The channel realizations are obtained by a step-wise procedure illustrated in Figure 7.5-1 and described below. It has to be noted that the geometric description covers arrival angles from the last bounce scatterers and respectively departure angles to the first scatterers interacted from the transmitting side. The propagation between the first and the last interaction is not defined. Thus, this approach can model also multiple interactions with the scattering media. This indicates also that e.g., the delay of a multipath component cannot be determined by the geometry. In the following steps, downlink is assumed. For uplink, arrival and departure parameters have to be swapped.

Note: the channel generation in this subclause is enough for at least the following cases.

- Case 1: For low complexity evaluations
- Case 2: To compare with earlier simulation results,
- Case 3: When none of the additional modelling components are turned on.

For other advanced simulations, e.g., spatially consistency, large bandwidth and arrays, oxygen absorption, blockage, absolute time of arrival, dual mobility, embedded devices, etc., some of the additional modelling components of Subclause 7.6 should be considered.

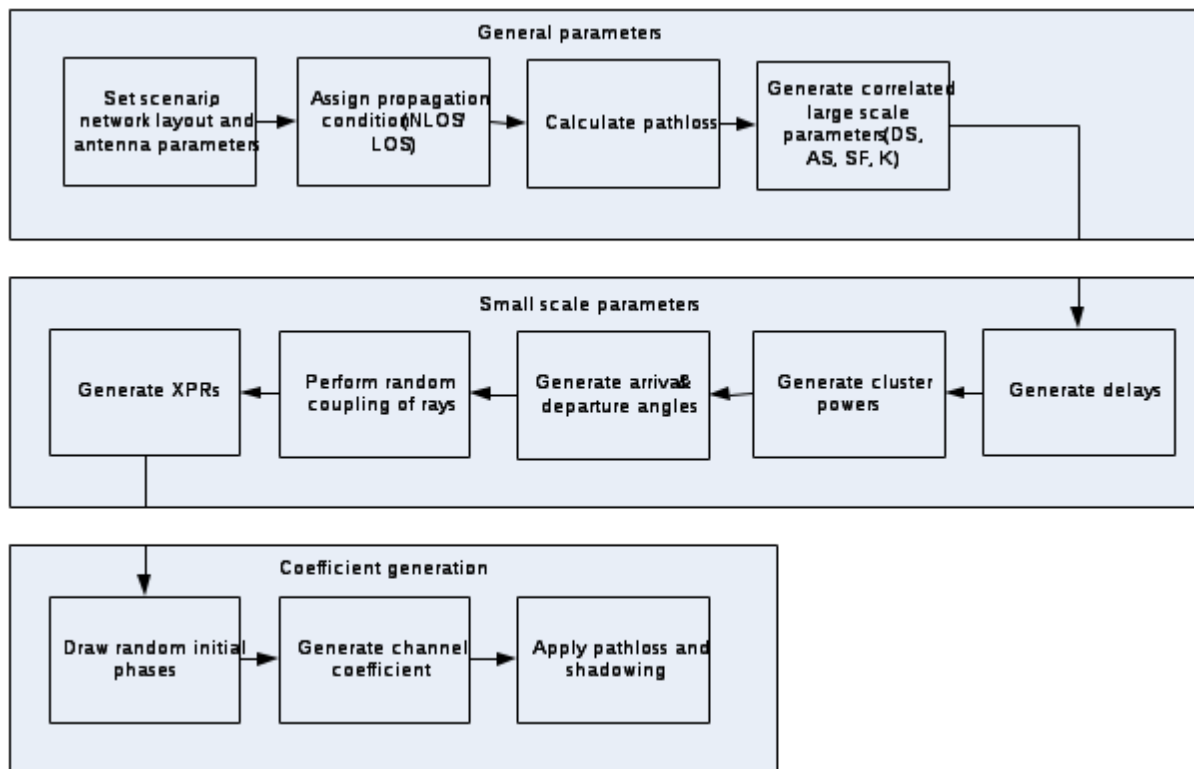


Figure 7.5-1 Channel coefficient generation procedure

Figure 7.5-2: Definition of a global coordinate system showing the zenith angle θ and the azimuth angle ϕ . $\theta=0^\circ$ points to zenith and $\theta=+90^\circ$ points to the horizon.

The spherical basis vectors $\hat{\theta}$ and $\hat{\phi}$ shown above are defined based on the direction of propagation \hat{n} .

Table 7.5-1: Notations in the global coordinate system (GCS)

Parameter	Notation
LOS AOD	$\phi_{\text{LOS,AOD}}$
LOS AOA	$\phi_{\text{LOS,AOA}}$
LOS ZOD	$\theta_{\text{LOS,ZOD}}$
LOS ZOA	$\theta_{\text{LOS,ZOA}}$
AOA for cluster n	$\phi_{n,\text{AOA}}$
AOD for cluster n	$\phi_{n,\text{AOD}}$
AOA for ray m in cluster n	$\phi_{n,m,\text{AOA}}$
AOD for ray m in cluster n	$\phi_{n,m,\text{AOD}}$
ZOA for cluster n	$\theta_{n,\text{ZOA}}$
ZOD for cluster n	$\theta_{n,\text{ZOD}}$
ZOA for ray m in cluster n	$\theta_{n,m,\text{ZOA}}$
ZOD for ray m in cluster n	$\theta_{n,m,\text{ZOD}}$
Receive antenna element u field pattern in the direction of the spherical basis vector $\hat{\theta}$	$F_{\text{rx},u,\theta}$
Receive antenna element u field pattern in the direction of the spherical basis vector $\hat{\phi}$	$F_{\text{rx},u,\phi}$
Transmit antenna element s field pattern in the direction of the spherical basis vector $\hat{\theta}$	$F_{\text{tx},s,\theta}$
Transmit antenna element s field pattern in the direction of the spherical basis vector $\hat{\phi}$	$F_{\text{tx},s,\phi}$

Step 1: Set environment, network layout, and antenna array parameters

- Choose one of the scenarios (e.g. UMa, UMi-Street Canyon, RMa, InH-Office or InF). Choose a global coordinate system and define zenith angle θ , azimuth angle ϕ , and spherical basis vectors $\hat{\theta}$, $\hat{\phi}$ as shown in Figure 7.3-2. Note: Scenario RMa is for up to 7GHz while others are for up to 100GHz
- Give number of BS and UT

- c) Give 3D locations of BS and UT, and determine LOS AOD ($\phi_{LOS,AOD}$), LOS ZOD ($\theta_{LOS,ZOD}$), LOS AOA ($\phi_{LOS,AOA}$), and LOS ZOA ($\theta_{LOS,ZOA}$) of each BS and UT in the global coordinate system
- d) Give BS and UT antenna field patterns F_{rx} and F_{tx} in the global coordinate system and array geometries
- e) Give BS and UT array orientations with respect to the global coordinate system. BS array orientation is defined by three angles $\Omega_{BS,\alpha}$ (BS bearing angle), $\Omega_{BS,\beta}$ (BS downtilt angle) and $\Omega_{BS,\gamma}$ (BS slant angle). UT array orientation is defined by three angles $\Omega_{UT,\alpha}$ (UT bearing angle), $\Omega_{UT,\beta}$ (UT downtilt angle) and $\Omega_{UT,\gamma}$ (UT slant angle).
- f) Give speed and direction of motion of UT in the global coordinate system
- g) Specify system centre frequency f_c and bandwidth B

Note: In case wrapping is used, each wrapping copy of a BS or site should be treated as a separate BS/site considering channel generation.

Large scale parameters:

Step 2: Assign propagation condition (LOS/NLOS) according to Table 7.4.2-1. The propagation conditions for different BS-UT links are uncorrelated.

Also, assign an indoor/outdoor state for each UT. It is noted that all the links from a UT have the same indoor/outdoor state.

Step 3: Calculate pathloss with formulas in Table 7.4.1-1 for each BS-UT link to be modelled.

Step 4: Generate large scale parameters, e.g. delay spread (DS), angular spreads (ASA, ASD, ZSA, ZSD), Ricean K factor (K) and shadow fading (SF) taking into account cross correlation according to Table 7.5-6 and using the procedure described in subclause 3.3.1 of [14] with the square root matrix $\sqrt{C_{MM}(0)}$ being generated using the Cholesky decomposition and the following order of the large scale parameter vector: $\mathbf{s}_M = [s_{SF}, s_K, s_{DS}, s_{ASD}, s_{ASA}, s_{ZSD}, s_{ZSA}]^T$.

These LSPs for different BS-UT links are uncorrelated, but the LSPs for links from co-sited sectors to a UT are the same. In addition, these LSPs for the links of UTs on different floors are uncorrelated.

Limit random RMS azimuth arrival and azimuth departure spread values to 104 degrees, i.e., $ASA = \min(ASA, 104^\circ)$, $ASD = \min(ASD, 104^\circ)$. Limit random RMS zenith arrival and zenith departure spread values to 52 degrees, i.e., $ZSA = \min(ZSA, 52^\circ)$, $ZSD = \min(ZSD, 52^\circ)$.

Small scale parameters:

Step 5: Generate cluster delays τ_n .

Delays are drawn randomly from the delay distribution defined in Table 7.5-6. With exponential delay distribution calculate

$$\tau'_n = -r_\tau DS \ln(X_n), \quad (7.5-1)$$

Where r_τ is the delay distribution proportionality factor, $X_n \sim \text{uniform}(0,1)$, and cluster index $n = 1, \dots, N$. With uniform delay distribution the delay values τ'_n are drawn from the corresponding range. Normalise the delays by subtracting the minimum delay and sort the normalised delays to ascending order:

$$\tau_n = \text{sort}(\tau'_n - \min(\tau'_n)) \quad (7.5-2)$$

In the case of LOS condition, additional scaling of delays is required to compensate for the effect of LOS peak addition to the delay spread. The heuristically determined Ricean K-factor dependent scaling constant is

$$C_\tau = 0.7705 - 0.0433K + 0.0002K^2 + 0.000017K^3, \quad (7.5-3)$$

where K [dB] is the Ricean K-factor as generated in Step 4. The scaled delays

$$\tau_n^{LOS} = \tau_n / C_\tau, \quad (7.5-4)$$

are **not** to be used in cluster power generation.

Step 6: Generate cluster powers P_n .

Cluster powers are calculated assuming a single slope exponential power delay profile. Power assignment depends on the delay distribution defined in Table 7.5-6. With exponential delay distribution the cluster powers are determined by

$$P_n' = \exp\left[-\tau_n \frac{r_\tau - 1}{r_\tau DS}\right] \cdot 10^{\frac{-Z_n}{10}} \quad (7.5-5)$$

where $Z_n \sim N(0, \zeta^2)$ is the per cluster shadowing term in [dB]. Normalize the cluster powers so that the sum of all cluster powers is equal to one, i.e.,

$$P_n = \frac{P_n'}{\sum_{n=1}^N P_n'} \quad (7.5-6)$$

In the case of LOS condition an additional specular component is added to the first cluster. Power of the single LOS ray is:

$$P_{1,LOS} = \frac{K_R}{K_R + 1} \quad (7.5-7)$$

and the cluster powers are not normalized as in equation (7.5-6), but:

$$P_n = \frac{1}{K_R + 1} \frac{P_n'}{\sum_{n=1}^N P_n'} + \delta(n-1) P_{1,LOS} \quad (7.5-8)$$

where $\delta(\cdot)$ is Dirac's delta function and K_R is the Ricean K -factor as generated in Step 4 converted to linear scale. These power values are used *only* in equations (7.5-9) and (7.5-14), but *not* in equation (7.5-22).

Assign the power of each ray within a cluster as P_n / M , where M is the number of rays per cluster.

Remove clusters with less than -25 dB power compared to the maximum cluster power. The scaling factors need not be changed after cluster elimination.

Step 7: Generate arrival angles and departure angles for both azimuth and elevation.

The composite PAS in azimuth of all clusters is modelled as wrapped Gaussian. The AOAs are determined by applying the inverse Gaussian function (7.5-9) with input parameters P_n and RMS angle spread ASA

$$\phi'_{n, AOA} = \frac{2(ASA/1.4)\sqrt{-\ln(P_n/\max(P_n))}}{C_\varphi}, \quad (7.5-9)$$

with C_φ defined as

$$C_\varphi = \begin{cases} C_\varphi^{NLOS} \cdot (1.1035 - 0.028K - 0.002K^2 + 0.0001K^3) & , \text{for LOS} \\ C_\varphi^{NLOS} & , \text{for NLOS} \end{cases}, \quad (7.5-10)$$

where C_φ^{NLOS} is defined as a scaling factor related to the total number of clusters and is given in Table 7.5-2:

Table 7.5-2: Scaling factors for AOA, AOD generation

# clusters	4	5	8	10	11	12	14	15	16	19	20	25
C_φ^{NLOS}	0.77 9	0.86 0	1.01 8	1.09 0	1.12 3	1.14 6	1.19 0	1.21 1	1.22 6	1.27 3	1.28 9	1.35 8

In the LOS case, constant C_φ also depends on the Ricean K-factor K in [dB], as generated in Step 4. Additional scaling of the angles is required to compensate for the effect of LOS peak addition to the angle spread.

Assign positive or negative sign to the angles by multiplying with a random variable X_n with uniform distribution to the discrete set of $\{1, -1\}$, and add component $Y_n \sim N(0, (ASA/7)^2)$ to introduce random variation

$$\phi_{n, AOA} = X_n \phi'_{n, AOA} + Y_n + \phi_{LOS, AOA}, \quad (7.5-11)$$

where $\phi_{LOS, AOA}$ is the LOS direction defined in the network layout description, see Step1c.

In the LOS case, substitute (7.5-11) by (7.5-12) to enforce the first cluster to the LOS direction $\phi_{LOS, AOA}$

$$\phi_{n, AOA} = (X_n \phi'_{n, AOA} + Y_n) - (X_1 \phi'_{1, AOA} + Y_1 - \phi_{LOS, AOA}) \quad (7.5-12)$$

Finally add offset angles α_m from Table 7.5-3 to the cluster angles

$$\phi_{n, m, AOA} = \phi_{n, AOA} + c_{ASA} \alpha_m, \quad (7.5-13)$$

where c_{ASA} is the cluster-wise rms azimuth spread of arrival angles (cluster ASA) in Table 7.5-6.

Table 7.5-3: Ray offset angles within a cluster, given for rms angle spread normalized to 1

Ray number m	Basis vector of offset angles α_m
1,2	± 0.0447
3,4	± 0.1413
5,6	± 0.2492
7,8	± 0.3715
9,10	± 0.5129
11,12	± 0.6797
13,14	± 0.8844
15,16	± 1.1481
17,18	± 1.5195
19,20	± 2.1551

The generation of AOD ($\varphi_{n,m,AOD}$) follows a procedure similar to AOA as described above.

The generation of ZOA assumes that the composite PAS in the zenith dimension of all clusters is Laplacian (see Table 7.5-6). The ZOAs are determined by applying the inverse Laplacian function (7.5-14) with input parameters P_n and RMS angle spread ZSA

$$\theta'_{n,ZOA} = -\frac{ZSA \ln(P_n / \max(P_n))}{C_\theta}, \quad (7.5-14)$$

with C_θ defined as

$$C_\theta = \begin{cases} C_\theta^{NLOS} \cdot (1.3086 + 0.0339 K - 0.0077 K^2 + 0.0002 K^3) & , \text{ for LOS} \\ C_\theta^{NLOS} & , \text{ for NLOS} \end{cases}, \quad (7.5-15)$$

Where C_θ^{NLOS} is a scaling factor related to the total number of clusters and is given in Table 7.5-4:

Table 7.5-4: Scaling factors for ZOA, ZOD generation

# clusters	8	10	11	12	15	19	20	25
C_θ^{NLOS}	0.88 9	0.95 7	1.03 1	1.10 4	1.108 8	1.18 4	1.17 8	1.28 2

In the LOS case, constant C_θ also depends on the Ricean K-factor K in [dB], as generated in Step 4. Additional scaling of the angles is required to compensate for the effect of LOS peak addition to the angle spread.

Assign positive or negative sign to the angles by multiplying with a random variable X_n with uniform distribution to the discrete set of $\{1, -1\}$, and add component $Y_n \sim N(0, (ZSA/7)^2)$ to introduce random variation

$$\theta_{n,ZOA} = X_n \theta'_{n,ZOA} + Y_n + \bar{\theta}_{ZOA}, \quad (7.5-16)$$

where $\bar{\theta}_{ZOA} = 90^\circ$ if the BS-UT link is O2I and $\bar{\theta}_{ZOA} = \theta_{LOS,ZOA}$ otherwise. The LOS direction is defined in the network layout description, see Step1c.

In the LOS case, substitute (7.5-16) by (7.5-17) to enforce the first cluster to the LOS direction $\theta_{LOS,ZOA}$

$$\theta_{n,ZOA} = (X_n \theta'_{n,ZOA} + Y_n) - (X_1 \theta'_{1,ZOA} + Y_1 - \theta_{LOS,ZOA}). \quad (7.5-17)$$

Finally add offset angles α_m from Table 7.5-3 to the cluster angles

$$\theta_{n,m,ZOA} = \theta_{n,ZOA} + c_{ZSA} \alpha_m, \quad (7.5-18)$$

where c_{ZSA} is the cluster-wise rms spread of ZOA (cluster ZSA) in Table 7.5-6. Assuming that $\theta_{n,m,ZOA}$ is wrapped within $[0, 360^\circ]$, if $\theta_{n,m,ZOA} \in [180^\circ, 360^\circ]$, then $\theta_{n,m,ZOA}$ is set to $(360^\circ - \theta_{n,m,ZOA})$.

The generation of ZOD follows the same procedure as ZOA described above except equation (7.5-16) is replaced by

$$\theta_{n,ZOD} = X_n \theta'_{n,ZOD} + Y_n + \theta_{LOS,ZOD} + \mu_{offset,ZOD}, \quad (7.5-19)$$

where variable X_n is with uniform distribution to the discrete set of $\{1,-1\}$, $Y_n \sim N(0, (ZSD/7)^2)$, $\mu_{\text{offset}, ZOD}$ is given in Tables 7.5-6/7/8 and equation (7.5-18) is replaced by

$$\theta_{n,m,ZOD} = \theta_{n,ZOD} + (3/8)(10^{\mu_{\text{lgZSD}}})\alpha_m \quad (7.5-20)$$

where μ_{lgZSD} is the mean of the ZSD log-normal distribution.

In the LOS case, the generation of ZOD follows the same procedure as ZOA described above using equation (7.5-17).

Step 8: Coupling of rays within a cluster for both azimuth and elevation

Couple randomly AOD angles $\phi_{n,m,AOD}$ to AOA angles $\phi_{n,m,AOA}$ within a cluster n , or within a sub-cluster in the case of two strongest clusters (see Step 11 and Table 7.5-3). Couple randomly ZOD angles $\theta_{n,m,ZOD}$ with ZOA angles $\theta_{n,m,ZOA}$ using the same procedure. Couple randomly AOD angles $\phi_{n,m,AOD}$ with ZOD angles $\theta_{n,m,ZOD}$ within a cluster n or within a sub-cluster in the case of two strongest clusters.

Step 9: Generate the cross polarization power ratios

Generate the cross polarization power ratios (XPR) κ for each ray m of each cluster n . XPR is log-Normal distributed. Draw XPR values as

$$\kappa_{n,m} = 10^{X_{n,m}/10}, \quad (7.5-21)$$

where $X_{n,m} \sim N(\mu_{\text{XPR}}, \sigma_{\text{XPR}}^2)$ is Gaussian distributed with σ_{XPR} and μ_{XPR} from Table 7.5-6.

Note: $X_{n,m}$ is independently drawn for each ray and each cluster.

The outcome of Steps 1-9 shall be identical for all the links from co-sited sectors to a UT.

Coefficient generation:

Step 10: Draw initial random phases

Draw random initial phase $\left[\Phi_{n,m}^{\theta\theta}, \Phi_{n,m}^{\theta\phi}, \Phi_{n,m}^{\phi\theta}, \Phi_{n,m}^{\phi\phi} \right]$ for each ray m of each cluster n and for four different polarisation combinations $(\theta\theta, \theta\phi, \phi\theta, \phi\phi)$. The distribution for initial phases is uniform within $(-\pi, \pi)$.

Step 11: Generate channel coefficients for each cluster n and each receiver and transmitter element pair u, s .

The method described below is used at least for *drop-based evaluations* irrespective of UT speeds. Relevant cases for drop-based evaluations are:

- Case 1: For low complexity evaluations
- Case 2: To compare with earlier simulation results,
- Case 3: When none of the additional modelling components are turned on.
- Case 4: When spatial consistency and/or blockage is modeled for MU-MIMO simulations

- Other cases are not precluded

For the $N - 2$ weakest clusters, say $n = 3, 4, \dots, N$, the channel coefficients are given by:

$$H_{u,s,n}^{\text{NLOS}}(t) = \sqrt{\frac{P_n}{M}} \sum_{m=1}^M \begin{bmatrix} F_{rx,u,\theta}(\theta_{n,m,ZOA}, \phi_{n,m,AOA}) \\ F_{rx,u,\phi}(\theta_{n,m,ZOA}, \phi_{n,m,AOA}) \end{bmatrix}^T \begin{bmatrix} \exp(j\Phi_{n,m}^{\theta\theta}) & \sqrt{\kappa_{n,m}^{-1}} \exp(j\Phi_{n,m}^{\theta\phi}) \\ \sqrt{\kappa_{n,m}^{-1}} \exp(j\Phi_{n,m}^{\phi\theta}) & \exp(j\Phi_{n,m}^{\phi\phi}) \end{bmatrix} \begin{bmatrix} F_{tx,s,\theta}(\theta_{n,m,ZOD}, \phi_{n,m,AOD}) \\ F_{tx,s,\phi}(\theta_{n,m,ZOD}, \phi_{n,m,AOD}) \end{bmatrix} \exp\left[\frac{j2\pi(\hat{r}_{rx,n,m}^T \cdot \bar{d}_{rx,u})}{\lambda_0}\right] \exp\left[\frac{j2\pi(\hat{r}_{tx,n,m}^T \cdot \bar{d}_{tx,s})}{\lambda_0}\right] \exp\left[j2\pi \frac{\hat{r}_{rx,n,m}^T \cdot \bar{v}}{\lambda_0} t\right] \quad (7.5-22)$$

where $F_{rx,u,\theta}$ and $F_{rx,u,\phi}$ are the field patterns of receive antenna element u according to (7.1-11) and in the direction of the spherical basis vectors, $\hat{\theta}$ and $\hat{\phi}$ respectively, $F_{tx,s,\theta}$ and $F_{tx,s,\phi}$ are the field patterns of transmit antenna element s in the direction of the spherical basis vectors, $\hat{\theta}$ and $\hat{\phi}$ respectively. Note that the patterns are given in the GCS and therefore include transformations with respect to antenna orientation as described in Subclause 7.1. $\hat{r}_{rx,n,m}$ is the spherical unit vector with azimuth arrival angle $\phi_{n,m,AOA}$ and elevation arrival angle $\theta_{n,m,ZOA}$, given by

$$\hat{r}_{rx,n,m} = \begin{bmatrix} \sin \theta_{n,m,ZOA} \cos \phi_{n,m,AOA} \\ \sin \theta_{n,m,ZOA} \sin \phi_{n,m,AOA} \\ \cos \theta_{n,m,ZOA} \end{bmatrix}, \quad (7.5-23)$$

where n denotes a cluster and m denotes a ray within cluster n . $\hat{r}_{tx,n,m}$ is the spherical unit vector with azimuth departure angle $\phi_{n,m,AOD}$ and elevation departure angle $\theta_{n,m,ZOD}$, given by

$$\hat{r}_{tx,n,m} = \begin{bmatrix} \sin \theta_{n,m,ZOD} \cos \phi_{n,m,AOD} \\ \sin \theta_{n,m,ZOD} \sin \phi_{n,m,AOD} \\ \cos \theta_{n,m,ZOD} \end{bmatrix}, \quad (7.5-24)$$

where n denotes a cluster and m denotes a ray within cluster n . Also, $\bar{d}_{rx,u}$ is the location vector of receive antenna element u and $\bar{d}_{tx,s}$ is the location vector of transmit antenna element s , $\kappa_{n,m}$ is the cross polarisation power ratio in linear scale, and λ_0 is the wavelength of the carrier frequency. If polarisation is not considered, the 2x2 polarisation matrix can be replaced by the scalar $\exp(j\Phi_{n,m})$ and only vertically polarised field patterns are applied.

The Doppler frequency component depends on the arrival angles (AOA, ZOA), and the UT velocity vector \bar{v} with speed v , travel azimuth angle ϕ_v , elevation angle θ_v and is given by

$$v_{n,m} = \frac{\hat{r}_{rx,n,m}^T \cdot \bar{v}}{\lambda_0}, \text{ where } \bar{v} = v \cdot \begin{bmatrix} \sin \theta_v \cos \phi_v & \sin \theta_v \sin \phi_v & \cos \theta_v \end{bmatrix}^T. \quad (7.5-25)$$

For the two strongest clusters, say $n = 1$ and 2, rays are spread in delay to three sub-clusters (per cluster), with fixed delay offset. The delays of the sub-clusters are

$$\begin{aligned} \tau_{n,1} &= \tau_n \\ \tau_{n,2} &= \tau_n + 1.28 \, c_{DS} \\ \tau_{n,3} &= \tau_n + 2.56 \, c_{DS} \end{aligned} \quad (7.5-26)$$

where C_{DS} is cluster delay spread specified in Table 7.5-6. When intra-cluster delay spread is unspecified (i.e., N/A) the value 3.91 ns is used; it is noted that this value results in the legacy behaviour with 5 and 10 ns sub-cluster delays.

Twenty rays of a cluster are mapped to sub-clusters as presented in Table 7.5-5 below. The corresponding offset angles are taken from Table 7.5-3 with mapping of Table 7.5-5.

Table 7.5-5: Sub-cluster information for intra cluster delay spread clusters

sub-cluster # i	mapping to rays R_i	Power $ R_i /M$	delay offset $\tau_{n,i} - \tau_n$
$i=1$	$R_1 = [1,2,3,4,5,6,7,8,19,20]$	10/20	0
$i=2$	$R_2 = [9,10,11,12,17,18]$	6/20	$1.28 C_{DS}$
$i=3$	$R_3 = [13,14,15,16]$	4/20	$2.56 C_{DS}$

Then, the channel impulse response is given by:

$$H_{u,s}^{\text{NLOS}}(\tau, t) = \sum_{n=1}^2 \sum_{i=1}^3 \sum_{m \in R_i} H_{u,s,n,m}^{\text{NLOS}}(t) \delta(\tau - \tau_{n,i}) + \sum_{n=3}^N H_{u,s,n}^{\text{NLOS}}(t) \delta(\tau - \tau_n) \quad (7.5-27)$$

where $H_{u,s,n}^{\text{NLOS}}(t)$ is given in (7.5-22) and $H_{u,s,n,m}^{\text{NLOS}}(t)$ defined as:

$$H_{u,s,n,m}^{\text{NLOS}}(t) = \sqrt{\frac{P_n}{M}} \begin{bmatrix} F_{rx,u,\theta}(\theta_{n,m,ZOA}, \varphi_{n,m,AOA}) \\ F_{rx,u,\varphi}(\theta_{n,m,ZOA}, \varphi_{n,m,AOA}) \end{bmatrix}^T \begin{bmatrix} \exp(j\Phi_{n,m}^{\theta\theta}) & \sqrt{\kappa_{n,m}-1} \exp(j\Phi_{n,m}^{\theta\varphi}) \\ \sqrt{\kappa_{n,m}-1} \exp(j\Phi_{n,m}^{\varphi\theta}) & \exp(j\Phi_{n,m}^{\varphi\varphi}) \end{bmatrix} \begin{bmatrix} F_{tx,s,\theta}(\theta_{n,m,ZOD}, \varphi_{n,m,AOD}) \\ F_{tx,s,\varphi}(\theta_{n,m,ZOD}, \varphi_{n,m,AOD}) \end{bmatrix} \exp\left(j2\pi \frac{\hat{r}_{rx,n,m}^T \cdot \bar{d}_{rx,u}}{\lambda_0}\right) \exp\left(j2\pi \frac{\hat{r}_{tx,n,m}^T \cdot \bar{d}_{tx,s}}{\lambda_0}\right) \exp\left(j2\pi \frac{\hat{r}_{rx,n,m}^T \cdot \bar{v}}{\lambda_0} t\right) \quad (7.5-28)$$

In the LOS case, determine the LOS channel coefficient by:

$$H_{u,s,1}^{\text{LOS}}(t) = \begin{bmatrix} F_{rx,u,\theta}(\theta_{LOS,ZOA}, \varphi_{LOS,AOA}) \\ F_{rx,u,\varphi}(\theta_{LOS,ZOA}, \varphi_{LOS,AOA}) \end{bmatrix}^T \begin{bmatrix} 1 & 0 \\ 0 & -1 \end{bmatrix} \begin{bmatrix} F_{tx,s,\theta}(\theta_{LOS,ZOD}, \varphi_{LOS,AOD}) \\ F_{tx,s,\varphi}(\theta_{LOS,ZOD}, \varphi_{LOS,AOD}) \end{bmatrix} \exp\left(-j2\pi \frac{d_{3D}}{\lambda_0}\right) \exp\left(j2\pi \frac{\hat{r}_{rx,LOS}^T \cdot \bar{d}_{rx,u}}{\lambda_0}\right) \exp\left(j2\pi \frac{\hat{r}_{tx,LOS}^T \cdot \bar{d}_{tx,s}}{\lambda_0}\right) \exp\left(j2\pi \frac{\hat{r}_{rx,LOS}^T \cdot \bar{v}}{\lambda_0} t\right) \quad (7.5-29)$$

where $\delta(\cdot)$ is the Dirac's delta function and K_R is the Ricean K-factor as generated in Step 4 converted to linear scale.

Then, the channel impulse response is given by adding the LOS channel coefficient to the NLOS channel impulse response and scaling both terms according to the desired K-factor K_R as

$$H_{u,s}^{\text{LOS}}(\tau, t) = \sqrt{\frac{1}{K_R + 1}} H_{u,s}^{\text{NLOS}}(\tau, t) + \sqrt{\frac{K_R}{K_R + 1}} H_{u,s,1}^{\text{LOS}}(t) \delta(\tau - \tau_1) \quad (7.5-30)$$

Step 12: Apply pathloss and shadowing for the channel coefficients.

Table 7.5-6 Part-1: Channel model parameters for UMi-Street Canyon and UMa

Scenarios		UMi - Street Canyon			UMa		
		LOS	NLOS	O2I	LOS	NLOS	O2I
Delay spread (DS) lgDS=log ₁₀ (DS/1s)	μ_{lgDS}	$-0.24 \log_{10}(1+f_c) - 7.14$	$-0.24 \log_{10}(1+f_c) - 6.83$	-6.62	$-6.955 - 0.0963 \log_{10}(f_c)$	$-6.28 - 0.204 \log_{10}(f_c)$	-6.62
	σ_{lgDS}	0.38	$0.16 \log_{10}(1+f_c) + 0.28$	0.32	0.66	0.39	0.32
AOD spread (ASD) lgASD=log ₁₀ (ASD/1°)	μ_{lgASD}	$-0.05 \log_{10}(1+f_c) + 1.21$	$-0.23 \log_{10}(1+f_c) + 1.53$	1.25	$1.06 + 0.1114 \log_{10}(f_c)$	$1.5 - 0.1144 \log_{10}(f_c)$	1.25
	σ_{lgASD}	0.41	$0.11 \log_{10}(1+f_c) + 0.33$	0.42	0.28	0.28	0.42
AOA spread (ASA) lgASA=log ₁₀ (ASA/1°)	μ_{lgASA}	$-0.08 \log_{10}(1+f_c) + 1.73$	$-0.08 \log_{10}(1+f_c) + 1.81$	1.76	1.81	$2.08 - 0.27 \log_{10}(f_c)$	1.76
	σ_{lgASA}	$0.014 \log_{10}(1+f_c) + 0.28$	$0.05 \log_{10}(1+f_c) + 0.3$	0.16	0.20	0.11	0.16
ZOA spread (ZSA) lgZSA=log ₁₀ (ZSA/1°)	μ_{lgZSA}	$-0.1 \log_{10}(1+f_c) + 0.73$	$-0.04 \log_{10}(1+f_c) + 0.92$	1.01	0.95	$-0.3236 \log_{10}(f_c) + 1.512$	1.01
	σ_{lgZSA}	$-0.04 \log_{10}(1+f_c) + 0.34$	$-0.07 \log_{10}(1+f_c) + 0.41$	0.43	0.16	0.16	0.43
Shadow fading (SF) [dB]	σ_{SF}	See Table 7.4.1-1	See Table 7.4.1-1	7	See Table 7.4.1-1	See Table 7.4.1-1	7
K-factor (K) [dB]	μ_K	9	N/A	N/A	9	N/A	N/A
	σ_K	5	N/A	N/A	3.5	N/A	N/A
Cross-Correlations	ASD vs DS	0.5	0	0.4	0.4	0.4	0.4
	ASA vs DS	0.8	0.4	0.4	0.8	0.6	0.4
	ASA vs SF	-0.4	-0.4	0	-0.5	0	0
	ASD vs SF	-0.5	0	0.2	-0.5	-0.6	0.2
	DS vs SF	-0.4	-0.7	-0.5	-0.4	-0.4	-0.5
	ASD vs ASA	0.4	0	0	0	0.4	0
	ASD vs K	-0.2	N/A	N/A	0	N/A	N/A
	ASA vs K	-0.3	N/A	N/A	-0.2	N/A	N/A
	DS vs K	-0.7	N/A	N/A	-0.4	N/A	N/A
Cross-Correlations ¹⁾	SF vs K	0.5	N/A	N/A	0	N/A	N/A
	ZSD vs SF	0	0	0	0	0	0
	ZSA vs SF	0	0	0	-0.8	-0.4	0
	ZSD vs K	0	N/A	N/A	0	N/A	N/A
	ZSA vs K	0	N/A	N/A	0	N/A	N/A
	ZSD vs DS	0	-0.5	-0.6	-0.2	-0.5	-0.6
	ZSA vs DS	0.2	0	-0.2	0	0	-0.2
	ZSD vs ASD	0.5	0.5	-0.2	0.5	0.5	-0.2
	ZSA vs ASD	0.3	0.5	0	0	-0.1	0
	ZSD vs ASA	0	0	0	-0.3	0	0
	ZSA vs ASA	0	0.2	0.5	0.4	0	0.5
	ZSD vs ZSA	0	0	0.5	0	0	0.5
Delay scaling parameter r_τ		3	2.1	2.2	2.5	2.3	2.2
XPR [dB]	μ_{XPR}	9	8.0	9	8	7	9
	σ_{XPR}	3	3	5	4	3	5
Number of clusters N		12	19	12	12	20	12

Number of rays per cluster M	20	20	20	20	20	20
Cluster DS (C_{DS}) in [ns]	5	11	11	$\max(0.25, 6.5622 - 3.4084 \log_{10}(f_c))$	$\max(0.25, 6.5622 - 3.4084 \log_{10}(f_c))$	11
Cluster ASD (C_{ASD}) in [deg]	3	10	5	5	2	5
Cluster ASA (C_{ASA}) in [deg]	17	22	8	11	15	8
Cluster ZSA (C_{ZSA}) in [deg]	7	7	3	7	7	3
Per cluster shadowing std ζ [dB]	3	3	4	3	3	4
Correlation distance in the horizontal plane [m]	DS	7	10	10	30	10
	ASD	8	10	11	18	11
	ASA	8	9	17	15	17
	SF	10	13	7	37	7
	K	15	N/A	N/A	12	N/A
	ZSA	12	10	25	15	25
	ZSD	12	10	25	15	25

f_c is carrier frequency in GHz; d_{2D} is BS-UT distance in km.

NOTE 1: DS = rms delay spread, ASD = rms azimuth spread of departure angles, ASA = rms azimuth spread of arrival angles, ZSD = rms zenith spread of departure angles, ZSA = rms zenith spread of arrival angles, SF = shadow fading, and K = Ricean K-factor.

NOTE 2: The sign of the shadow fading is defined so that positive SF means more received power at UT than predicted by the path loss model.

NOTE 3: All large scale parameters are assumed to have no correlation between different floors.

NOTE 4: The following notation for mean ($\mu_{\log X} = \text{mean}\{\log_{10}(X)\}$) and standard deviation ($\sigma_{\log X} = \text{std}\{\log_{10}(X)\}$) is used for logarithmized parameters X .

NOTE 5: For all considered scenarios the AOD/AOA distributions are modelled by a wrapped Gaussian distribution, the ZOD/ZOA distributions are modelled by a Laplacian distribution and the delay distribution is modelled by an exponential distribution.

NOTE 6: For UMa and frequencies below 6 GHz, use $f_c = 6$ when determining the values of the frequency-dependent LSP values

NOTE 7: For UMi and frequencies below 2 GHz, use $f_c = 2$ when determining the values of the frequency-dependent LSP values

Table 7.5-6 Part-2: Channel model parameters for RMa (up to 7GHz) and Indoor-Office

Scenarios		RMa			Indoor-Office	
		LOS	NLOS	O2I	LOS	NLOS
Delay spread (DS) lgDS=log ₁₀ (DS/1s)	μ_{lgDS}	-7.49	-7.43	-7.47	$-0.01 \log_{10}(1+f_c) - 7.692$	$-0.28 \log_{10}(1+f_c) - 7.173$
	σ_{lgDS}	0.55	0.48	0.24	0.18	$0.10 \log_{10}(1+f_c) + 0.055$
AOD spread (ASD) lgASD=log ₁₀ (ASD/1°)	μ_{lgASD}	0.90	0.95	0.67	1.60	1.62
	σ_{lgASD}	0.38	0.45	0.18	0.18	0.25
AOA spread (ASA) lgASA=log ₁₀ (ASA/1°)	μ_{lgASA}	1.52	1.52	1.66	$-0.19 \log_{10}(1+f_c) + 1.781$	$-0.11 \log_{10}(1+f_c) + 1.863$
	σ_{lgASA}	0.24	0.13	0.21	$0.12 \log_{10}(1+f_c) + 0.119$	$0.12 \log_{10}(1+f_c) + 0.059$
ZOA spread (ZSA) lgZSA=log ₁₀ (ZSA/1°)	μ_{lgZSA}	0.47	0.58	0.93	$-0.26 \log_{10}(1+f_c) + 1.44$	$-0.15 \log_{10}(1+f_c) + 1.387$
	σ_{lgZSA}	0.40	0.37	0.22	$-0.04 \log_{10}(1+f_c) + 0.264$	$-0.09 \log_{10}(1+f_c) + 0.746$
Shadow fading (SF) [dB]	σ_{SF}	See Table 7.4.1-1			See Table 7.4.1-1	
K-factor (K) [dB]	μ_K	7	N/A	N/A	7	N/A
	σ_K	4	N/A	N/A	4	N/A
Cross-Correlations	ASD vs DS	0	-0.4	0	0.6	0.4
	ASA vs DS	0	0	0	0.8	0
	ASA vs SF	0	0	0	-0.5	-0.4
	ASD vs SF	0	0.6	0	-0.4	0
	DS vs SF	-0.5	-0.5	0	-0.8	-0.5
	ASD vs ASA	0	0	-0.7	0.4	0
	ASD vs K	0	N/A	N/A	0	N/A
	ASA vs K	0	N/A	N/A	0	N/A
	DS vs K	0	N/A	N/A	-0.5	N/A
	SF vs K	0	N/A	N/A	0.5	N/A
Cross-Correlations ¹⁾	ZSD vs SF	0.01	-0.04	0	0.2	0
	ZSA vs SF	-0.17	-0.25	0	0.3	0
	ZSD vs K	0	N/A	N/A	0	N/A
	ZSA vs K	-0.02	N/A	N/A	0.1	N/A
	ZSD vs DS	-0.05	-0.10	0	0.1	-0.27
	ZSA vs DS	0.27	-0.40	0	0.2	-0.06
	ZSD vs ASD	0.73	0.42	0.66	0.5	0.35
	ZSA vs ASD	-0.14	-0.27	0.47	0	0.23
	ZSD vs ASA	-0.20	-0.18	-0.55	0	-0.08
	ZSA vs ASA	0.24	0.26	-0.22	0.5	0.43
	ZSD vs ZSA	-0.07	-0.27	0	0	0.42
Delay scaling parameter r_r		3.8	1.7	1.7	3.6	3
XPR [dB]	μ_{XPR}	12	7	7	11	10
	σ_{XPR}	4	3	3	4	4
Number of clusters N		11	10	10	15	19

Number of rays per cluster M	20	20	20	20	20
Cluster DS (C_{DS}) in [ns]	N/A	N/A	N/A	N/A	N/A
Cluster ASD (C_{ASD}) in [deg]	2	2	2	5	5
Cluster ASA (C_{ASA}) in [deg]	3	3	3	8	11
Cluster ZSA (C_{ZSA}) in [deg]	3	3	3	9	9
Per cluster shadowing std ζ [dB]	3	3	3	6	3
Correlation distance in the horizontal plane [m]	DS	50	36	36	8
	ASD	25	30	30	7
	ASA	35	40	40	5
	SF	37	120	120	10
	K	40	N/A	N/A	4
	ZSA	15	50	50	4
	ZSD	15	50	50	4
<p>f_c is carrier frequency in GHz; d_{2D} is BS-UT distance in km.</p> <p>NOTE 1: DS = rms delay spread, ASD = rms azimuth spread of departure angles, ASA = rms azimuth spread of arrival angles, ZSD = rms zenith spread of departure angles, ZSA = rms zenith spread of arrival angles, SF = shadow fading, and K = Ricean K-factor.</p> <p>NOTE 2: The sign of the shadow fading is defined so that positive SF means more received power at UT than predicted by the path loss model.</p> <p>NOTE 3: The following notation for mean ($\mu_{\log X} = \text{mean}\{\log_{10}(X)\}$) and standard deviation ($\sigma_{\log X} = \text{std}\{\log_{10}(X)\}$) is used for logarithmized parameters X.</p> <p>NOTE 4: Void.</p> <p>NOTE 5: For all considered scenarios the AOD/AOA distributions are modelled by a wrapped Gaussian distribution, the ZOD/ZOA distributions are modelled by a Laplacian distribution and the delay distribution is modelled by an exponential distribution.</p> <p>NOTE 6: For InH and frequencies below 6 GHz, use $f_c = 6$ when determining the values of the frequency-dependent LSP values</p>					

Table 7.5-6 Part-3: Channel model parameters for InF

Scenarios		InF	
		LOS	NLOS
Delay spread (DS) $\lg DS = \log_{10}(DS/1s)$ ⁴⁾	$\mu_{\lg DS}$	$\log_{10}(26(V/S)+14)-9.35$	$\log_{10}(30(V/S)+32)-9.44$
	$\sigma_{\lg DS}$	0.15	0.19
AOD spread (ASD) $\lg ASD = \log_{10}(ASD/1^\circ)$	$\mu_{\lg ASD}$	1.56	1.57
	$\sigma_{\lg ASD}$	0.25	0.2
AOA spread (ASA) $\lg ASA = \log_{10}(ASA/1^\circ)$	$\mu_{\lg ASA}$	$-0.18 \cdot \log_{10}(1+fc) + 1.78$	1.72
	$\sigma_{\lg ASA}$	$0.12 \cdot \log_{10}(1+fc) + 0.2$	0.3
ZOA spread (ZSA) $\lg ZSA = \log_{10}(ZSA/1^\circ)$	$\mu_{\lg ZSA}$	$-0.2 \cdot \log_{10}(1+fc) + 1.5$	$-0.13 \cdot \log_{10}(1+fc) + 1.45$
	$\sigma_{\lg ZSA}$	0.35	0.45
Shadow fading (SF) [dB]	σ_{SF}	Specified as part of path loss models	
K-factor (K) [dB]	μ_K	7	N/A
	σ_K	8	N/A
Cross-Correlations	ASD vs DS	0	0
	ASA vs DS	0	0
	ASA vs SF	0	0
	ASD vs SF	0	0
	DS vs SF	0	0
	ASD vs ASA	0	0
	ASD vs K	-0.5	N/A
	ASA vs K	0	N/A
	DS vs K	-0.7	N/A
Cross-Correlations ¹⁾	SF vs K	0	N/A
	ZSD vs SF	0	0
	ZSA vs SF	0	0
	ZSD vs K	0	N/A
	ZSA vs K	0	N/A
	ZSD vs DS	0	0
	ZSA vs DS	0	0
	ZSD vs ASD	0	0
	ZSA vs ASD	0	0
	ZSD vs ASA	0	0
	ZSA vs ASA	0	0
	ZSD vs ZSA	0	0
Delay scaling parameter r_τ		2.7	3
XPR [dB]	μ_{XPR}	12	11
	σ_{XPR}	6	6
Number of clusters N		25	25
Number of rays per cluster M		20	20
Cluster DS (C_{DS}) in [ns]		N/A	N/A
Cluster ASD (C_{ASD}) in [deg]		5	5
Cluster ASA (C_{ASA}) in [deg]		8	8
Cluster ZSA (C_{ZSA}) in [deg]		9	9
Per cluster shadowing std ζ [dB]		4	3
Correlation distance in the horizontal plane [m] ⁵⁾	DS	10	10
	ASD	10	10
	ASA	10	10
	SF	10	10
	K	10	N/A
	ZSA	10	10
	ZSD	10	10

f_c is carrier frequency in GHz; d_{2D} is BS-UT distance in km.

NOTE 1: DS = rms delay spread, ASD = rms azimuth spread of departure angles, ASA = rms azimuth spread of arrival angles, ZSD = rms zenith spread of departure angles, ZSA = rms zenith spread of arrival angles, SF = shadow fading, and K = Ricean K-factor.

NOTE 2: The sign of the shadow fading is defined so that positive SF means more received power at UT than predicted by the path loss model.

NOTE 3: The following notation for mean ($\mu_{\lg X} = \text{mean}\{\log_{10}(X)\}$) and standard deviation ($\sigma_{\lg X} = \text{std}\{\log_{10}(X)\}$) is used for logarithmized parameters X .

NOTE 4: V = hall volume in m^3 , S = total surface area of hall in m^2 (walls+floor+ceiling)

NOTE 5: When the simulation scenario is small it is recommended to consider methods to improve the statistical confidence, such as using multiple random seeds in simulations.

Table 7.5-7: ZSD and ZOD offset parameters for UMa

Scenarios		LOS	NLOS
ZOD spread (ZSD) $\lg ZSD = \log_{10}(ZSD/1^\circ)$	$\mu_{\lg ZSD}$	$\max[-0.5, -2.1(d_{2D}/1000) - 0.01(h_{UT} - 1.5) + 0.75]$	$\max[-0.5, -2.1(d_{2D}/1000) - 0.01(h_{UT} - 1.5) + 0.9]$
	$\sigma_{\lg ZSD}$	0.40	0.49
ZOD offset	$\mu_{\text{offset}, ZOD}$	0	$e(f_c) - 10^{\{a(f_c) \log_{10}(\max(b(f_c), d_{2D})) + c(f_c) - 0.07(h_{UT} - 1.5)\}}$
Note: For NLOS ZOD offset: $a(f_c) = 0.208 \log_{10}(f_c) - 0.782$; $b(f_c) = 25$; $c(f_c) = -0.13 \log_{10}(f_c) + 2.03$; $e(f_c) = 7.66 \log_{10}(f_c) - 5.96$.			

Table 7.5-8: ZSD and ZOD offset parameters for UMi – Street Canyon

Scenarios		LOS	NLOS
ZOD spread (ZSD) $\lg ZSD = \log_{10}(ZSD/1^\circ)$	$\mu_{\lg ZSD}$	$\max[-0.21, -14.8(d_{2D}/1000) + 0.01 h_{UT} - h_{BS} + 0.83]$	$\max[-0.5, -3.1(d_{2D}/1000) + 0.01 \max(h_{UT} - h_{BS}, 0) + 0.2]$
	$\sigma_{\lg ZSD}$	0.35	0.35
ZOD offset	$\mu_{\text{offset}, ZOD}$	0	$-10^{\{-1.5 \log_{10}(\max(10, d_{2D})) + 3.3\}}$

Table 7.5-9: ZSD and ZOD offset parameters for RMa

Scenarios		LOS	NLOS	O2I
ZOD spread (ZSD) $\lg ZSD = \log_{10}(ZSD/1^\circ)$	$\mu_{\lg ZSD}$	$\max[-1, -0.17(d_{2D}/1000) - 0.01(h_{UT} - 1.5) + 0.22]$	$\max[-1, -0.19(d_{2D}/1000) - 0.01(h_{UT} - 1.5) + 0.28]$	$\max[-1, -0.19(d_{2D}/1000) - 0.01(h_{UT} - 1.5) + 0.28]$
	$\sigma_{\lg ZSD}$	0.34	0.30	0.30
ZOD offset	$\mu_{\text{offset}, ZOD}$	0	$\arctan((35 - 3.5)/d_{2D}) - \arctan((35 - 1.5)/d_{2D})$	$\arctan((35 - 3.5)/d_{2D}) - \arctan((35 - 1.5)/d_{2D})$

Table 7.5-10: ZSD and ZOD offset parameters for Indoor-Office

Scenarios		LOS	NLOS
ZOD spread (ZSD) $\lg ZSD = \log_{10}(ZSD/1^\circ)$	$\mu_{\lg ZSD}$	$-1.43 \log_{10}(1 + f_c) + 2.228$	1.08
	$\sigma_{\lg ZSD}$	$0.13 \log_{10}(1 + f_c) + 0.30$	0.36
ZOD offset	$\mu_{\text{offset}, ZOD}$	0	0

Table 7.5-11: ZSD and ZOD offset parameters for InF

Scenarios		LOS	NLOS
ZOD spread (ZSD) $\lg ZSD = \log_{10}(ZSD/1^\circ)$	$\mu_{\lg ZSD}$	1.35	1.2
	$\sigma_{\lg ZSD}$	0.35	0.55
ZOD offset	$\mu_{\text{offset}, ZOD}$	0	0

Notes for Tables 7.5-7, 7.5-8, 7.5-9, 7.5-10, 7.5-11:

NOTE 1: f_c is center frequency in GHz; d_{2D} is BS-UT distance in m.

NOTE 2: h_{BS} and h_{UT} are antenna heights in m for BS and UT **respectively**.

NOTE 3: The following notation for mean ($\mu_{\lg X} = \text{mean}\{\log_{10}(X)\}$) and standard deviation ($\sigma_{\lg X} = \text{std}\{\log_{10}(X)\}$) is used for logarithmized parameters X.

NOTE 4: For frequencies below 6 GHz, use $f_c = 6$ when determining the values of the frequency-dependent ZSD and ZOD offset parameters in Table 7.5-7 and 7.5-10

NOTE 5: The ZSD parameters for O2I links are the same parameters that are used for outdoor links, depending on the LOS condition of the outdoor link part in Tables 7.5-7 and 7.5-8.

7.6 Additional modelling components

The additional modelling components in this subclause are to support advanced simulations, such as simulations with very large arrays and large bandwidth, simulations affected by oxygen absorption (frequencies between 53 and 67 GHz), simulations in which spatial consistency is important (e.g. high number of closely located user), simulations of mobility, simulations of blockage effects, simulations of absolute time of arrival, simulations of dual mobility, simulations that include sources of EM interference, and simulations of devices embedded in machinery or enclosures. These modelling components affect some of the steps between Step 1 and Step 12 in Subclause 7.5.

These extensions are computationally more expensive and might not be required in all evaluation cases.

7.6.1 Oxygen absorption

Oxygen absorption loss is applied to the cluster responses generated in Step 11 in Subclause 7.5. The additional loss, $OL_n(f_c)$ for cluster n at centre frequency f_c is modelled as:

$$OL_n(f_c) = \frac{\alpha(f_c)}{1000} \cdot (d_{3D} + c \cdot (\tau_n + \tau_\Delta)) \quad [\text{dB}] \quad (7.6-1)$$

where:

- $\alpha(f_c)$ is frequency dependent oxygen loss [dB/km] characterized in Table 7.6.1-1;
- c is the speed of light [m/s]; and d_{3D} is the distance [m];
- τ_n is the n -th cluster delay [s] in Step 11 in Subclause 7.5;
- τ_Δ is 0 in the LOS case and $\min(\tau_n')$ otherwise, where $\min(\tau_n')$ is the minimum delay in Step 5.

For centre frequencies not specified in this table, the frequency dependent oxygen loss $\alpha(f_c)$ is obtained from a linear interpolation between two loss values corresponding to the two adjacent centre frequencies of the centre frequency f_c .

Table 7.6.1-1 Frequency dependent oxygen loss $\alpha(f)$ [dB/km]

f in [GHz]	0-52	53	54	55	56	57	58	59	60	61	62	63	64	65	66	67	68-100
$\alpha(f)$ in [dB/km]	0	1	2.2	4	6.6	9.7	12.6	14.6	15	14.6	14.3	10.5	6.8	3.9	1.9	1	0

For large channel bandwidth, first transform the time-domain channel response of each cluster (all rays within one cluster share common oxygen absorption loss for simplicity) into frequency-domain channel response, and apply the oxygen absorption loss to the cluster's frequency-domain channel response for frequency $f_c + \Delta f$ within the considered bandwidth. The oxygen loss, $OL_n(f_c + \Delta f)$ for cluster n at frequency $f_c + \Delta f$ is modelled as:

$$OL_n(f_c + \Delta f) = \frac{\alpha(f_c + \Delta f)}{1000} (d_{3D} + c(\tau_n + \tau_\Delta)) \quad [\text{dB}] \quad (7.6-2)$$

where:

- $\alpha(f_c + \Delta f)$ is the oxygen loss (dB/km) at frequency $f_c + \Delta f$ characterized in Table 7.6.1-1. Note that Δf is in $[-B/2, B/2]$, where B is the bandwidth. Linear interpolation is applied for frequencies not provided in Table 7.6.1-1.

The final frequency-domain channel response is obtained by the summation of frequency-domain channel responses of all clusters.

Time-domain channel response is obtained by the reverse transform from the obtained frequency-domain channel response.

7.6.2 Large bandwidth and large antenna array

7.6.2.1 Modelling of the propagation delay

The modelling in this subclause applies only when the bandwidth B is greater than c/D Hz, where

- D is the maximum antenna aperture in either azimuth or elevation (m)
- c is the speed of light (m/s)

Each ray within a cluster for a given u (Rx) and s (Tx) has unique time of arrival (TOA). The channel coefficient generation step (Step 11 in Subclause 7.5) is updated to model individual rays. In this case, the channel response of ray m in cluster n for a link between Rx antenna u and Tx antenna s at delay τ at time t is given by:

$$H_{u,s,n,m}^{\text{NLOS}}(t; \tau) = \sqrt{P_{n,m}} \begin{bmatrix} F_{rx,u,\theta}(\theta_{n,m,ZOA}, \varphi_{n,m,AOA}) \\ F_{rx,u,\varphi}(\theta_{n,m,ZOA}, \varphi_{n,m,AOA}) \end{bmatrix}^T \begin{bmatrix} \exp(j\Phi_{n,m}^{\theta\theta}) & \sqrt{\kappa_{n,m-1}} \exp(j\Phi_{n,m}^{\theta\varphi}) \\ \sqrt{\kappa_{n,m-1}} \exp(j\Phi_{n,m}^{\varphi\theta}) & \exp(j\Phi_{n,m}^{\varphi\varphi}) \end{bmatrix} \\ \begin{bmatrix} F_{tx,s,\theta}(\theta_{n,m,ZOD}, \varphi_{n,m,AOD}) \\ F_{tx,s,\varphi}(\theta_{n,m,ZOD}, \varphi_{n,m,AOD}) \end{bmatrix} \exp\left(\frac{j2\pi(\hat{r}_{rx,n,m}^T \cdot \bar{d}_{rx,u})}{\lambda(f)}\right) \exp\left(\frac{j2\pi(\hat{r}_{tx,n,m}^T \cdot \bar{d}_{tx,s})}{\lambda(f)}\right) \\ \exp\left(j2\pi \frac{\hat{r}_{rx,n,m}^T \cdot \bar{v}}{\lambda_0} t\right) \delta(\tau - \tau_{n,m}) \quad (7.6-3)$$

3)

with $\lambda(f)$ is the wavelength on frequency $f \in \left[f_c - \frac{B}{2}, f_c + \frac{B}{2}\right]$, which can be implemented by user's own method. The delay (TOA) for ray m in cluster n for a link between Rx antenna u and Tx antenna s is given by:

$$\tau_{u,s,n,m} = \tau_{n,m} - \frac{1}{c} \hat{r}_{rx,n,m}^T \cdot \bar{d}_{rx,u} - \frac{1}{c} \hat{r}_{tx,n,m}^T \cdot \bar{d}_{tx,s} \quad (7.6-4)$$

Note that Equation (7.6-3) only considers the delays $\tau_{n,m}$ intentionally. If unequal ray powers are considered,

$P_{n,m}$ are generated according to Subclause 7.6.2.2. Otherwise, ray powers are equal within a cluster, i.e., $P_{n,m} = P_n / M$ for all m . Note: this model is developed assuming plane wave propagation.

7.6.2.2 Modelling of intra-cluster angular and delay spreads

With large antenna arrays or large bandwidths, the angle and/or delay resolution can be larger than what the fast fading model in Subclause 7.5 is designed to support. To model this effect, the following modifications to Step 7 in Subclause 7.5 can be optionally used.

1. The offset angles α_m in (7.5-13), (7.5-18) and (7.5-20) are generated independently per cluster and ray using:

$$\alpha_{n,m,|AOA,AOD,ZOA,ZOD|} \sim \text{unif}(-2,2) \quad (7.6-5)$$

where $\text{unif}(a,b)$ denotes the continuous uniform distribution in the interval $[a,b]$. These random variables may further be modelled as spatially consistent with correlation distance equal to the cluster-specific random variable correlation distance of Table 7.6.3.1-2.

2. The relative delay of m -th ray is given by $\tau'_{n,m} = \tau''_{n,m} - \min \left(\left(\tau''_{n,i} \right)_{i=1}^M \right)$, where n is the cluster index,

$\tau''_{n,m} \sim \text{unif}(0, 2c_{DS})$, the cluster DS c_{DS} is given in Table 7.5-6. These random variables may further be modelled as spatially consistent with correlation distance equal to the cluster-specific random variable correlation distance of Table 7.6.3.1-2. In this case, the sub-cluster mapping according to (7.5-26) and Table 7.5-

5 shall not be applied. The delays to be used in Equation (7.6-3) are given by $\tau_{n,m} = \tau_n + \tau'_{n,m}$.

3. Ray powers are determined unequally by the following process:

$$P_{n,m} = P_n \cdot \frac{P'_{n,m}}{\sum_{m=1}^M P'_{n,m}}$$

The power of m -th ray in n -th cluster is given by for $m = 1, \dots, M$, where

$$P'_{n,m} = \exp\left(-\frac{\tau'_{n,m}}{c_{DS}}\right) \exp\left(-\frac{\sqrt{2}|\alpha_{n,m,AOA}|}{c_{ASA}}\right) \exp\left(-\frac{\sqrt{2}|\alpha_{n,m,AOD}|}{c_{ASD}}\right) \exp\left(-\frac{\sqrt{2}|\alpha_{n,m,ZOA}|}{c_{ZSA}}\right) \exp\left(-\frac{\sqrt{2}|\alpha_{n,m,ZOD}|}{c_{ZSD}}\right) \quad (7.6-6)$$

and c_{DS} , c_{ASA} , c_{ASD} , and c_{ZSA} are respectively the intra-cluster delay spread and the corresponding intra-cluster angular spread that are given in Table 7.5-6. The cluster zenith spread of departure is given by

$$c_{ZSD} = \frac{3}{8} 10^{\mu_{lgZSD}}, \quad (7.6-7)$$

with μ_{lgZSD} being defined in Tables 7.5-7, 7.5-8, 7.5-9, 7.5-10 and 7.5-11.

4. The number of rays per cluster shall be calculated as follows:

$$M = \min \left\{ \max \left(M_t, M_{AOD}, M_{ZOD}, 20 \right), M_{\max} \right\} \quad (7.6-8)$$

where:

$$M_t = \lceil 4kc_{DS}B \rceil$$

$$M_{AOD} = \lceil 4kc_{ASD} \frac{\pi \cdot D_h}{180 \cdot \lambda} \rceil$$

$$M_{ZOD} = \lceil 4kc_{ZSD} \frac{\pi \cdot D_v}{180 \cdot \lambda} \rceil$$

- M_{\max} is the upper limit of M , and it should be selected by the user of channel model based on the trade-off between simulation complexity and accuracy.
- D_h and D_v are the array size in m in horizontal and vertical dimension, B is bandwidth in Hz, C_{ASD} and C_{ZSD} are the cluster spreads in degrees, and λ is the wavelength.
- k is a "sparseness" parameter with value 0.5.

It is noted that each MPC may have different AOD, ZOD, and delay.

7.6.3 Spatial consistency

7.6.3.1 Spatial consistency procedure

A new procedure, namely a *spatial consistency procedure*, can be used for both cluster-specific and ray-specific random variables to be generated in various channel generation steps in Subclause 7.5, so that they are spatially consistent for drop-based simulations. Alternatively, this can be used together with Procedure B described in Subclause 7.6.3.2 for spatially consistent mobility simulations.

The procedure can be considered as a 2D random process (in the horizontal plane) given the UT locations based on the parameter-specific correlation distance values for spatial consistency, specified in Table 7.6.3.1-2. The cluster specific random variables include:

- Cluster specific random delay in Step 5;
- Cluster specific shadowing in Step 6; and
- Cluster specific offset for AOD/AOA/ZOD/ZOA in Step 7.
- Cluster specific sign for AOD/AOA/ZOD/ZOA in Step 7.
- Optionally in case of large bandwidth as described in Subclause 7.6.2.2 the procedure may apply as well for the parameters of rays within a cluster.

The procedure shall apply to each cluster before sorting the delay. Cluster specific sign for AOD/AOA/ZOD/ZOA in Step 7 shall be kept unchanged per simulation drop even if UT position changes during simulation. The ray specific random variables include:

- Random coupling of rays in Step 8;
- XPR in Step 9; and
- Random phase in Step 10.

The random coupling of rays in Step 8 and the intra-cluster delays in Step 11 shall be kept unchanged per simulation drop even if UT position changes during simulation.

Table 7.6.3.1-2 Correlation distance for spatial consistency

Correlation distance in [m]	RMa			UMi			UMa			Indoor	InF
	LOS	NLOS	O2I	LOS	NLOS	O2I	LOS	NLOS	O2I		
Cluster and ray specific random variables	50	60	15	12	15	15	40	50	15	10	10
LOS/NLOS state	60			50			50			10	$d_{clutter}/2$
Indoor/outdoor state	50			50			50			N/A	N/A

7.6.3.2 Spatially-consistent UT/BS mobility modelling

For mobility simulation enhancement, two alternative spatial consistency procedures – Procedure A and Procedure B – are described as follows. The procedures presented below consider the downlink direction same as in Subclause 7.5.

Procedure A:

For $t_0=0$ when a UT/BS is dropped into the network, spatially consistent powers/delays/angles of clusters are generated according to Subclause 7.6.3.1.

The updated distance of UT/BS should be limited within 1 meter, i.e. when $v_{\Delta t} < 1 \text{ m}$, and the updated procedure in the following should take the closest realization instead of $t_0=0$. In case the absolute time of arrival modeling of clause 7.6.9 is simultaneously used, the update distance should be the minimum of 1 meter and $d_{3D}/10$.

At $t_k = t_{k-1} + \Delta t$, update channel cluster power/delay/angles based on UT/BS channel cluster power/delay/angles, moving speed moving direction and UT position at t_{k-1} .

Cluster delay is updated as:

$$\tilde{\tau}_n(t_k) = \begin{cases} \tilde{\tau}_n(t_{k-1}) - \frac{\hat{r}_{rx,n}(t_{k-1})^T \dot{v}_{rx}(t_{k-1}) + \hat{r}_{tx,n}(t_{k-1})^T \dot{v}_{tx}(t_{k-1})}{c} \Delta t & \text{for } k > 0 \\ \tau_n(t_0) + \tau_{\Delta}(t_0) + \frac{d_{3D}(t_0)}{c} & \text{for } k = 0 \end{cases} \quad (7.6-9)$$

where

c is the speed of light in [m/s] $v(\cos(\phi_v(t_0)), \sin(\phi_v(t_0)), 0)$;

$\dot{v}_{tx}(t_k)$ and $\dot{v}_{rx}(t_k)$ are the BS and UT velocity vector respectively with $\|\bar{v}_{tx}(t_k)\|_2 = v_{tx}$ and $\|\bar{v}_{rx}(t_k)\|_2 = v_{rx}$;

$d_{3D}(t_0)$ is the 3D distance between Rx antenna and Tx antenna at t_0 in [m];

$\tau_n(t_0)$ are the cluster delays in [s] as in Step 11 in Subclause 7.5;

$\tau_{\Delta}(t_0) = \begin{cases} 0 & \text{for LOS} \\ \min(\tau_n') & \text{for NLOS} \end{cases}$, where τ_n' are the delays from Equation (7.5-1). In case the absolute

time of arrival modelling of clause 7.6.9 is simultaneously used, $\tau_{\Delta}(t_0) = \begin{cases} 0 & \text{for LOS} \\ \Delta\tau & \text{for NLOS} \end{cases}$ where $\Delta\tau$ is determined according to clause 7.6.9.

Also,

$$\hat{r}_{rx,n}(t_{k-1}) = \begin{pmatrix} \sin(\theta_{n,ZOA}(t_{k-1})) \cos(\phi_{n,AOA}(t_{k-1})) \\ \sin(\theta_{n,ZOA}(t_{k-1})) \sin(\phi_{n,AOA}(t_{k-1})) \\ \cos(\theta_{n,ZOA}(t_{k-1})) \end{pmatrix}$$

$$\overrightarrow{p_n(t_0)} = (\sin(\theta_{n,ZOA}(t_0)) \cos(\phi_{n,AOA}(t_0)), \sin(\theta_{n,ZOA}(t_0)) \sin(\phi_{n,AOA}(t_0)), \cos(\theta_{n,ZOA}(t_0))) \quad (7.6-10)$$

where $\theta_{n,ZOA}$ and $\phi_{n,AOA}$ are cluster specific zenith and azimuth angles of arrival.

$$\hat{r}_{tx,n}(t_{k-1}) = \begin{bmatrix} \sin(\theta_{n,ZOD}(t_{k-1})) \cos(\phi_{n,AOD}(t_{k-1})) \\ \sin(\theta_{n,ZOD}(t_{k-1})) \sin(\phi_{n,AOD}(t_{k-1})) \\ \cos(\theta_{n,ZOD}(t_{k-1})) \end{bmatrix} \quad (7.6-10a)$$

where $\theta_{n,ZOD}$ and $\phi_{n,AOD}$ are the cluster specific zenith and azimuth angles of departure.

After updating the delays according to equation (7.6-9), the delays over the mobility range are normalized. Equation (7.5-2) of the fast fading model is replaced by

$$\tau_n(t_k) = \tilde{\tau}_n(t_k) - \min \left(\left(\tilde{\tau}_n(t_k) \right)_{n=1}^N \right) \quad (7.6-10a)$$

in which t_k covers the entire duration of the mobility model.

Cluster powers are updated as in Step 6 using the cluster delays from Equation (7.6-10a) $\tau_n(t_0 + t)$.

Cluster departure angles ($\theta_{n,ZOD}$ and $\phi_{n,AOD}$) and arrival angles ($\theta_{n,ZOA}$ and $\phi_{n,AOA}$) are updated using a cluster-wise transformation of the UT/BS velocity vector given by

$$\dot{v}'_{n,rx}(t_k) = \begin{cases} \dot{v}_{rx}(t_k) - \dot{v}_{tx}(t_k) & \text{for LOS} \\ R_{n,rx} \cdot \dot{v}_{rx}(t_k) - \dot{v}_{tx}(t_k) & \text{for NLOS} \end{cases} \quad (7.6-10b)$$

$$\dot{v}'_{n,tx}(t_k) = \begin{cases} \dot{v}_{tx}(t_k) - \dot{v}_{rx}(t_k) & \text{for LOS} \\ R_{n,tx} \cdot \dot{v}_{tx}(t_k) - \dot{v}_{rx}(t_k) & \text{for NLOS} \end{cases} \quad (7.6-10c)$$

with

$$R_{n,rx} = R_Z(\phi_{n,AOD}(t_k) + \pi) \cdot R_Y\left(\frac{\pi}{2} - \theta_{n,ZOD}(t_k)\right) \cdot \begin{bmatrix} 1 & 0 & 0 \\ 0 & X_n & 0 \\ 0 & 0 & 1 \end{bmatrix} \cdot R_Y\left(\frac{\pi}{2} - \theta_{n,ZOA}(t_k)\right) \cdot R_Z(-\phi_{n,AOA}(t_k)) ,$$

and

$$R_{n,tx} = R_Z(-\phi_{n,AOD}(t_k)) \cdot R_Y\left(\frac{\pi}{2} - \theta_{n,ZOD}(t_k)\right) \cdot \begin{bmatrix} 1 & 0 & 0 \\ 0 & X_n & 0 \\ 0 & 0 & 1 \end{bmatrix} \cdot R_Y\left(\frac{\pi}{2} - \theta_{n,ZOA}(t_k)\right) \cdot R_Z(\phi_{n,AOA}(t_k) + \pi) ,$$

where $R_Y(\beta)$ and $R_Z(\alpha)$ being the rotation matrices around y-axis and z-axis as defined in Equation (7.1-2).

Random variable $X_n \in [1, -1]$ is sampled from a uniform distribution on a NLOS cluster basis and is not changed during the UT mobility within a drop. The cluster specific decorrelation distances are 60m, 15m, 50m and 10m for RMa, UMi, UMa and Indoor scenarios, respectively.

Now, the departure and arrival angles in radians are updated as:

$$\phi_{n,AOD}(t_k) = \phi_{n,AOD}(t_{k-1}) + \frac{\dot{v}'_{n,rx}(t_{k-1})^T \hat{\phi}(\theta_{n,ZOD}(t_{k-1}), \phi_{n,AOD}(t_{k-1}))}{c \cdot \tilde{\tau}_n(t_{k-1}) \sin(\theta_{n,ZOD}(t_{k-1}))} \Delta t \quad (7.6-11)$$

$$\theta_{n,ZOD}(t_k) = \theta_{n,ZOD}(t_{k-1}) + \frac{\dot{v}'_{n,rx}(t_{k-1})^T \hat{\theta}(\theta_{n,ZOD}(t_{k-1}), \phi_{n,AOD}(t_{k-1}))}{c \cdot \tilde{\tau}_n(t_{k-1})} \Delta t \quad (7.6-12)$$

and

$$\phi_{n,AOA}(t_k) = \phi_{n,AOA}(t_{k-1}) - \frac{\dot{v}'_{n,tx}(t_{k-1})^T \hat{\phi}(\theta_{n,ZOA}(t_{k-1}), \phi_{n,AOA}(t_{k-1}))}{c \cdot \tilde{\tau}_n(t_{k-1}) \sin(\theta_{n,ZOA}(t_{k-1}))} \Delta t \quad (7.6-13)$$

$$\theta_{n,ZOA}(t_k) = \theta_{n,ZOA}(t_{k-1}) - \frac{\dot{v}'_{n,tx}(t_{k-1})^T \hat{\theta}(\theta_{n,ZOA}(t_{k-1}), \phi_{n,AOA}(t_{k-1}))}{c \cdot \tilde{\tau}_n(t_{k-1})} \Delta t, \quad (7.6-14)$$

with $\hat{\theta}(\theta, \phi)$ and $\hat{\phi}(\theta, \phi)$ being the spherical unit vectors defined in Equations (7.1-13) and (7.1-14).

Procedure B:

In procedure B, spatial or time evolution of the channel is obtained by generating channel realizations separately for all links to different Rx positions using Steps 1-12 of Subclause 7.5 together with the spatially consistent procedure of Subclause 7.6.3.1. In the case of mobility these positions may be a function of time along one or more Rx trajectories. Furthermore, to ensure that the spatial or time evolution of delays and angles are within reasonable limits, Steps 5, 6, and 7 in Subclause 7.5 should be replaced by the below procedure.

Note: For implementation purposes, LSPs and SSPs may be interpolated within the coherence length or time of the respective parameter.

Step 5: Generate cluster delays τ_n , with $n \in [1, N]$.

N delays are drawn randomly from a uniform distribution.

$$\tau'_n \sim \text{unif}(0, 2 \cdot 10^{\mu_{\text{lgDS}} + \sigma_{\text{lgDS}}}) \quad (7.6-15)$$

Normalise the delays by subtracting the minimum delay: $\tau_n = \tau'_n - \min(\tau'_n)$. The autocorrelation distance for τ'_n is $2c \cdot 10^{\mu_{\text{lgDS}} + \sigma_{\text{lgDS}}}$.

In the case of LOS, set the delay of the first cluster τ_1 to 0.

Step 6: Generate N arrival angles and departure angles for both azimuth and elevation using (7.6-16) instead of (7.5-9) and (7.5-14).

$$\phi'_{n,AOA} \sim 2 \cdot 10^{\mu_{\text{lgASA}} + \sigma_{\text{lgASA}}} \text{unif}(-1, 1) \quad (7.6-16)$$

with $n \in [1, N]$. This step is repeated independently for AOD, AOA, ZOD, and ZOA with corresponding maximum angles for the uniform distribution. In case of LOS, set the angles of the first cluster ($\phi'_{1,AOA}$, etc) to 0.

The autocorrelation distances are $\tau_{\text{max}} \cdot c_0 = 2c \cdot 10^{\mu_{\text{lgDS}} + \sigma_{\text{lgDS}}}$ for AOD, and ZOD, while they are fixed to 50m for AOA, and ZOA.

Offset angles etc are applied in the modified Step 7b below after cluster powers have been calculated.

Step 7: Generate cluster powers P_n P

Cluster powers are calculated assuming a single slope exponential power profile and Laplacian angular power profiles. The cluster powers are determined by

$$P'_n = \exp\left(\frac{-\tau'_n}{DS}\right) \exp\left(\frac{-\sqrt{2}|\varphi'_{n,AOA}|}{ASA}\right) \exp\left(\frac{-\sqrt{2}|\varphi'_{n,AOD}|}{ASD}\right) \exp\left(\frac{-\sqrt{2}|\theta'_{n,ZOA}|}{ZSA}\right) \exp\left(\frac{-\sqrt{2}|\theta'_{n,ZOD}|}{ZSD}\right) \cdot 10^{\frac{-Z_n}{10}} \quad (7.6-17)$$

where $Z_n \sim N(0, \zeta^2)$ (autocorrelation distance same as for shadow fading) is the per cluster shadowing term in [dB]. Delay spread DS and angular spreads ASA , ASD , ZSA , ZSD are generated in Step 4 of Subclause 7.5. Normalize the cluster powers so that the sum of all cluster powers is equal to one, i.e.,

$$P_n = \frac{P'_n}{\sum_{n=1}^N P'_n} \quad (7.6-17a)$$

In the case of LOS condition, substitute DS with $\sqrt{1+K_R}/2 \cdot DS$ and $\{ASA, ASD, ZSA, ZSD\}$ with $\{\sqrt{1+K_R} \cdot ASA, \sqrt{1+K_R} \cdot ASD, \sqrt{1+K_R} \cdot ZSA, \sqrt{1+K_R} \cdot ZSD\}$

respectively to preserve the delay and angular spreads. K_R is the Ricean K-factor as generated in Step 4 converted to linear scale. Furthermore, an additional specular component is added to the first cluster. Power of the single LOS ray is:

$$P_{1,LOS} = \frac{K_R}{K_R + 1} \quad (7.6-17b)$$

and the cluster powers are not normalized as in equation (7.6-17a), but:

$$P_n = \frac{1}{K_R + 1} \frac{P'_n}{\sum_{n=1}^N P'_n} + \delta(n-1) P_{1,LOS} \quad (7.6-17c)$$

where $\delta(\cdot)$ is Dirac's delta function.

Assign the power of each ray within a cluster as P_n/M , where M is the number of rays per cluster.

Step 7b: Apply offset angles

The ray AOA angles are determined by

$$\varphi_{n,m,AOA} = \varphi'_{n,AOA} + \varphi_{LOS,AOA} + c_{ASA} \alpha_m \quad (7.6-17d)$$

where $\varphi_{LOS,AOA}$ is the LOS direction defined in the network layout description, see Step1c.

The generation of AOD ($\varphi_{n,m,AOD}$) follows a procedure similar to AOA as described above.

The ZOA angles are determined by

$$\theta_{n,m,ZOA} = \varphi'_{n,ZOA} + \bar{\theta}_{ZOA} + c_{ZSA} \alpha_m \quad (7.6-17e)$$

where $\bar{\theta}_{ZOA} = 90^\circ$ if the BS-UT link is O2I and $\bar{\theta}_{ZOA} = \theta_{LOS,ZOA}$ otherwise. The LOS direction is defined in the network layout description, see Step1c.

The ZOA angles are determined by

$$\theta_{n,m,ZOD} = \phi'_{n,ZOD} + \theta_{LOS,ZOD} + \mu_{offset,ZOD} + (3/8) \left(10^{\mu_{lgZSD}} \right) \alpha_m \quad (7.6-17f)$$

where μ_{lgZSD} is the mean of the ZSD log-normal distribution.

Some of the delay and angle spreads and standard deviations used in equations (7.6-15) and (7.6-16) may be frequency-dependent. In the case of multi-frequency simulations according to Subclause 7.6.5, the largest value among all the simulated frequencies should be used in (7.6-15) and (7.6-16) so that the cluster and ray delays and angles (but not the powers or the resulting delay or angular spreads) are the same for all frequencies.

7.6.3.3 LOS/NLOS, indoor states and O2I parameters

The LOS state can be determined according to the spatial consistency procedure for random variables as mentioned in Subclause 7.6.3.1, by comparing a realization of a random variable generated with distance-dependent LOS probability. If the realization is less than the LOS probability, the state is LOS; otherwise NLOS. Decision of LOS and NLOS status should be used in Step 2 in Subclause 7.5 if this advanced simulation is performed.

The same procedure can be applied for determining the indoor state, with the indoor probability instead of the LOS probability.

The correlation distance for LOS state and indoor/outdoor is specified in Table 7.6.3.1-2.

The indoor distance can be modeled as the minimum of two spatially consistent uniform random variables within (0, 25) meters with correlation distance 25m.

Note in case the UT is in an indoor state, the pathloss model changes and a penetration loss is considered. For details on the model, see Subclause 7.4.3. Here, the focus is on modelling aspects with respect to spatial consistency. As described in Subclause 7.4.3, the penetration loss deviation σ_p represents variations within and between buildings of the same type. For spatial consistency this can be modeled as a spatially consistent random variable with correlation distance 10m, see Subclause 7.6.3.1. The "building type" is determined using a spatially consistent uniform random variable with correlation distance 50 m. The building type is determined by comparing the random variable with P_1 , where P_1 is the probability of the building type with low loss penetration. If the realization of the random variable is less than P_1 , the building type is low loss; otherwise the building type is high loss.

The cluster-specific and ray-specific random variables as defined in Subclause 7.6.3.1 on the same floor are generated in the spatial consistency modelling; otherwise, these variables across different floors are uncorrelated.

In case there is a transition from LOS to NLOS due to UT mobility, there will be a hard transition in the channel response. This is because pathloss and LS parameters are different for these states, leading automatically to very different channel realizations. To circumvent such hard transitions the optional soft LOS state can be considered to determine the PL and the channel impulse responses containing characteristics of both LOS and NLOS. Soft LOS state

LOS_{soft} is generated by floating numbers between 0 (NLOS) and 1 (LOS) in the spatial consistency modelling. The value of LOS_{soft} is determined by

$$LOS_{soft} = \frac{1}{2} + \frac{1}{\pi} \arctan \left(\sqrt{\frac{20}{\lambda}} (G + F(d)) \right) \quad (7.6-18)$$

$$LOS_{soft} = \frac{1}{2} + \frac{1}{\pi} \arctan \left(\sqrt{\frac{d_{LOS}}{\lambda}} (G + F(d)) \right) \quad \text{where:}$$

- G is a spatially consistent Gaussian random variable with correlation distance according to Table 7.6.3.1-2;

- $F(d) = \sqrt{2} \operatorname{erf}^{-1}(2 \operatorname{Pr}_{\text{LOS}}(d) - 1)$ $F(d) = \sqrt{2} \operatorname{erf}^{-1}(2 P_{\text{LOS}}(d) - 1)$; and
- $\operatorname{Pr}_{\text{LOS}}(d)$ $P_{\text{LOS}}(d)$ is the distance dependent LOS probability function.

After LOS_{soft} is obtained, Steps 2-12 of the channel coefficient generation described in Subclause 7.5 are performed twice, once with the propagation condition in Step 2 set as LOS and once with the propagation condition in Step 2 set as NLOS. The resulting channel coefficients are denoted as H^{LOS} and H^{NLOS} respectively, where H^{LOS} is generated with the LOS path loss formula and channel model parameters while H^{NLOS} is generated using the NLOS path loss formula and channel model parameters. The channel matrix H with soft LOS state is determined from a linear combination of H^{LOS} and H^{NLOS} as:

$$H(\text{LOS}_{\text{soft}}) = H^{\text{LOS}} \text{LOS}_{\text{soft}} + H^{\text{NLOS}} \sqrt{1 - \text{LOS}_{\text{soft}}^2} \quad (7.6-19)$$

It is noted that soft indoor/outdoor states are not modelled in this TR. Thus the model does not support transitions between indoor/outdoor states in mobility simulations.

7.6.3.4 Applicability of spatial consistency

According to the characteristics of different cluster specific parameters and ray specific parameters, the following types on spatial consistency are defined:

- Site-specific: parameters for different BS-UT links are uncorrelated, but the parameters for links from co-sited sectors to a UT are correlated.
- All-correlated: BS-UT links are correlated.

In Table 7.6.3.4-1, correlation type for each large scale parameter, cluster specific parameter and ray specific parameter is clarified.

Table 7.6.3.4-1: Correlation type among TRPs

Parameters	Correlation type
Delays	Site-specific
Cluster powers	Site-specific
AOA/ZOA/AOD/ZOD offset	Site-specific
AOA/ZOA/AOD/ZOD sign	Site-specific
Random coupling	Site-specific
XPR	Site-specific
Initial random phase	Site-specific
LOS/NLOS states	Site-specific
Blockage (Model A)	All-correlated
O2I penetration loss	All-correlated
Indoor distance	All-correlated
Indoor states	All-correlated

Spatial consistency is not modelled in the following situations:

- Different link types, e.g., outdoor LOS, outdoor NLOS or O2I
- UE locates on different floors

Table 7.6.3.4-2, lists conditions in which each large scale parameter, cluster specific parameter and ray specific parameter is assumed not spatially correlated.

Table 7.6.3.4-2: Conditions when parameters are not spatially correlated.

Parameters	Uncorrelated states
Delays	Outdoor LOS/outdoor NLOS/O2I (different floors)
Cluster powers	Outdoor LOS/outdoor NLOS/O2I (different floors)
AOA/ZOA/AOD/ZOD offset	Outdoor LOS/outdoor NLOS/O2I (different floors)
AOA/ZOA/AOD/ZOD sign	Outdoor LOS/outdoor NLOS/O2I (different floors)
Random coupling	Outdoor LOS/outdoor NLOS/O2I (different floors)
XPR	Outdoor LOS/outdoor NLOS/O2I (different floors)
Initial random phase	Outdoor LOS/outdoor NLOS/O2I (different floors)
Blockage	Outdoor/O2I (different floors)
Standard deviation for O2I penetration loss	Different building types, i.e., high/low loss

7.6.4 Blockage

Blockage modelling is an add-on feature to the channel model. The method described in the following applies only when this feature is turned on. In addition, the temporal variability of the blockage modelling parameters is on-demand basis. It is also noted that the modelling of the blockage does not change LOS/NLOS state of each link.

When blockage model is applied, the channel generation in Subclause 7.5 should have several additional steps between Step 9 and 10 as illustrated in Figure 7.6.4-1.

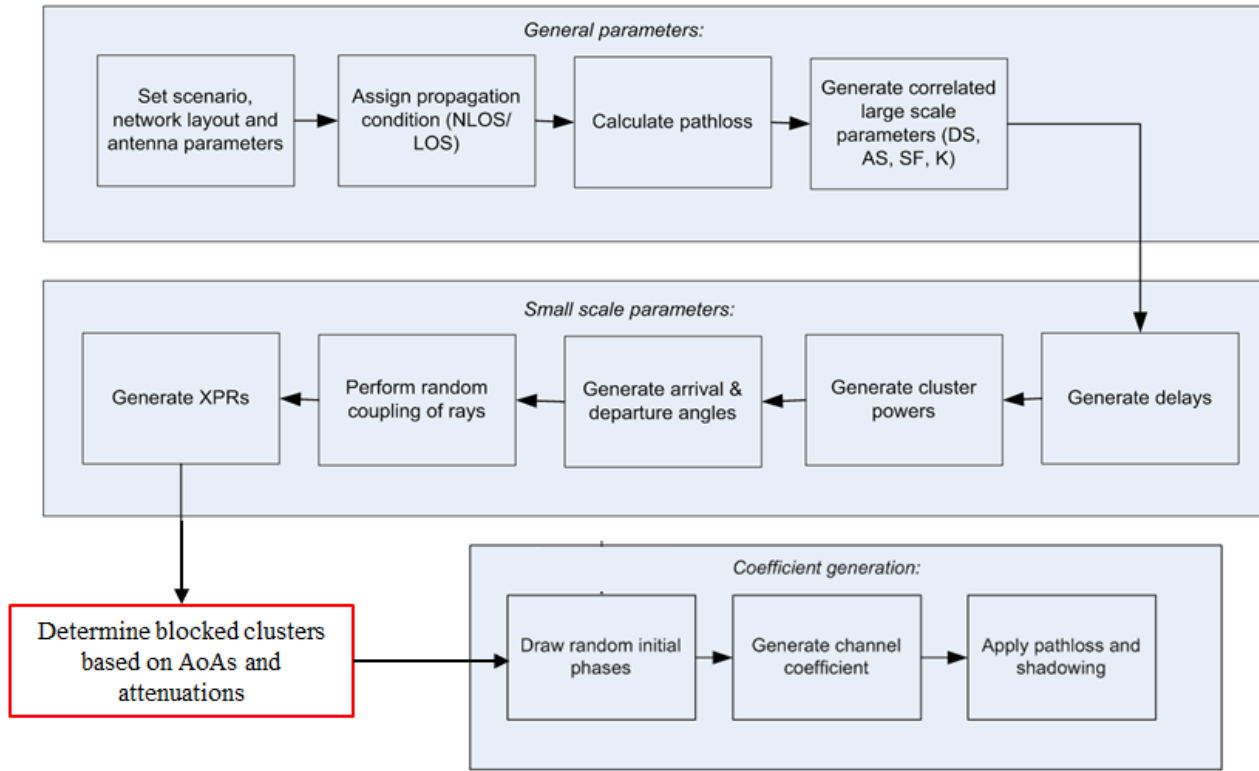


Figure.7.6.4-1 Channel generation procedure with blockage model

Two alternative models (Model A and Model B) are provided for the blockage modelling. Both approaches have their own use cases. Model A is applicable when a generic and computationally efficient blockage modelling is desired. Model B is applicable when a specific and more realistic blocking modelling is desired.

7.6.4.1 Blockage model A

Model A adopts a stochastic method for capturing human and vehicular blocking.

Step a: Determine the number of blockers.

Multiple 2-dimensional (2D) angular blocking regions, in terms of centre angle, azimuth and elevation angular span are generated around the UT. There is one self-blocking region, and $K = 4$ non-self-blocking regions, where K may be changed for certain scenarios (e.g., higher blocker density). Note that the self-blocking component of the model is important in capturing the effects of human body blocking.

Step b: Generate the size and location of each blocker.

For self-blocking, the blocking region in UT LCS is defined in terms of elevation and azimuth angles, $(\theta'_{sb}, \varphi'_{sb})$ and azimuth and elevation angular span (x_{sb}, y_{sb}) .

$$\left\{ (\theta', \varphi') \left| \left(\theta'_{sb} - \frac{y_{sb}}{2} \leq \theta' \leq \theta'_{sb} + \frac{y_{sb}}{2}, \varphi'_{sb} - \frac{x_{sb}}{2} \leq \varphi' \leq \varphi'_{sb} + \frac{x_{sb}}{2} \right) \right. \right\} \quad (7.6-20)$$

where the parameters are described in Table 7.6.4.1-1.

Table 7.6.4.1-1: Self-blocking region parameters.

	φ'_{sb}	x_{sb}	θ'_{sb}	y_{sb}
Portrait mode	260°	120°	100°	80°
Landscape mode	40°	160°	110°	75°

For non-self-blocking $k = 1, \dots, 4$, the blocking region in GCS is defined by

$$\left\{ (\theta, \varphi) \mid \left(\theta_k - \frac{y_k}{2} \leq \theta \leq \theta_k + \frac{y_k}{2}, \varphi_k - \frac{x_k}{2} \leq \varphi \leq \varphi_k + \frac{x_k}{2} \right) \right\} \quad (7.6-21)$$

where the parameters are described in Table 7.6.4.1-2, as well as the distance r between the UT and the blocker.

Table 7.6.4.1-2: Blocking region parameters.

Blocker index ($k = 1, \dots, 4$)	φ_k	x_k	θ_k	y_k	r
InH scenario	Uniform in [0°, 360°]	Uniform in [15°, 45°]	90°	Uniform in [5°, 15°]	2 m
UMi, UMa, RMa scenarios	Uniform in [0°, 360°]	Uniform in [5°, 15°]	90°	5°	10 m

Step c: Determine the attenuation of each cluster due to blockers.

The attenuation of each cluster due to self-blocking corresponding to the centre angle pair $(\theta'_{sb}, \varphi'_{sb})$, is 30 dB provided that $|\varphi_{AoA} - \varphi_1| < \frac{x_1}{2}$, $|\varphi'_{AoA} - \varphi'_{sb}| < \frac{x_{sb}}{2}$ and $|\theta_{ZoA} - \theta_1| < \frac{y_1}{2}$, $|\theta'_{ZoA} - \theta'_{sb}| < \frac{y_{sb}}{2}$. Otherwise, the attenuation is 0 dB.

The attenuation of each cluster due to the non-self-blocking regions ($k=1, \dots, 4$) is given by

$$L_{dB} = -20 \log_{10} \left(1 - (F_{A_1} + F_{A_2}) (F_{Z_1} + F_{Z_2}) \right) \quad (7.6-22)$$

provided that $|\varphi_{AoA} - \varphi_k| < x_k$, $|\varphi_{AoA} - \varphi_k| < x_k$ and $|\theta_{ZoA} - \theta_k| < y_k$, $|\theta_{ZoA} - \theta_k| < y_k$. Otherwise, the attenuation is 0 dB. The terms in the above equation are given as

$$F_{A_1|A_2|Z_1|Z_2} = \frac{\tan^{-1} \left(\pm \frac{\pi}{2} \sqrt{\frac{\pi}{\lambda} r \left(\frac{1}{\cos(A_1|A_2|Z_1|Z_2)} - 1 \right)} \right)}{\pi} \quad (7.6-23)$$

where

$$A_1 = \varphi_{AoA} - \left(\varphi_k + \frac{x_k}{2} \right), \quad (7.6-24)$$

$$A_2 = \varphi_{AoA} - \left(\varphi_k - \frac{x_k}{2} \right), \quad (7.6-25)$$

$$Z_1 = \theta_{ZoA} - \left(\theta_k + \frac{y_k}{2} \right), \quad (7.6-26)$$

$$Z_2 = \theta_{\text{ZOA}} - \left(\theta_k - \frac{y_k}{2} \right). \quad (7.6-27)$$

In the above formula for $F_{A_1|A_2|Z_1|Z_2}$, λ is the wavelength. The appropriate signs (\pm) within the \tan^{-1} term are described in Table 7.6.4.1-3.

Table 7.6.4.1-3: Description of signs

	$-y_k < \theta_{\text{ZOA}} - \theta_k \leq -\frac{y}{2}$	$-\frac{y_k}{2} < \theta_{\text{ZOA}} - \theta_k \leq \frac{y}{2}$	$\frac{y_k}{2} < \theta_{\text{ZOA}} - \theta_k \leq y$
$\frac{x_k}{2} < \varphi_{\text{AOA}} - \varphi_k \leq x_k$	(-, +) for (A_1, A_2) (+, -) for (Z_1, Z_2)	(-, +) for (A_1, A_2) (A_1, A_2) (+, +) for (Z_1, Z_2)	(-, +) for (A_1, A_2) (A_1, A_2) (-, +) for (Z_1, Z_2) (Z_1, Z_2)
$-\frac{x_k}{2} < \varphi_{\text{AOA}} - \varphi_k \leq \frac{x}{2}$	(+, +) for (A_1, A_2) (A_1, A_2) (+, -) for (Z_1, Z_2)	(+, +) for (A_1, A_2) (A_1, A_2) (+, +) for (Z_1, Z_2) (Z_1, Z_2)	(+, +) for (A_1, A_2) (A_1, A_2) (-, +) for (Z_1, Z_2) (Z_1, Z_2)
$-x_k < \varphi_{\text{AOA}} - \varphi_k \leq -\frac{x}{2}$	(+, -) for (A_1, A_2) (A_1, A_2) (+, -) for (Z_1, Z_2) (Z_1, Z_2)	(+, -) for (A_1, A_2) (A_1, A_2) (+, +) for (Z_1, Z_2) (Z_1, Z_2)	(+, -) for (A_1, A_2) (A_1, A_2) (-, +) for (Z_1, Z_2) (Z_1, Z_2)

Step d: Spatial and temporal consistency of each blocker.

The centre of the blocker is generated based on a uniformly distributed random variable, which is temporally and spatially consistent. The two-dimensional autocorrelation function $R(\Delta_x, \Delta_t) = R(\Delta_x, \Delta_t)$ can be described with sufficient accuracy by the exponential function

$$R(\Delta_x, \Delta_t) = \exp \left(- \left(\frac{|\Delta_x|}{d_{\text{corr}}} + \frac{|\Delta_t|}{t_{\text{corr}}} \right) \right) \quad (7.6-28)$$

The spatial correlation distance d_{corr} for the random variable determining the centre of the blocker is given in Table 7.6.4.1-4 for different scenarios.

Table 7.6.4.1-4: Spatial correlation distance for different scenarios.

Spatial correlation distance d_{corr} in [m] for the random variable determining the centre of the blocker	UMi			UMa			RMa			InH	
	LOS	NLOS	O2I	LOS	NLOS	O2I	LOS	NLOS	O2I	LOS	NLOS
	10	10	5	10	10	5	10	10	5	5	5

The correlation time is defined by $t_{\text{corr}} = d_{\text{corr}} / v$, where v is the speed of the moving blocker.

Note: The rectangular blocker description is chosen for self-blocking region with the specific choices of $(\theta'_{sb}, \phi'_{sb})$ assumed here. Generalization of this description to other choices should be done with care as the rectangular description may not be accurate.

7.6.4.2 Blockage model B

Model B adopts a geometric method for capturing e.g., human and vehicular blocking.

Step a: Determine blockers

A number, K , of blockers are modelled as rectangular screens that are physically placed on the map. Each screen has the dimension by height (h_k) and width (w_k), with the screen centre at coordinate (x_k, y_k, z_k) .

Note:

- The number of blockers (K), their vertical and horizontal extensions (h_k and w_k), locations (x_k, y_k, z_k) , density, and movement pattern (if non-stationary) are all simulation assumptions, to allow different blocking scenarios to be constructed depending on the need of the particular simulation study.

Recommended parameters for typical blockers are provided in Table 7.6.4.2-5.

- The blocking effect diminishes with increasing distance to the blocker. For implementation purposes it may be sufficient to consider only the K nearest blockers or the blockers closer than some distance from a specific UT.

Table 7.6.4.2-5: Recommended blocker parameters

	Typical set of blockers	Blocker dimensions	Mobility pattern
Indoor; Outdoor; InF	Human	Cartesian: w=0.3m; h=1.7m	Stationary or up to 3 km/h
Outdoor	Vehicle	Cartesian: w=4.8m; h=1.4m	Stationary or up to 100 km/h
InF	AGV	Cartesian: w=3m; h=1.5m	Up to 30 km/h
InF	Industrial robot	Cartesian: w=2m; h=0.2m	Up to 3 m/s

Step b: Determine the blockage attenuation per sub-path

Attenuation caused by each blocker to each sub-path is modelled using a simple knife edge diffraction model and is given by

$$L_{dB} = -20 \log_{10} \left(1 - (F_{h_1} + F_{h_2})(F_{w_1} + F_{w_2}) \right) \quad (7.6-29)$$

where F_{h_1} , F_{h_2} and F_{w_1} , F_{w_2} account for knife edge diffraction at the four edges, and are given by

$$F_{h_1|h_2|w_1|w_2} = \begin{cases} \frac{\tan^{-1} \left(\pm \frac{\pi}{2} \sqrt{\frac{\pi}{\lambda} (D1_{h_1|h_2|w_1|w_2} + D2_{h_1|h_2|w_1|w_2} - r)} \right)}{\pi}, & \text{for direct path in LOS} \\ \frac{\tan^{-1} \left(\pm \frac{\pi}{2} \sqrt{\frac{\pi}{\lambda} (D1_{h_1|h_2|w_1|w_2} - r')} \right)}{\pi}, & \text{for all other paths} \end{cases} \quad (7.6-30)$$

where λ is the wave length. As shown in Figure 7.6.4.2-2, $D1_{h1|h2|w1 \vee w2}$ and $D1_{h1|h2|w1|w2}$ are the projected (onto the side and top view planes) distances between the receiver and four edges of the corresponding blocker, and $D2_{h1|h2|w1 \vee w2}$ and $D2_{h1|h2|w1|w2}$ are the projected (onto the side and top view planes) distances between the transmitter and four edges of the corresponding blocker. The side view plane is perpendicular to the horizontal ground plane. The top view is perpendicular to the side view. For each cluster, the blocker screen is rotated around its centre such that the arrival direction of the corresponding path is always perpendicular to the screen. It should be noted that different rotations are required for each individual sub-path. Meanwhile, the base and top edges of the screens are always parallel to the horizontal plane. As the screen is perpendicular to each sub-path, r is the distance between the transmitter and receiver for the direct path in LOS, and r' is the distance between the blocker screen and receiver, projected onto the incoming sub-path direction, for all the other (NLOS) paths. In the equation of $F_{h1|h2|w1|w2}$, the plus and minus signs are determined in such a way that, as shown in Figure 7.6.4.2-2,

- if the sub-path (terminated at the receiver or transmitter) does not intersect the screen in side view, minus sign is applied for the shortest path among $D1_{h1}$ and $D1_{h2}$ in the NLOS case ($D1_{h1} + D2_{h1}$ and $D1_{h2} + D2_{h2}$ in the LOS case) and plus sign is applied for the other edge.
- if the sub-path (terminated at the receiver or transmitter) does not intersect the screen in top view, minus sign is applied for the shortest path among $D1_{w1}$ and $D1_{w2}$ in the NLOS case ($D1_{w1} + D2_{w1}$ and $D1_{w2} + D2_{w2}$ for the LOS case) and plus sign is applied for the other edge.
- if the sub-path intersects the screen plus signs are applied for both edges.

For the case of multiple screens the total loss is given by summing the losses of each contributing screen in dB units.

The model according to option B is consistent in time, frequency and space, and is more appropriate to be used for simulations with arbitrarily designated blocker density.

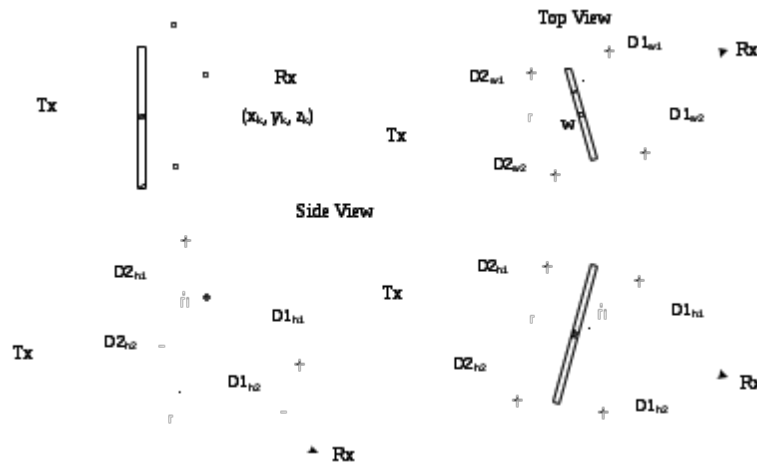


Figure 7.6.4.2-2(a): Illustration of the geometric relation among blocker, receiver and transmitter for the LOS path

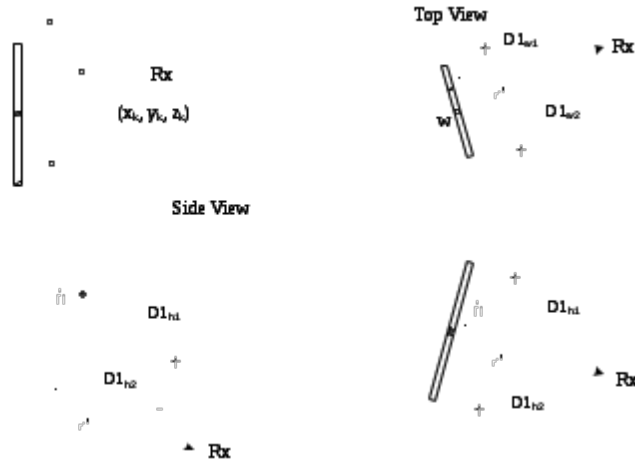


Figure 7.6.4.2-2(b): Illustration of the geometric relation between blocker and receiver for NLOS paths

7.6.5 Correlation modelling for multi-frequency simulations

This subclause describes how to generate parameters to reflect correlation across different frequencies for a BS-UT link, for simulations involved with multiple frequencies.

For those simulations, the steps in Subclause 7.5 should be revised according to the following:

- The parameters generated in Step 1 are the same for all the frequencies, except for antenna patterns, array geometries, system center frequency and bandwidth.
- Propagation conditions generated in Step 2 are the same for all the frequencies. It is noted that soft LOS states may be different due to frequency dependent function.
- The parameters generated in Step 4 are the same for all the frequencies, except for possibly frequency-dependent scaling of e.g. delay spread and angular spreads according to the LSP tables. I.e. let x be a random variable drawn from a Gaussian distribution: $x \sim N(0,1)$. Then the delay spread at frequency f is $DS(f) = 10^{(\mu_{lgDS}(f) + \sigma_{lgDS}(f) \cdot x)}$, where the same value of x is used for all frequencies. A corresponding procedure applies to each of the angular spreads.
- The cluster delays and angles resulting from Steps 5-7 are the same for all frequency bands
- Per-cluster shadowing Z_n in Step 6 are independently generated for the frequency bands.
- Cluster powers in Step 6 may be frequency-dependent.
- Steps 8-11 are independently applied for the frequency bands.

In addition, when blockage is modeled according to Subclause 7.6.4, the positions of blockers are the same across all the frequencies.

Note: The requirements above may not be fully aligned with the behavior of the model according to Subclause 7.5, since cluster delays and angles will be frequency-dependent in scenarios where the DS or AS is frequency-dependent. The procedure below may alternatively be used to ensure that cluster delays and angles are frequency-independently generated.

7.6.5.1 Alternative channel generation method

The alternative method replaces Steps 5-7 in Subclause 7.5 with the below Steps 5'-7'. The inputs to the alternative method are the delay and angular spreads determined according to Step 4 at an anchor frequency, e.g. 2 GHz: DS_0 , ASD_0 , ASA_0 , ZSD_0 , ZSA_0 , the delay and angular spreads determined according to Step 4 at a frequency of interest: DS , ASD , ASA , ZSD , ZSA , and the number of clusters N from Table 7.5-6.

Step 5': Generate nominal delays τ'_n and angles $\phi'_{AOD,n}$, $\phi'_{AOA,n}$, $\theta'_{ZOD,n}$, $\theta'_{ZOA,n}$.

Generate N delays from a single-sided exponential distribution with zero mean and standard deviation of $r \cdot DS_0$, according to $\tau'_n = -r \cdot DS_0 \ln(X_n)$ with $X_n \sim \text{unif}(0, 1)$.

Generate N AODs from a wrapped Gaussian distribution with zero mean and standard deviation of $r \cdot ASD_0$, according to $\phi'_{AOD,n} = \arg(\exp(-j \cdot r \cdot ASD_0 Y_n))$ with $Y_n \sim N(0, 1)$.

Generate N AOAs from a wrapped Gaussian distribution with zero mean and standard deviation of $r \cdot ASA_0$, according to $\phi'_{AOA,n} = \arg(\exp(-j \cdot r \cdot ASA_0 Z_n))$ with $Z_n \sim N(0, 1)$.

Generate N ZODs from a wrapped Laplacian distribution with zero mean and standard deviation of $r \cdot ZSD_0$, according to $\theta'_{ZOD,n} = \arg(\exp(-j \cdot r \cdot ZSD_0 \text{sgn}(V_n - 0.5) \ln(1 - 2|V_n - 0.5|/\sqrt{2})))$ with $V_n \sim \text{unif}(0, 1)$.

Generate N ZOAs from a wrapped Laplacian distribution with zero mean and standard deviation of $r \cdot ZSA_0$, according to $\theta'_{ZOA,n} = \arg(\exp(-j \cdot r \cdot ZSA_0 \text{sgn}(W_n - 0.5) \ln(1 - 2|W_n - 0.5|/\sqrt{2})))$ with $W_n \sim \text{unif}(0, 1)$.

r is a proportionality factor, $r=1.5$. The principal value of the arg function should be used, e.g. $(-180, 180)$.

In case of LOS, set $\tau'_1=0$, $\phi'_{AOD,1}=0$, $\phi'_{AOA,1}=0$, $\theta'_{ZOD,1}=0$, and $\theta'_{ZOA,1}=0$.

Step 6': Generate cluster powers P_n .

Generate cluster powers as

$$P'_n = \exp\left(-\tau'_n g_{DS} - \left(\frac{\phi'_{AOD,n} g_{ASD}}{\sqrt{2}}\right)^2 - \left(\frac{\phi'_{AOA,n} g_{ASA}}{\sqrt{2}}\right)^2 - \sqrt{2}|\theta'_{ZOD,n}|g_{ZSD} - \sqrt{2}|\theta'_{ZOA,n}|g_{ZSA}\right) \cdot 10^{-Q_n/10} \quad (7.6.30a)$$

where $Q_n \sim N(0, \zeta^2)$ is the per cluster shadowing term in [dB] and

$$g_{DS} = \frac{\max(r \cdot DS_0 - DS, 0)}{DS \cdot r \cdot DS_0} \quad (7.6.30b)$$

$$g_{ASD} = \frac{\sqrt{\max((r \cdot ASD_0)^2 - ASD^2, 0)}}{ASD \cdot r \cdot ASD_0} \quad (7.6.30c)$$

$$g_{ASA} = \frac{\sqrt{\max((r \cdot ASA_0)^2 - ASA^2, 0)}}{ASA \cdot r \cdot ASA_0} \quad (7.6.30d)$$

$$g_{\text{ZSD}} = \frac{\max(r \cdot \text{ZSD}_0 - \text{ZSD}, 0)}{\text{ZSD} \cdot r \cdot \text{ZSD}_0} \quad (7.6.30\text{e})$$

$$g_{\text{ZSA}} = \frac{\max(r \cdot \text{ZSA}_0 - \text{ZSA}, 0)}{\text{ZSA} \cdot r \cdot \text{ZSA}_0} \quad (7.6.30\text{f})$$

Normalize the cluster powers so that the sum of all cluster powers is equal to one, i.e.,

$$P_n = \frac{P'_n}{\sum_{n=1}^N P'_n} \quad (7.6.30\text{g})$$

or, in the case of LOS, so that

$$P_n = \frac{1}{1+K_R} \frac{P'_n}{\sum_{n=1}^N P'_n} + \frac{K_R}{1+K_R} \delta(n-1) \quad (7.6.30\text{h})$$

where K_R is the K-factor converted to linear scale.

Step 7': Generate delays τ_n and angles $\varphi_{\text{AOD},n}$, $\varphi_{\text{AOA},n}$, $\theta_{\text{ZOD},n}$, $\theta_{\text{ZOA},n}$.

$$\tau_n = \begin{cases} \tau'_n & , \text{for NLOS} \\ \sqrt{1 + \frac{K_R}{2}} \tau'_n & , \text{for LOS} \end{cases} \quad (7.6.30\text{i})$$

$$\varphi_{n,m,\text{AOA}} = \begin{cases} \varphi'_{n,\text{AOA}} + \varphi_{\text{LOS},\text{AOA}} + c_{\text{ASA}} \alpha_m & , \text{for NLOS} \\ \sqrt{1+K_R} \varphi'_{n,\text{AOA}} + \varphi_{\text{LOS},\text{AOA}} + c_{\text{ASA}} \alpha_m & , \text{for LOS} \end{cases} \quad (7.6.30\text{j})$$

$$\varphi_{n,m,\text{AOD}} = \begin{cases} \varphi'_{n,\text{AOD}} + \varphi_{\text{LOS},\text{AOD}} + c_{\text{ASD}} \alpha_m & , \text{for NLOS} \\ \sqrt{1+K_R} \varphi'_{n,\text{AOD}} + \varphi_{\text{LOS},\text{AOD}} + c_{\text{ASD}} \alpha_m & , \text{for LOS} \end{cases} \quad (7.6.30\text{k})$$

$$\theta_{n,m,\text{ZOA}} = \begin{cases} \theta'_{n,\text{ZOA}} + \theta_{\text{LOS},\text{ZOA}} + c_{\text{ZSA}} \alpha_m & , \text{for NLOS} \\ \sqrt{1+K_R} \theta'_{n,\text{ZOA}} + \theta_{\text{LOS},\text{ZOA}} + c_{\text{ZSA}} \alpha_m & , \text{for LOS} \end{cases} \quad (7.6.30\text{l})$$

$$\theta_{n,m,\text{ZOD}} = \begin{cases} \theta'_{n,\text{ZOD}} + \theta_{\text{LOS},\text{ZOD}} + c_{\text{ZSD}} \alpha_m & , \text{for NLOS} \\ \sqrt{1+K_R} \theta'_{n,\text{ZOD}} + \theta_{\text{LOS},\text{ZOD}} + c_{\text{ZSD}} \alpha_m & , \text{for LOS} \end{cases} \quad (7.6.30\text{m})$$

Repeat Steps 6'-7' for each frequency of interest, reusing the delays and angles from Step 5' for all frequencies.

Note: The resulting delay and angular spreads of channels generated with this alternative method will be similar but not identical to when using Steps 5-7 in Subclause 7.5.

7.6.6 Time-varying Doppler shift

The Doppler shift generally depends on the time evolution of the channel as it is defined as the derivative of the channels phase over time. It can be the result from Tx, Rx, or scatterer movement. The more general form of the exponential Doppler term as used in Equation (7.5-22) is given by

$$\exp\left(j2\pi\int_{t_0}^t \frac{\hat{r}_{rx,n,m}^T(\tilde{t}) \cdot \vec{v}(\tilde{t})}{\lambda_0} d\tilde{t}\right) \quad (7.6-31)$$

Here, $\hat{r}_{rx,n,m}(t)$ is the normalized vector that points into the direction of the incoming wave as seen from the Rx at time t . $\vec{v}(t)$ denotes the velocity vector of the Rx at time t , while t_0 denotes a reference point in time that defines the initial phase, e.g. $t_0=0$.

Note that Equation (7.5-22) only holds for time-invariant Doppler shift, i.e. $\hat{r}_{rx,n,m}^T(t) \cdot \vec{v}(t) = \hat{r}_{rx,n,m}^T \cdot \vec{v}$.

7.6.7 UT rotation

UT rotation modelling is an add-on feature. When modelled, Step 1 in Subclause 7.5 shall consider UT rotational motion.

Step 1:

Add: h) Give rotational motion of UT in terms of its bearing angle, downtilt angle and slant angle.

7.6.8 Explicit ground reflection model

In case the ground reflection shall be modelled explicitly, Equation (7.5-30) has to be replaced by

$$H_{u,s}^{\text{LOS}}(\tau, t) = \sqrt{\frac{1}{K_R + 1}} H_{u,s}^{\text{NLOS}}(\tau - \tau_{\text{LOS}}, t) + \sqrt{\frac{K_R}{K_R + 1}} \left(H_{u,s,1}^{\text{LOS}}(t) \delta(\tau - \tau_{\text{LOS}}) + \frac{d_{3D}}{d_{\text{GR}}} H_{u,s}^{\text{GR}}(t) \delta(\tau - \tau_{\text{GR}}) \right) \quad (7.6-32)$$

with the delays for the ground reflected and the LOS paths being defined by their lengths, according to the Tx-Rx separation d_{2D} and the Tx and Rx heights h_{tx} and h_{rx} respectively, as

$$\tau_{\text{GR}} = \frac{d_{\text{GR}}}{c} = \frac{\sqrt{(h_{\text{tx}} + h_{\text{rx}})^2 + d_{2D}^2}}{c}, \quad (7.6-33)$$

and

$$\tau_{\text{LOS}} = \frac{d_{3D}}{c} = \frac{\sqrt{(h_{\text{tx}} - h_{\text{rx}})^2 + d_{2D}^2}}{c}. \quad (7.6-34)$$

The channel coefficient for the ground reflected path is given by

$$H_{u,s}^{\text{GR}}(t) = \begin{bmatrix} F_{\text{rx},u,\theta}(\theta_{\text{GR,ZOA}}, \varphi_{\text{GR,AOA}}) \\ F_{\text{rx},u,\varphi}(\theta_{\text{GR,ZOA}}, \varphi_{\text{GR,AOA}}) \end{bmatrix}^T \begin{bmatrix} R_{\parallel}^{\text{GR}} & 0 \\ 0 & -R_{\perp}^{\text{GR}} \end{bmatrix} \begin{bmatrix} F_{\text{tx},s,\theta}(\theta_{\text{GR,ZOD}}, \varphi_{\text{GR,AOD}}) \\ F_{\text{tx},s,\varphi}(\theta_{\text{GR,ZOD}}, \varphi_{\text{GR,AOD}}) \end{bmatrix} \\ \cdot \exp\left(-j2\pi \frac{d_{\text{GR}}}{\lambda_0}\right) \exp\left(j2\pi \frac{\hat{r}_{\text{rx,GR}}^T \cdot \bar{d}_{\text{rx},u}}{\lambda_0}\right) \exp\left(j2\pi \frac{\hat{r}_{\text{tx,GR}}^T \cdot \bar{d}_{\text{tx},s}}{\lambda_0}\right) \exp\left(j2\pi \frac{\hat{r}_{\text{rx,GR}}^T \cdot \bar{v}}{\lambda_0} t\right) \quad (7.6-35)$$

with the normalized vectors pointing towards the ground reflection point from the Tx

$$\hat{r}_{\text{tx,GR}} = e_r(\theta_{\text{GR,ZOD}}, \varphi_{\text{GR,AOD}}) = \begin{bmatrix} \sin \theta_{\text{GR,ZOD}} \cos \varphi_{\text{GR,AOD}} \\ \sin \theta_{\text{GR,ZOD}} \sin \varphi_{\text{GR,AOD}} \\ \cos \theta_{\text{GR,ZOD}} \end{bmatrix} \quad (7.6-36)$$

and from the Rx side

$$\hat{r}_{\text{rx,GR}} = e_r(\theta_{\text{GR,ZOA}}, \varphi_{\text{GR,AOA}}) = \begin{bmatrix} \sin \theta_{\text{GR,ZOA}} \cos \varphi_{\text{GR,AOA}} \\ \sin \theta_{\text{GR,ZOA}} \sin \varphi_{\text{GR,AOA}} \\ \cos \theta_{\text{GR,ZOA}} \end{bmatrix} . \quad (7.6-37)$$

The angles for the ground reflected path are given by the geometry assuming a flat surface with its normal pointing into z-direction. The angles at the Tx side can be determined by

$$\theta_{\text{GR,ZOD}} = 180^\circ - \text{atan}\left(\frac{d_{2D}}{h_{\text{tx}} + h_{\text{tx}}}\right) \quad (7.6-37a)$$

$$\varphi_{\text{GR,AOD}} = \varphi_{\text{LOS,AOD}} \quad (7.6-37b)$$

and at the Rx side by

$$\theta_{\text{GR,ZOA}} = \theta_{\text{GR,ZOD}} \quad (7.6-37c)$$

$$\varphi_{\text{GR,AOA}} = \varphi_{\text{GR,AOD}} + 180^\circ . \quad (7.6-37d)$$

The reflection coefficients for parallel and perpendicular polarization on the ground, cf. [21], are given by

$$R_{\parallel}^{\text{GR}} = \frac{\frac{\epsilon_{\text{GR}}}{\epsilon_0} \cos(\theta_{\text{GR,ZOD}}) + \sqrt{\frac{\epsilon_{\text{GR}}}{\epsilon_0} - \sin^2(\theta_{\text{GR,ZOD}})}}{\frac{\epsilon_{\text{GR}}}{\epsilon_0} \cos(\theta_{\text{GR,ZOD}}) - \sqrt{\frac{\epsilon_{\text{GR}}}{\epsilon_0} - \sin^2(\theta_{\text{GR,ZOD}})}} , \quad (7.6-38)$$

and

$$R_{\perp}^{\text{GR}} = \frac{\cos(\theta_{\text{GR,ZOD}}) + \sqrt{\frac{\epsilon_{\text{GR}}}{\epsilon_0} - \sin^2(\theta_{\text{GR,ZOD}})}}{\cos(\theta_{\text{GR,ZOD}}) - \sqrt{\frac{\epsilon_{\text{GR}}}{\epsilon_0} - \sin^2(\theta_{\text{GR,ZOD}})}} , \quad (7.6-39)$$

with the complex relative permittivity of the ground material given by

$$\frac{\varepsilon_{\text{GR}}}{\varepsilon_0} = \varepsilon_r - j \frac{\sigma}{2\pi f_c \varepsilon_0} \quad (7.6-40)$$

The electric constant ε_0 is given by $8.854187817... \times 10^{-12} \text{ F}\cdot\text{m}^{-1}$.

For applicable frequency ranges, the real relative permittivity can be modelled by

$$\varepsilon_r = a_\varepsilon \cdot \left(\frac{f_c}{10^9} \right)^{b_\varepsilon}, \quad (7.6-41)$$

while the conductivity in [S/m] may be modelled by

$$\sigma = c_\sigma \cdot \left(\frac{f_c}{10^9} \right)^{d_\sigma}, \quad (7.6-42)$$

with f_c being the center frequency in Hz.

A selection of material properties from [19] is given below. Since the simplified models for conductivity and relative permittivity are only applicable for frequencies between 1 and 10 GHz, Figure 7.6.8-1 presents curves up to 100 GHz at least for very, medium dry and wet ground, cf. [20].

Table 7.6.8-1 Material properties [19]

Material class	Relative permittivity		Conductivity		Frequency range in [GHz]
	a_ε	b_ε	c_σ	d_σ	
Concrete	5.31	0	0.0326	0.809 5	1-100
Brick	3.75	0	0.038	0	1-10
Plasterboard	2.94	0	0.0116	0.707 6	1-100
Wood	1.99	0	0.0047	1.071 8	0.001-100
Floorboard	3.66	0	0.0044	1.351 5	50-100
Metal	1	0	10^7	0	1-100
Very dry ground	3	0	0.0001 5	2.52	1-10
Medium dry ground	15	-0.1	0.035	1.63	1-10
Wet ground	30	-0.4	0.15	1.30	1-10

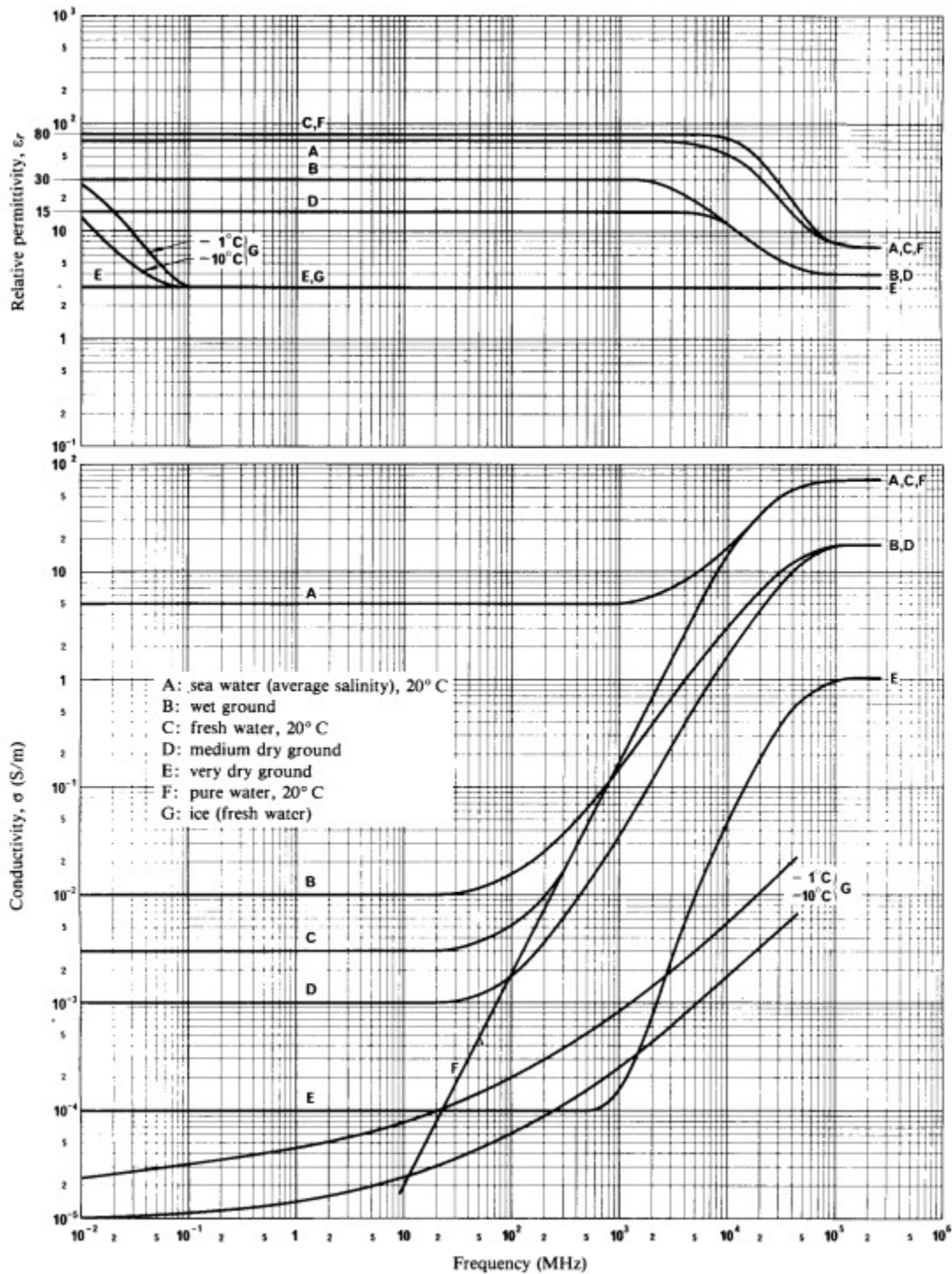


Figure 7.6.8-1: Relative permittivity and conductivity as a function of frequency [20]

7.6.9 Absolute time of arrival

To support simulations in which absolute time of arrival is important, the propagation time delay due to the total path length is considered in step 11 of the fast fading model as follows. The impulse response in NLOS is determined using equation (7.6-43) instead of (7.5-27) and the impulse response in LOS is determined using equation (7.6-44) instead of (7.5-30), where c is the speed of light. $\Delta\tau$ is generated from a lognormal distribution with parameters according to Table 7.6.9-1. $\Delta\tau$ is generated independently for links between the same UT and different BS sites. The excess delay in NLOS, $\Delta\tau$, should further be upper bounded by $2L/c$, where L is the largest dimension of the factory hall, i.e. $L = \max(\text{length, width, height})$.

$$H_{u,s}^{NLOS}(\tau, t) = \sum_{n=1}^2 \sum_{i=1}^3 \sum_{m \in R_i} H_{u,s,n,m}^{NLOS}(t) \delta(\tau - \tau_{n,i} - d_{3D}/c - \Delta\tau) + \sum_{n=3}^N H_{u,s,n}^{NLOS}(t) \delta(\tau - \tau_n - d_{3D}/c - \Delta\tau) \quad (7.6-43)$$

$$H_{u,s}^{LOS}(\tau, t) = \sqrt{\frac{1}{K_R+1}} H_{u,s}^{NLOS}(\tau, t) + \sqrt{\frac{K_R}{K_R+1}} H_{u,s,1}^{LOS}(t) \delta(\tau - \tau_1 - d_{3D}/c) \quad (7.6-44)$$

Table 7.6.9-1: Parameters for the absolute time of arrival model

Scenarios		InF-SL, InF-DL	InF-SH, InF-DH
$\lg \Delta\tau = \log_{10}(\Delta\tau / 1s)$	$\mu_{\lg \Delta\tau}$	-7.5	-7.5
	$\sigma_{\lg \Delta\tau}$	0.4	0.4
Correlation distance in the horizontal plane [m]		6	11

7.6.10 Dual mobility

To support simulations that involve dual Tx and Rx mobility or scatterer mobility, the Doppler frequency component in the channel coefficient generation in step 11 in clause 7.5 should be updated as follows.

For the LOS path, the Doppler frequency is given by

$$v_{n,m} = \frac{\hat{r}_{rx,n,m}^T \cdot \dot{v}_{rx} + \hat{r}_{tx,n,m}^T \cdot \dot{v}_{tx}}{\lambda_0} \quad (7.6-45)$$

where $\hat{r}_{rx,n,m}$ and $\hat{r}_{tx,n,m}$ are defined in (7.5-23) and (7.5-24) respectively, and

$$\bar{v}_{rx} = v_{rx} \begin{bmatrix} \sin \theta_{v,rx} \cos \phi_{v,rx} & \sin \theta_{v,rx} \sin \phi_{v,rx} & \cos \theta_{v,rx} \end{bmatrix}^T$$

$$\bar{v}_{tx} = v_{tx} \begin{bmatrix} \sin \theta_{v,tx} \cos \phi_{v,tx} & \sin \theta_{v,tx} \sin \phi_{v,tx} & \cos \theta_{v,tx} \end{bmatrix}^T$$

For all other paths, the Doppler frequency component is given by:

$$v_{n,m} = \frac{\hat{r}_{rx,n,m}^T \cdot \dot{v}_{rx} + \hat{r}_{tx,n,m}^T \cdot \dot{v}_{tx} + 2\alpha_{n,m} D_{n,m}}{\lambda_0} \quad (7.6-46)$$

where $D_{n,m}$ is a random variable from $-v_{scatt}$ to v_{scatt} , $\alpha_{n,m}$ is a random variable of Bernoulli distribution with mean p , and v_{scatt} is the maximum speed of the clutter. A typical value of p is 0.2.

7.6.11 Sources of EM interference

When the simulation includes sources of EM interference in industrial scenarios, the channel(s) between the interferer(s) and the BS or UT should be modeled using the appropriate sub-scenario(s), e.g. clutter-embedded or elevated Tx or Rx and low or high clutter density. Characterization of EM interference sources is out of the scope of the channel model.

7.6.12 Embedded devices

To simulate devices that are embedded inside machinery or enclosures, an additional loss parameter L_{embedded} is added to the path loss in step 12. The additional path loss parameter L_{embedded} to embedded devices is left as a simulation assumption, where it may be formulated e.g. as a value or range, or derived using a methodology similar to the building penetration loss in clause 7.4.3.1.

7.7 Channel models for link-level evaluations

7.7.1 Clustered Delay Line (CDL) models

The CDL models are defined for the full frequency range from 0.5 GHz to 100 GHz with a maximum bandwidth of 2 GHz. CDL models can be implemented by e.g., coefficient generation Step 10 and Step 11 in Subclause 7.5 or generating TDL model using spatial filter from Subclause 7.7.4. Three CDL models, namely CDL-A, CDL-B and CDL-C are constructed to represent three different channel profiles for NLOS while CDL-D and CDL-E are constructed for LOS, the parameters of which can be found respectively in Table 7.7.1-1, Table 7.7.1-2, Table 7.7.1-3, Table 7.7.1-4 and Table 7.7.1-5.

Each CDL model can be scaled in delay so that the model achieves a desired RMS delay spread, according to the procedure described in Subclause 7.7.3. Each CDL model can also be scaled in angles so that the model achieves desired angle spreads, according to the procedure described in Subclause 7.7.5.1.

For LOS channel models, the K-factor of CDL-D and CDL-E can be set to a desired value following the procedure described in Subclause 7.7.6.

For modelling effect of beamforming in a simplified way, a brick-wall window can be applied to a delay-scaled CDL model. The power shall be normalized after applying the window. A TDL model for simplified evaluations can be obtained from the CDL model, according to this method.

The following step by step procedure should be used to generate channel coefficients using the CDL models.

Step 1: Generate departure and arrival angles

Generate arrival angles of azimuth using the following equation

$$\varphi_{n,m, \text{AOA}} = \varphi_{n, \text{AOA}} + c_{\text{ASA}} \alpha_m, \quad (7.7-0a)$$

Where $\varphi_{n, \text{AOA}}$ is the cluster AOA and c_{ASA} is the cluster-wise rms azimuth spread of arrival angles (cluster ASA) in Tables 7.7.1.1 – 7.7.1.5 below, and α_m denotes the ray offset angles within a cluster given by Table 7.5-3. If angular

scaling according to Subclause 7.7.5.1 is used, this is applied to the ray angles $\varphi_{n,m, \text{AOA}}$. The generation of AOD ($\varphi_{n,m, \text{AOD}}$), ZSA ($\theta_{n,m, \text{ZOA}}$), and ZSD ($\theta_{n,m, \text{ZOD}}$) follows a procedure similar to AOA as described above.

Step 2: Coupling of rays within a cluster for both azimuth and elevation

Couple randomly AOD angles $\varphi_{n,m, \text{AOD}}$ to AOA angles $\varphi_{n,m, \text{AOA}}$ within a cluster n . Couple randomly ZOD angles $\theta_{n,m, \text{ZOD}}$ with ZOA angles $\theta_{n,m, \text{ZOA}}$ using the same procedure. Couple randomly AOD angles $\varphi_{n,m, \text{AOD}}$ with ZOD angles $\theta_{n,m, \text{ZOD}}$ within a cluster n .

Step 3: Generate the cross polarization power ratios

Generate the cross polarization power ratios (XPR) κ for each ray m of each cluster n as

$$\kappa_{n,m} = 10^{X/10}, \quad (7.7-0b)$$

where X is the per-cluster XPR in dB from Tables 7.7.1.1 – 7.7.1.5.

Step 4: Coefficient generation

Follow the same procedure as in Steps 10 and 11 in Subclause 7.5, with the exception that all clusters are treated as "weaker cluster", i.e. no further sub-clusters in delay should be generated. Additional clusters representing delay spread of the stronger clusters are already provided in Tables 7.7.1.1 – 7.7.1.5.

Table 7.7.1-1. CDL-A

Cluster #	Normalized delay	Power in [dB]	AOD in [°]	AOA in [°]	ZOD in [°]	ZOA in [°]
1	0.0000	-13.4	-178.1	51.3	50.2	125.4
2	0.3819	0	-4.2	-152.7	93.2	91.3
3	0.4025	-2.2	-4.2	-152.7	93.2	91.3
4	0.5868	-4	-4.2	-152.7	93.2	91.3
5	0.4610	-6	90.2	76.6	122	94
6	0.5375	-8.2	90.2	76.6	122	94
7	0.6708	-9.9	90.2	76.6	122	94
8	0.5750	-10.5	121.5	-1.8	150.2	47.1
9	0.7618	-7.5	-81.7	-41.9	55.2	56
10	1.5375	-15.9	158.4	94.2	26.4	30.1
11	1.8978	-6.6	-83	51.9	126.4	58.8
12	2.2242	-16.7	134.8	-115.9	171.6	26
13	2.1718	-12.4	-153	26.6	151.4	49.2
14	2.4942	-15.2	-172	76.6	157.2	143.1
15	2.5119	-10.8	-129.9	-7	47.2	117.4
16	3.0582	-11.3	-136	-23	40.4	122.7
17	4.0810	-12.7	165.4	-47.2	43.3	123.2
18	4.4579	-16.2	148.4	110.4	161.8	32.6
19	4.5695	-18.3	132.7	144.5	10.8	27.2
20	4.7966	-18.9	-118.6	155.3	16.7	15.2
21	5.0066	-16.6	-154.1	102	171.7	146
22	5.3043	-19.9	126.5	-151.8	22.7	150.7
23	9.6586	-29.7	-56.2	55.2	144.9	156.1
Per-Cluster Parameters						
Parameter	C_{ASD} in [°]	C_{ASA} in [°]	C_{ZSD} in [°]	C_{ZSA} in [°]	XPR in [dB]	
Value	5	11	3	3	10	

Table 7.7.1-2. CDL-B

Cluster #	Normalized delay	Power in [dB]	AOD in [°]	AOA in [°]	ZOD in [°]	ZOA in [°]
1	0.0000	0	9.3	-173.3	105.8	78.9
2	0.1072	-2.2	9.3	-173.3	105.8	78.9
3	0.2155	-4	9.3	-173.3	105.8	78.9
4	0.2095	-3.2	-34.1	125.5	115.3	63.3
5	0.2870	-9.8	-65.4	-88.0	119.3	59.9
6	0.2986	-1.2	-11.4	155.1	103.2	67.5
7	0.3752	-3.4	-11.4	155.1	103.2	67.5
8	0.5055	-5.2	-11.4	155.1	103.2	67.5
9	0.3681	-7.6	-67.2	-89.8	118.2	82.6
10	0.3697	-3	52.5	132.1	102.0	66.3
11	0.5700	-8.9	-72	-83.6	100.4	61.6
12	0.5283	-9	74.3	95.3	98.3	58.0
13	1.1021	-4.8	-52.2	103.7	103.4	78.2
14	1.2756	-5.7	-50.5	-87.8	102.5	82.0
15	1.5474	-7.5	61.4	-92.5	101.4	62.4
16	1.7842	-1.9	30.6	-139.1	103.0	78.0
17	2.0169	-7.6	-72.5	-90.6	100.0	60.9
18	2.8294	-12.2	-90.6	58.6	115.2	82.9
19	3.0219	-9.8	-77.6	-79.0	100.5	60.8
20	3.6187	-11.4	-82.6	65.8	119.6	57.3
21	4.1067	-14.9	-103.6	52.7	118.7	59.9
22	4.2790	-9.2	75.6	88.7	117.8	60.1
23	4.7834	-11.3	-77.6	-60.4	115.7	62.3
Per-Cluster Parameters						
Parameter	c_{ASD} in [°]	c_{ASA} in [°]	c_{ZSD} in [°]	c_{ZSA} in [°]	XPR in [dB]	
Value	10	22	3	7	8	

Table 7.7.1-3. CDL-C

Cluster #	Normalized delay	Power in [dB]	AOD in [°]	AOA in [°]	ZOD in [°]	ZOA in [°]
1	0	-4.4	-46.6	-101	97.2	87.6
2	0.2099	-1.2	-22.8	120	98.6	72.1
3	0.2219	-3.5	-22.8	120	98.6	72.1
4	0.2329	-5.2	-22.8	120	98.6	72.1
5	0.2176	-2.5	-40.7	-127.5	100.6	70.1
6	0.6366	0	0.3	170.4	99.2	75.3
7	0.6448	-2.2	0.3	170.4	99.2	75.3
8	0.6560	-3.9	0.3	170.4	99.2	75.3
9	0.6584	-7.4	73.1	55.4	105.2	67.4
10	0.7935	-7.1	-64.5	66.5	95.3	63.8
11	0.8213	-10.7	80.2	-48.1	106.1	71.4
12	0.9336	-11.1	-97.1	46.9	93.5	60.5
13	1.2285	-5.1	-55.3	68.1	103.7	90.6
14	1.3083	-6.8	-64.3	-68.7	104.2	60.1
15	2.1704	-8.7	-78.5	81.5	93.0	61.0
16	2.7105	-13.2	102.7	30.7	104.2	100.7
17	4.2589	-13.9	99.2	-16.4	94.9	62.3
18	4.6003	-13.9	88.8	3.8	93.1	66.7
19	5.4902	-15.8	-101.9	-13.7	92.2	52.9
20	5.6077	-17.1	92.2	9.7	106.7	61.8
21	6.3065	-16	93.3	5.6	93.0	51.9
22	6.6374	-15.7	106.6	0.7	92.9	61.7
23	7.0427	-21.6	119.5	-21.9	105.2	58
24	8.6523	-22.8	-123.8	33.6	107.8	57
Per-Cluster Parameters						
Parameter	c_{ASD} in [°]	c_{ASA} in [°]	c_{ZSD} in [°]	c_{ZSA} in [°]	XPR in [dB]	
Value	2	15	3	7	7	

Table 7.7.1-4. CDL-D.

Cluster #	Cluster PAS	Normalized Delay	Power in [dB]	AOD in [°]	AOA in [°]	ZOD in [°]	ZOA in [°]
1	Specular(LOS path)	0	-0.2	0	-180	98.5	81.5
	Laplacian	0	-13.5	0	-180	98.5	81.5
2	Laplacian	0.035	-18.8	89.2	89.2	85.5	86.9
3	Laplacian	0.612	-21	89.2	89.2	85.5	86.9
4	Laplacian	1.363	-22.8	89.2	89.2	85.5	86.9
5	Laplacian	1.405	-17.9	13	163	97.5	79.4
6	Laplacian	1.804	-20.1	13	163	97.5	79.4
7	Laplacian	2.596	-21.9	13	163	97.5	79.4
8	Laplacian	1.775	-22.9	34.6	-137	98.5	78.2
9	Laplacian	4.042	-27.8	-64.5	74.5	88.4	73.6
10	Laplacian	7.937	-23.6	-32.9	127.7	91.3	78.3
11	Laplacian	9.424	-24.8	52.6	-119.6	103.8	87
12	Laplacian	9.708	-30.0	-132.1	-9.1	80.3	70.6
13	Laplacian	12.525	-27.7	77.2	-83.8	86.5	72.9
Per-Cluster Parameters							
Parameter		C _{ASD} in [°]	C _{ASA} in [°]	C _{ZSD} in [°]	C _{ZSA} in [°]	XPR in [dB]	
Value		5	8	3	3	11	

Table 7.7.1-5. CDL-E.

Cluster #	Cluster PAS	Normalized Delay	Power in [dB]	AOD in [°]	AOA in [°]	ZOD in [°]	ZOA in [°]
1	Specular (LOS path)	0.000	-0.03	0	-180	99.6	80.4
	Laplacian	0.000	-22.03	0	-180	99.6	80.4
2	Laplacian	0.5133	-15.8	57.5	18.2	104.2	80.4
3	Laplacian	0.5440	-18.1	57.5	18.2	104.2	80.4
4	Laplacian	0.5630	-19.8	57.5	18.2	104.2	80.4
5	Laplacian	0.5440	-22.9	-20.1	101.8	99.4	80.8
6	Laplacian	0.7112	-22.4	16.2	112.9	100.8	86.3
7	Laplacian	1.9092	-18.6	9.3	-155.5	98.8	82.7
8	Laplacian	1.9293	-20.8	9.3	-155.5	98.8	82.7
9	Laplacian	1.9589	-22.6	9.3	-155.5	98.8	82.7
10	Laplacian	2.6426	-22.3	19	-143.3	100.8	82.9
11	Laplacian	3.7136	-25.6	32.7	-94.7	96.4	88
12	Laplacian	5.4524	-20.2	0.5	147	98.9	81
13	Laplacian	12.0034	-29.8	55.9	-36.2	95.6	88.6
14	Laplacian	20.6419	-29.2	57.6	-26	104.6	78.3
Per-Cluster Parameters							
Parameter		C _{ASD} in [°]	C _{ASA} in [°]	C _{ZSD} in [°]	C _{ZSA} in [°]	XPR in [dB]	
Value		5	11	3	7	8	

7.7.2 Tapped Delay Line (TDL) models

The TDL models for simplified evaluations, e.g., for non-MIMO evaluations, are defined for the full frequency range from 0.5 GHz to 100 GHz with a maximum bandwidth of 2 GHz.

Three TDL models, namely TDL-A, TDL-B and TDL-C, are constructed to represent three different channel profiles for NLOS while TDL-D and TDL-E are constructed for LOS, the parameters of which can be found respectively in Table 7.7.2-1, Table 7.7.2-2, Table 7.7.2-3, Table 7.7.2-4 and Table 7.7.2-5.

The Doppler spectrum for each tap is characterized by a classical (Jakes) spectrum shape and a maximum Doppler shift

f_D where $f_D = |\vec{v}|/\lambda_0$. Due to the presence of a LOS path, the first tap in TDL-D and TDL-E follows a Ricean

fading distribution. For those taps the Doppler spectrum additionally contains a peak at the Doppler shift $f_s = 0.7 f_D$ with an amplitude such that the resulting fading distribution has the specified K-factor.

Each TDL model can be scaled in delay so that the model achieves a desired RMS delay spread, according to the procedure described in Subclause 7.7.3.

For LOS channel models, the K-factor of TDL-D and TDL-E can be set to a desired value following the procedure described in Subclause 7.7.6.

Table 7.7.2-1. TDL-A

Tap #	Normalized delay	Power in [dB]	Fading distribution
1	0.0000	-13.4	Rayleigh
2	0.3819	0	Rayleigh
3	0.4025	-2.2	Rayleigh
4	0.5868	-4	Rayleigh
5	0.4610	-6	Rayleigh
6	0.5375	-8.2	Rayleigh
7	0.6708	-9.9	Rayleigh
8	0.5750	-10.5	Rayleigh
9	0.7618	-7.5	Rayleigh
10	1.5375	-15.9	Rayleigh
11	1.8978	-6.6	Rayleigh
12	2.2242	-16.7	Rayleigh
13	2.1718	-12.4	Rayleigh
14	2.4942	-15.2	Rayleigh
15	2.5119	-10.8	Rayleigh
16	3.0582	-11.3	Rayleigh
17	4.0810	-12.7	Rayleigh
18	4.4579	-16.2	Rayleigh
19	4.5695	-18.3	Rayleigh
20	4.7966	-18.9	Rayleigh
21	5.0066	-16.6	Rayleigh
22	5.3043	-19.9	Rayleigh
23	9.6586	-29.7	Rayleigh

Table 7.7.2-2. TDL-B

Tap #	Normalized delay	Power in [dB]	Fading distribution
1	0.0000	0	Rayleigh
2	0.1072	-2.2	Rayleigh
3	0.2155	-4	Rayleigh
4	0.2095	-3.2	Rayleigh
5	0.2870	-9.8	Rayleigh
6	0.2986	-1.2	Rayleigh
7	0.3752	-3.4	Rayleigh
8	0.5055	-5.2	Rayleigh
9	0.3681	-7.6	Rayleigh
10	0.3697	-3	Rayleigh
11	0.5700	-8.9	Rayleigh
12	0.5283	-9	Rayleigh
13	1.1021	-4.8	Rayleigh
14	1.2756	-5.7	Rayleigh
15	1.5474	-7.5	Rayleigh
16	1.7842	-1.9	Rayleigh
17	2.0169	-7.6	Rayleigh
18	2.8294	-12.2	Rayleigh
19	3.0219	-9.8	Rayleigh
20	3.6187	-11.4	Rayleigh
21	4.1067	-14.9	Rayleigh
22	4.2790	-9.2	Rayleigh
23	4.7834	-11.3	Rayleigh

Table 7.7.2-3. TDL-C

Tap #	Normalized delays	Power in [dB]	Fading distribution
1	0	-4.4	Rayleigh
2	0.2099	-1.2	Rayleigh
3	0.2219	-3.5	Rayleigh
4	0.2329	-5.2	Rayleigh
5	0.2176	-2.5	Rayleigh
6	0.6366	0	Rayleigh
7	0.6448	-2.2	Rayleigh
8	0.6560	-3.9	Rayleigh
9	0.6584	-7.4	Rayleigh
10	0.7935	-7.1	Rayleigh
11	0.8213	-10.7	Rayleigh
12	0.9336	-11.1	Rayleigh
13	1.2285	-5.1	Rayleigh
14	1.3083	-6.8	Rayleigh
15	2.1704	-8.7	Rayleigh
16	2.7105	-13.2	Rayleigh
17	4.2589	-13.9	Rayleigh
18	4.6003	-13.9	Rayleigh
19	5.4902	-15.8	Rayleigh
20	5.6077	-17.1	Rayleigh
21	6.3065	-16	Rayleigh
22	6.6374	-15.7	Rayleigh
23	7.0427	-21.6	Rayleigh
24	8.6523	-22.8	Rayleigh

Table 7.7.2-4. TDL-D.

Tap #	Normalized delay	Power in [dB]	Fading distribution
1	0	-0.2	LOS path
	0	-13.5	Rayleigh
2	0.035	-18.8	Rayleigh
3	0.612	-21	Rayleigh
4	1.363	-22.8	Rayleigh
5	1.405	-17.9	Rayleigh
6	1.804	-20.1	Rayleigh
7	2.596	-21.9	Rayleigh
8	1.775	-22.9	Rayleigh
9	4.042	-27.8	Rayleigh
10	7.937	-23.6	Rayleigh
11	9.424	-24.8	Rayleigh
12	9.708	-30.0	Rayleigh
13	12.525	-27.7	Rayleigh

NOTE: The first tap follows a Ricean distribution with a K-factor of $K_1 = 13.3$ dB and a mean power of 0dB.

Table 7.7.2-5. TDL-E.

Tap #	Normalized delay	Power in [dB]	Fading distribution
1	0	-0.03	LOS path
	0	-22.03	Rayleigh
2	0.5133	-15.8	Rayleigh
3	0.5440	-18.1	Rayleigh
4	0.5630	-19.8	Rayleigh
5	0.5440	-22.9	Rayleigh
6	0.7112	-22.4	Rayleigh
7	1.9092	-18.6	Rayleigh
8	1.9293	-20.8	Rayleigh
9	1.9589	-22.6	Rayleigh
10	2.6426	-22.3	Rayleigh
11	3.7136	-25.6	Rayleigh
12	5.4524	-20.2	Rayleigh
13	12.0034	-29.8	Rayleigh
14	20.6519	-29.2	Rayleigh

NOTE: The first tap follows a Ricean distribution with a K-factor of $K_1 = 22$ dB and a mean power of 0dB.

7.7.3 Scaling of delays

The RMS delay spread values of both CDL and TDL models are normalized and they can be scaled in delay so that a desired RMS delay spread can be achieved. The scaled delays can be obtained according to the following equation:

$$\tau_{n,\text{scaled}} = \tau_{n,\text{model}} \cdot DS_{\text{desired}} \quad (7.7-1)$$

in which

$\tau_{n,\text{model}}$ is the normalized delay value of the n th cluster in a CDL or a TDL model

$\tau_{n,\text{scaled}}$ is the new delay value (in [ns]) of the n th cluster

DS_{desired} is the wanted delay spread (in [ns])

The example scaling parameters are selected according to Table 7.7.3-1 where the values have been chosen such that the RMS delay spreads span the range observed in measurements corresponding to the typical 5G evaluation scenarios. For information purposes, examples of such RMS delay spreads for the different scenarios are given in Table 7.7.3-2 where the "short-delay profile" corresponds to the median RMS delay spread for LOS scenarios, while "normal-delay profile" and "long-delay profile" correspond to the median and the 90th percentile RMS delay spread for NLOS scenarios

according to the channel parameters in Table 7.5-6. It can therefore be understood that a particular RMS delay spread in Table 7.7.3-1 may occur in any scenario; however certain values may be more likely in some scenarios than in others.

The example parameters given in Table 7.7.3-1 does not preclude the use of other scaling values if this is found appropriate, for instance if additional scenarios are introduced or if e.g. the effect of beamforming needs to be captured in a TDL. Both of these examples can potentially result in an increased range of experienced RMS delay spreads.

Table 7.7.3-1. Example scaling parameters for CDL and TDL models.

Model	$DS_{desired}$
Very short delay spread	10 ns
Short delay spread	30 ns
Nominal delay spread	100 ns
Long delay spread	300 ns
Very long delay spread	1000 ns

Table 7.7.3-2. Scenario specific scaling factors - for information only

Proposed Scaling Factor	$DS_{desired}$ in [ns]	Frequency [GHz]						
		2	6	15	28	39	60	70
Indoor office	Short-delay profile	20	16	16	16	16	16	16
	Normal-delay profile	39	30	24	20	18	16	16
	Long-delay profile	59	53	47	43	41	38	37
UMi Street-canyon	Short-delay profile	65	45	37	32	30	27	26
	Normal-delay profile	129	93	76	66	61	55	53
	Long-delay profile	634	316	307	301	297	293	291
UMa	Short-delay profile	93	93	85	80	78	75	74
	Normal-delay profile	363	363	302	266	249	228	221
	Long-delay profile	1148	1148	955	841	786	720	698
RMa & RMa O2I	Short-delay profile	32	32	N/A	N/A	N/A	N/A	N/A
	Normal-delay profile	37	37	N/A	N/A	N/A	N/A	N/A
	Long-delay profile	153	153	N/A	N/A	N/A	N/A	N/A
UMi / UMa O2I	Normal-delay profile	240						
	Long-delay profile	616						

7.7.4 Spatial filter for generating TDL channel model

The TDL models described in Subclause 7.7.2 are generated from the CDL models assuming ideal isotropic antennas at both Tx and Rx. It is also possible to generate TDL models by assuming non-isotropic antennas like directive horn antennas or array antennas.

The basic idea to generate a TDL model based on a filtered CDL model is shown in Figure 7.7.4-1 below.

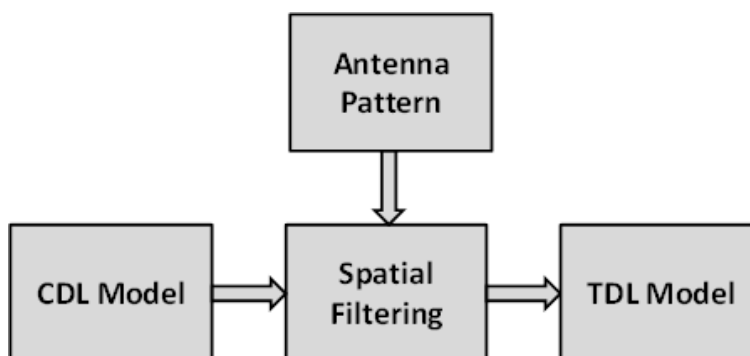


Figure 7.7.4-1 The basic idea for filtering the CDL model to TDL model.

7.7.4.1 Exemplary filters/antenna patterns

Note that any filter/pattern can be applied on a CDL to derive a TDL for evaluating directional algorithms.

Example 1: Isotropic pattern

$$A'_{\{tx,rx\}}(\theta', \varphi') = 1 \quad (7.7-2)$$

Example 2: Rectangular mask

$$A'_{\{tx,rx\}}(\theta', \varphi', BW) = \begin{cases} 1, & |\theta' - 90^\circ| \leq \frac{BW}{2} \wedge |\varphi'| \leq \frac{BW}{2} \\ 0, & \text{otherwise.} \end{cases} \quad (7.7-3)$$

with BW denotes beamwidth.

Example 3: Simplified antenna pattern given in [ITU-R M.2135]

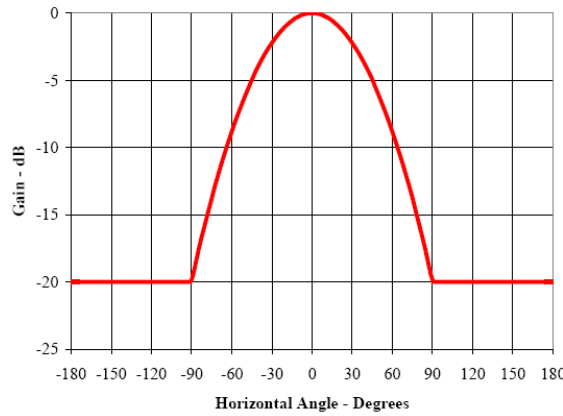


Figure 7.7.4-2 Simplified antenna pattern [ITU-R M.2135].

7.7.4.2 Generation procedure

1. The following steps are needed to generate tapped delay line (TDL) models: Choose a CDL model (e.g. CDL-A). Note that the models may be scaled according to Subclause 7.7.5.1 prior to the filtering in order to represent different angular spreads.

2. Choose spatial filters A'_{tx} and A'_{rx} defined in LCS

3. Transform the spatial filter into GCS to obtain A_{tx} and A_{rx} such that the pointing direction (θ_p, φ_p) is centered within the filter. The pointing direction (θ_i, φ_i) may be defined

- a. by the dominant path $(\theta_p, \varphi_p) = (\theta_i, \varphi_i)$ with $i = \operatorname{argmax}_n (P_n^{\text{CDL}})$ $i = \operatorname{argmax}_n (P_n^{\text{CDL}})$, where P_n^{CDL} denotes the CDL cluster power values

- b. Or an arbitrary direction

4. Calculate TDL cluster power values P_n^{TDL} given the following equation

$$P_n^{\text{TDL}} = P_n^{\text{CDL}} A_{rx}(\theta_{n,ZOA}, \varphi_{n,AOA}) A_{tx}(\theta_{n,ZOD}, \varphi_{n,AOD}) \quad (7.7-4)$$

7.7.5 Extension for MIMO simulations

Extended MIMO link-level channel models can be constructed according to two alternative methods described in the following.

7.7.5.1 CDL extension: Scaling of angles

The angle values of CDL models are fixed, which is not very suitable for MIMO simulations for several reasons; The PMI statistics can become biased, and a fixed precoder may perform better than open-loop and on par with closed-loop or reciprocity beamforming. Furthermore, a CDL only represents a single channel realization. The predefined angle values in the CDL models can be generalized by introducing angular translation and scaling. By translation, mean angle can be changed to $\mu_{\phi, \text{desired}}$ and angular spread can be changed by scaling. The translated and scaled ray angles can be obtained according to the following equation:

$$\varphi_{n, \text{scaled}} = \frac{AS_{\text{desired}}}{AS_{\text{model}}} (\varphi_{n, \text{model}} - \mu_{\phi, \text{model}}) + \mu_{\phi, \text{desired}} \quad (7.7-5)$$

in which:

$\varphi_{n, \text{model}}$ $\phi_{n,0}$ is the tabulated CDL ray angle

AS_{model} $\sigma_{\phi,0}$ is the rms angular spread of the tabulated CDL including the offset ray angles, calculated using the angular spread definition in Annex A

$\mu_{\phi, \text{model}}$ $\mu_{\phi,0}$ is the mean angle of the tabulated CDL, calculated using the definition in Annex A

$\mu_{\phi, \text{desired}}$ $\Delta\phi$ is the desired mean angle

AS_{desired} σ_{ϕ} is the desired rms angular spread

$\varphi_{n, \text{scaled}}$ ϕ_n is the resulting scaled ray angle.

The angular scaling is applied on the ray angles including offsets from the tabulated cluster angles. Typical angular spreads for different scenarios can be obtained from the system-level model.

Example scaling values are:

- AOD spread (ASD) for each CDL model: {5, 10, 15, 25} degrees.
- AOA spread (ASA) for each CDL model: {30, 45, 60} degrees.
- ZOA spread (ZSA) for each CDL model: {5, 10, 15} degrees.
- ZOD spread (ZSD) for each CDL model: {1, 3, 5} degrees.

The angular scaling and translation can be applied to some or all of the azimuth and zenith angles of departure and arrival.

Note: The azimuth angles may need to be wrapped around to be within [0, 360] degrees, while the zenith angles may need to be clipped to be within [0, 180] degrees.

7.7.5.2 TDL extension: Applying a correlation matrix

The TDLs and the spatial-filtered TDLs can be used with the correlation matrices for MIMO link-level simulations. Typical correlation parameters can be derived from 1) delay & angular scaled CDLs with antenna array assumptions, 2)

system-level model with antenna array assumptions, or 3) by selecting extreme cases, e.g. uncorrelated, highly correlated etc. For example, these following options can be considered:

- 1) Zero correlation (IID channel coefficients) can be used for any number of antenna elements
- 2) The correlation matrix construction method from 3GPP TS36.101/104 [15][16] can be used for linear and planar (single- or dual-polarized) arrays.
 - Other correlation parameters α , β , γ than those specified in 3GPP TS36.101/104 [15][16] and extensions to larger antenna arrays can be considered. For typical scenarios, α and β will be in the range 0-1
 - A representative set of values is {0,0.7,0.9,0.99}

Note: This approach can be applied to TDLs derived from spatially filtered CDLs to emulate hybrid BF system

Note: Other methodologies could also be developed, e.g.

- extending the 3GPP TS36.101/104 [15][16] procedure to planar arrays or more elements
- using CDLs in combination with array assumptions to derive per-tap correlation matrices as in [17].
- using the system-level model in combination with array assumptions to derive per-tap or per-channel correlation matrices

7.7.6 K-factor for LOS channel models

For the LOS channel models of CDL/TDL-D and CDL/TDL-E, the K-factor values may be changed by the user. Mean and standard deviation of K-factor values can be found in Table 7.5-6, although other values may also be used.

If the K-factor of a model shall be changed to K_{desired} [dB], the cluster powers for the Laplacian clusters (in case of CDL) or the tap powers for the Rayleigh fading taps (in case of TDL) are determined by

$$P_{n,\text{scaled}} = P_{n,\text{model}} - K_{\text{desired}} + K_{\text{model}}, \quad (7.7.6-1)$$

where $P_{n,\text{scaled}}$ and $P_{n,\text{model}}$ denote the scaled and the model path power (as given in the tables) of tap/cluster n . The model's K-factor K_{model} is defined as

$$K_{\text{model}} = P_{1,\text{model}}^{\text{LOS}} - 10 \log_{10} \left(\sum_{n=1}^N 10^{P_{n,\text{model}}/10} \right). \quad (7.7.6-2)$$

After scaling the powers, the delay spread needs to be re-normalized. This is done through the two steps below.

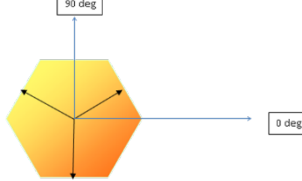
- 1) Calculate the actual RMS delay spread after the K-factor adjustment.
- 2) Divide the delays by that value to obtain DS = 1.

7.8 Channel model calibration

7.8.1 Large scale calibration

For large scale calibration, fast fading is not modeled. The calibration parameters can be found in Table 7.8-1. The calibration results based on TR 38.900 V14.0.0 can be found in R1-165974.

Table 7.8-1: Simulation assumptions for large scale calibration

Parameter	Values
Scenarios	UMa, UMi-Street Canyon, Indoor-office (open office)
Sectorization	3 sectors per cell site: 30, 150 and 270 degrees 
BS antenna configurations	$M_g = N_g = 1$; $(M, N, P) = (10, 1, 1)$, $d_v = 0.5\lambda$
BS port mapping	The 10 elements are mapped to a single CRS port
BS antenna electrical downtilting	102 degrees for UMa and UMi Street Canyon 110 degrees for indoor
Antenna virtualization	DFT precoding according to TR 36.897 with application of panning and tilting angles
BS Tx power	44 dBm for UMi-Street Canyon, 49 for UMa at 6GHz 35 dBm at 30GHz and 70 GHz for UMa and UMi-Street canyon 24 dBm for Indoor for all carrier frequencies
Bandwidth	20MHz for 6GHz, and 100MHz for 30GHz and 70 GHz
UT antenna configurations	1 element (vertically polarized), Isotropic antenna gain pattern
Handover margin (for calibration)	0dB
UT distribution	Following TR36.873 for UMa and UMi, (3D dropping) uniform dropping for indoor with minimum distance (2D) of 0 m
UT attachment	Based on pathloss considering LOS angle
UT noise figure	9 dB
Fast fading channel	Fast fading channel is not modelled
O2I penetration loss	50% low loss and 50% high loss
Carrier Frequency	6 GHz, 30 GHz, 70GHz
Wrapping method for UMa and UMi	geographical distance based wrapping (mandatory) radio distance (optional)
Metrics	1) Coupling loss – serving cell (based on LOS pathloss) 2) Geometry (based on LOS pathloss) with and without white noise

7.8.2 Full calibration

The calibration parameters for full calibration including the fast fading modelling can be found in Table 7.8-2. Unspecified parameters in Table 7.8-2 are the same as those in Table 7.8-1. When $P=2$, X-pol (+/-45 degree) is used for BS antenna configuration 1 and X-pol (0/+90 degree) is used for UT antenna configuration. The calibration results based on TR 38.900 V14.0.0 can be found in R1-165975.

Table 7.8-2: Simulation assumptions for full calibration

Parameter	Values
Scenarios	UMa, UMi-street Canyon, Indoor-office (open office)
Carrier Frequency	6 GHz, 30 GHz, 60GHz, 70GHz
Bandwidth	20MHz for 6GHz, and 100MHz for 30GHz, 60 GHz and 70 GHz
BS Tx power	44 dBm for UMi-Street Canyon, 49 for UMa at 6GHz 35 dBm at 30GHz, 60 GHz and 70 GHz for UMa and UMi-Street canyon 24 dBm for Indoor for all carrier frequencies
BS antenna configurations	Config 1: $M = 4, N = 4, P = 2, M_g = 1, N_g = 2, d_H = d_V = 0.5\lambda, d_{H,g} = d_{V,g} = 2.5\lambda$... calibration metrics 1), 2), 3) are calibrated Config 2: $M_g = N_g = 1, M = N = 2, P = 1$... calibration metrics 1), 2), 4) are calibrated
BS port mapping	Config 1: all 16 elements for each polarization on each panel are mapped to a single CRS port; panning angles of the two subarrays: (0,0) degs; same downtilt angles as used for the large-scale calibrations Config 2: each antenna element is mapped to one CRS port
UT antenna configurations	$M_g = N_g = 1, M = N = 1, P = 2$
UT distribution	Following TR36.873 for UMa and UMi, (3D dropping) uniform dropping for indoor with minimum distance (2D) of 0 m
UT attachment	Based on RSRP (formula) from CRS port 0
Polarized antenna modelling	Model-2 in TR36.873
UT array orientation	$\Omega_{UT,\alpha}$ uniformly distributed on [0,360] degree, $\Omega_{UT,\beta} = 90$ degree, $\Omega_{UT,\gamma} = 0$ degree
UT antenna pattern	Isotropic
Metrics	1) Coupling loss – serving cell
	2) Wideband SIR before receiver without noise
	3) CDF of Delay Spread and Angle Spread (ASD, ZSD, ASA, ZSA) from the serving cell (according to circular angle spread definition of TR 25.996)
	4) CDF of largest (1 st) PRB singular values (serving cell) at $t=0$ plotted in $10 \cdot \log_{10}$ scale. CDF of smallest (2 nd) PRB singular values (serving cell) at $t=0$ plotted in $10 \cdot \log_{10}$ scale. CDF of the ratio between the largest PRB singular value and the smallest PRB singular value (serving cell) at $t=0$ plotted in $10 \cdot \log_{10}$ scale. Note: The PRB singular values of a PRB are the eigenvalues of the mean covariance matrix in the PRB.

7.8.3 Calibration of additional features

The calibration parameters for the calibration of oxygen absorption, large bandwidth and large antenna array, spatial consistency, and blockage can be respectively found in Table 7.8-3, 7.8-4, 7.8-5, and 7.8-6. Unspecified parameters in these tables are the same as those in Tables 7.8-1 and 7.8-2. When $P=2$, X-pol (+/-45 degree) is used for BS antenna configuration 1 and X-pol (0/+90 degree) is used for UT antenna configuration. The calibration results based on TR 38.900 V14.0.0 can be found in R1-1700990.

Table 7.8-3: Simulation assumptions for calibration for oxygen absorption

Parameter	Values
Scenarios	UMi-street Canyon
Carrier Frequency	60 GHz
BS antenna configurations	$M = 4, N = 4, P = 2, M_g = 1, N_g = 2, d_H = d_V = 0.5\lambda, d_{H,g} = d_{V,g} = 2.5\lambda$
BS port mapping	all 16 elements for each polarization on each panel are mapped to a single CRS port; panning angles of the two subarrays: (0,0) degs; same downtilt angles as used for the large-scale calibrations
Calibration method	Drop multiple users in the multiple cells randomly, and collect the following metrics for each user after attachment.
Metrics	1) CDF of coupling loss (serving cell) 2) Wideband SINR before receiver – determined from RSRP (formula) from CRS port 0 3) CDF of Delay Spread from the serving cell

Table 7.8-4: Simulation assumptions for calibration for large bandwidth and large antenna array

Parameter	Values
Scenarios	UMi-street Canyon
Carrier Frequency	30GHz
Bandwidth	2GHz
BS antenna configurations	$M = 8, N = 8, P = 2, M_g = 1, N_g = 4, d_H = d_V = 0.5\lambda, d_{H,g} = d_{V,g} = 4\lambda$
BS port mapping	all 64 elements for each polarization on each panel are mapped to a single CRS port; panning angles of the two subarrays: (0,0) degs; same downtilt angles as used for the large-scale calibrations
The number of rays per cluster	$N_{MPC} = 40$
Calibration method	Drop multiple users in the multiple cells randomly, and collect the following metrics for each user after attachment.
Metrics	1) CDF of coupling loss (serving cell) 2) Wideband SINR before receiver – determined from RSRP (formula) from CRS port 0 3) CDF of largest (1 st) PRB singular values (serving cell) at t=0 plotted in $10^{\log_{10}}$ scale

Table 7.8-5: Simulation assumptions for calibration for spatial consistency

Parameter	Values
Scenarios	UMi-street Canyon
Carrier Frequency	30 GHz
BS antenna configurations	$M = 4, N = 4, P = 2, M_g = 1, N_g = 2, d_H = d_V = 0.5\lambda, d_{H,g} = d_{V,g} = 2.5\lambda$
BS port mapping	all 16 elements for each polarization on each panel are mapped to a single CRS port; panning angles of the two subarrays: (0,0) degs; same downtilt angles as used for the large-scale calibrations
UE distribution	Following TR36.873, 3D dropping uniform dropping for indoor with minimum distance of 0 m For Config1: 100% UE indoor and in the 1 st floor For Config2: 100% UE outdoor
Mobility	Config1: UE is stationary Config2: UE is moving with random direction and fixed speed, e.g., 30 km/h
Calibration method	For Config1: Drop multiple UEs in a single cell, determine all permutations of pairs of UEs, collect the variables for each pair and bin them into certain distance ranges, e.g., 1m/2m/10m, to get enough samples. Collect the following metrics 1) –6). For Config2: Drop multiple users in the single cell, and collect metric 1)-2) and 7)-9) for each user after attachment.
Metrics	1) CDF of coupling loss (serving cell) 2) Wideband SINR before receiver – determined from RSRP (formula) from CRS port 0 3) Cross-correlation coefficient of delay for the third cluster between paired UEs, see note 1 4) Cross-correlation coefficient of AOA for the third cluster between paired UEs 5) Cross-correlation coefficient of LOS/NLOS status between paired UEs 6) Cross correlation coefficient of the channel response in Step 11 on the first non-DC subcarrier in an OFDM symbol on antenna port 0 received on the first UE antenna over multiple realizations between paired UEs 7) CDF of average varying rate of power for the third cluster, see note 2 8) CDF of average varying rate of delay for the third cluster (ns) 9) CDF of average varying rate of AOA for the third cluster (degree)
NOTE 1	For the UT pair at a certain distance range, the variables collected by two UEs can be denoted as X and Y, respectively, then the cross-correlation coefficient for real number can be written as $\frac{[E(XY)-E(X)E(Y)]}{\sqrt{[E(X^2)-E(X)^2]}\sqrt{[E(Y^2)-E(Y)^2]}}$, the cross-correlation coefficient for complex number can be written as $\frac{[E(XY^*)-E(X)E(Y)^*]}{\sqrt{[E(XX^*)-E(X)E(X)^*]}\sqrt{[E(YY^*)-E(Y)E(Y)^*]}}$.
NOTE 2	For the average varying rate, we assume the collecting interval, e.g., 100ms, and then get the samples for a certain UE, the varying rate can be written as the standard variance of the samples per 100ms.

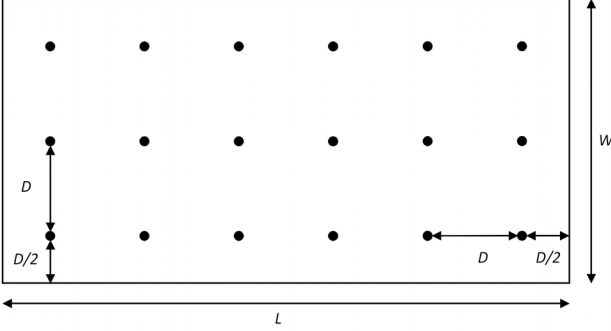
Table 7.8-6: Simulation assumptions for calibration for blockage

Parameter	Values
Scenarios	UMi-street Canyon
Carrier Frequency	30 GHz
BS antenna configurations	$M = 4$, $N = 4$, $P = 2$, $M_g = 1$, $N_g = 2$, $d_H = d_V = 0.5\lambda$, $d_{H,g} = d_{V,g} = 2.5\lambda$
BS port mapping	all 16 elements for each polarization on each panel are mapped to a single CRS port; panning angles of the two subarrays: (0,0) degs; same downtilt angles as used for the large-scale calibrations
Calibration method	<p>For Model A: Drop multiple users in the multiple cells, and collect the following metrics 1) – 3) for each user after attachment. Optional self-blocking feature is made mandatory in the Landscape mode only for calibration purposes.</p> <p>For Model B: Drop a BS in (0,0,30) and a UT in (100,0,1.5), Jump directly to Step 11 and replace the channel with CDL-E. Drop a blocking screen of size $h=10\text{m}$, $w = 2\text{m}$ in (80,10,1.5) Move the UT from (100,0,1.5) to (100,20,1.5) in small increments. For each UT position, translate all the AODs and AOAs of CDL-E such that the specular (LOS path) of CDL-E is pointing along the direct path between the BS and UT. Collect metric 4)</p>
Metrics	<ol style="list-style-type: none"> 1) CDF of coupling loss (serving cell) 2) Wideband SINR before receiver – determined from RSRP (formula) from CRS port 0 3) CDF of ASA from the serving cell 4) RSRP as a function of UT position

7.8.4 Calibration of the indoor factory scenario

For the InF, the calibration parameters can be found in Table 7.8-7. The calibration results can be found in R1-1909704.

Table 7.8-7: Simulation assumptions for large scale calibration for the indoor factory scenario

Parameter	Values
Scenario	InF-SL, InF-DL, InF-SH, InF-DH
Hall size	InF-SL: 120x60 m InF-DL: 300x150 m InF-SH: 300x150 m InF-DH: 120x60 m
Room height	10 m
Sectorization	None
BS antenna configurations	1 element (vertically polarized), Isotropic antenna gain pattern
UT antenna configurations	1 element (vertically polarized), Isotropic antenna gain pattern
Handover margin (for calibration)	0dB
BS deployment	<p>18 BSs on a square lattice with spacing D, located $D/2$ from the walls.</p> <ul style="list-style-type: none"> - for the small hall ($L=120\text{m} \times W=60\text{m}$): $D=20\text{m}$ - for the big hall ($L=300\text{m} \times W=150\text{m}$): $D=50\text{m}$  <p>BS height = 1.5 m for InF-SL and InF-DL BS-height = 8 m for for InF-SH and InF-DH</p>
UT distribution	uniform dropping for indoor with minimum 2D distance of 1 m UT height = 1.5 m
UT attachment	Based on pathloss
UT noise figure	9 dB
Carrier frequency	3.5 GHz, 28 GHz
Bandwidth	100 MHz
Clutter density: r	Low clutter density: 20% High clutter density: 60%
Clutter height: h_c	Low clutter density: 2 m High clutter density: 6 m
Clutter size: $d_{clutter}$	Low clutter density: 10 m High clutter density: 2 m
Metrics	1) Coupling loss – serving cell 2) Geometry with and without noise 3) CDF of delay and angle spread (ASD, ZSD, ASA, ZSA) according to the definition in Annex A.1 4) CDF of first path excess delay for serving cell

8 Map-based hybrid channel model (Alternative channel model methodology)

Map-based hybrid model is composed of a deterministic component following, e.g., METIS work [6] and a stochastic component following mainly the model described in clause 7. The channel model methodology described in this clause is an alternative to the methodology specified in clause 7, and can be used if:

- The system performance is desired to be evaluated or predicted with the use of digital map to take into account the impacts from environmental structures and materials.

The map-based hybrid model defined in this clause is not calibrated and can be used per company basis.

8.1 Coordinate system

The same coordinate system as defined in Subclause 7.1 is applied.

8.2 Scenarios

The same scenarios as in Subclause 7.2 can be applied.

8.3 Antenna modelling

The same antenna modelling as defined in Subclause 7.3 can be applied.

8.4 Channel generation

The radio channels are created using the deterministic ray-tracing upon a digitized map and emulating certain stochastic components according to the statistic parameters listed in Tables 7.5-6 to 7.5-11 [Note: Not all parameters listed in these tables are used in hybrid model]. The channel realizations are obtained by a step-wise procedure illustrated in Figure 8.4-1 and described below. In the following steps, downlink is assumed. For uplink, arrival and departure parameters have to be swapped.

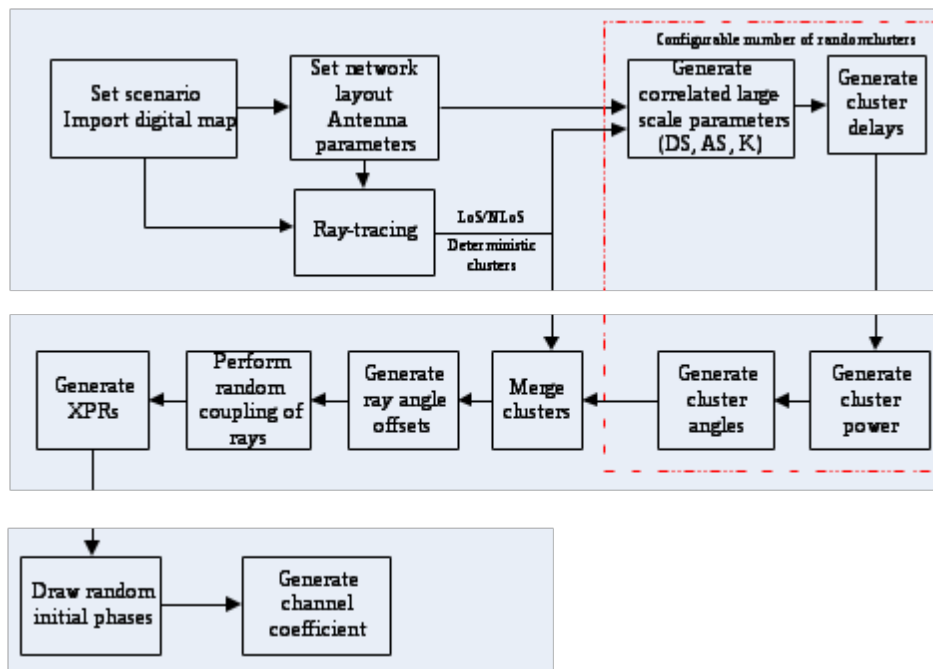


Figure 8.4-1: Channel coefficient generation procedure

Step-wise procedure:

Step 1: Set environment and import digitized map accordingly

- a) Choose scenario. Choose a global coordinate system and define zenith angle θ , azimuth angle ϕ , and spherical basis vectors $\hat{\theta}$, $\hat{\phi}$ as shown in Figure 7.5-2.
- b) Import digitized map according to the chosen scenario. The digitized map should at least contain the following information:

- The 3D geometric information for each of major structures involving with buildings or rooms. The external building walls and internal room walls are represented by surfaces and identified by the coordinates of the vertices on each wall.
- The material and thickness of each wall as well as the corresponding electromagnetic properties including permittivity and conductivity.
- Random small objects in certain scenarios (e.g, UMi outdoor)

The format of digitized map, including additional information besides above-mentioned, is per implementation wise and out of scope of this description.

Step 2: Set network layout, and antenna array parameters

- a) Give number of BS and UT.
- b) Give 3D locations of BS and UT, and calculate LOS AOD ($\phi_{LOS,AOD}$), LOS ZOD ($\theta_{LOS,ZOD}$), LOS AOA ($\phi_{LOS,AOA}$), LOS ZOA ($\theta_{LOS,ZOA}$) of each BS and UT in the global coordinate system
- c) Give BS and UT antenna field patterns F_{rx} and F_{tx} in the global coordinate system and array geometries
- d) Give BS and UT array orientations with respect to the global coordinate system. BS array orientation is defined by three angles $\Omega_{BS,\alpha}$ (BS bearing angle), $\Omega_{BS,\beta}$ (BS downtilt angle) and $\Omega_{BS,\gamma}$ (BS slant angle). UT array orientation is defined by three angles $\Omega_{UT,\alpha}$ (UT bearing angle), $\Omega_{UT,\beta}$ (UT downtilt angle) and $\Omega_{UT,\gamma}$ (UT slant angle). Give rotational motion of UT in terms of its bearing angle, downtilt angle and slant angle if UT rotation is modelled.
- e) Give speed and direction of motion of UT in the global coordinate system for virtual motion.
- f) Give system centre frequency/frequencies and bandwidth(s) for each of BS-UT links

If the bandwidth (denoted as B) is greater than c/D Hz, where c is the speed of light and D is the maximum antenna aperture in either azimuth or elevation, the whole bandwidth is split into K_B equal-sized frequency

bins, where $K_B \geq \lceil \frac{B}{c/D} \rceil$ is a per-implementation parameter taking into account the channel constancy as well as other potential evaluation needs, and the bandwidth of each frequency bin is $\Delta B = \frac{B}{K_B}$. Within k -th frequency bin, the channel power attenuation, phase rotation, Doppler are assumed constant, whose corresponding values are calculated based on the centre frequency of k -th frequency bin

$f_k = f_c - \frac{K_B - 2k + 1}{2} \Delta B$ for $1 \leq k \leq K_B$, where f_c is the centre frequency of the corresponding BS-UT link.

Step 3: Apply ray-tracing to each pair of link ends (i.e., end-to-end propagation between pair of Tx/Rx arrays).

- a) Perform geometric calculations in ray-tracing to identify propagation interaction types, including LOS, reflections, diffractions, penetrations and scattering (in case the digitized map contains random small objects), for each propagation path. In general, some maximum orders of different interaction types can be set.
 - The theoretical principles and procedures of geometric tracing calculations can be found in [6]~[10][12]. This description does not intend to mandate new concepts and/or procedures to the conventional ray-tracing algorithms; on the other hand, the implementation-based variations aiming to reduce computation complexity are allowed within limits of acceptable calibration tolerances.
 - The same geometric calculation is shared among all K_B frequency bins.
- b) Perform electric field calculations over propagation path, based on identified propagation interaction types (LOS, reflection, diffraction, penetration and scattering) and centre frequencies of frequency bins.

The details of electric field calculation can be found in [6]~[13].

The modelling algorithms in geometry and electric field calculations for different propagation interactions are summarized in the table below.

Table 8.4-1 Principles applied in ray-tracing

	Geometry calculation	Electric field calculation
LOS	Free space LOS	Friis equation [11]
Reflection	Snell's law with image-based method [7]	Fresnel equation [7]
Diffraction	Fermat's principle [12]	UTD [13]
Penetration	Snell's law for transmission through slab [8]	Fresnel equation [7]
Scattering (upon small objects)	Isotropic scattering [6]	RCS-based scattering coefficient [6]

Note: For reasons of simplicity and simulation speed, the maximum order of reflection on a path without diffraction is configurable from {1,2,3}; the maximum order of diffraction on a path without reflection is configurable from {1,2}; the path containing both reflection and diffraction has 1-order reflection and 1-order diffraction, besides any potential penetrations; and the maximum order of penetration on a path is configurable, with the recommended value equal to 5.

The outputs from Step 3 should at least contain following for each pair of link ends:

- the LOS/NLOS flag to indicate whether a LOS propagation mechanism exists;
- the number of deterministic propagation paths L_{RT} (also referred as deterministic clusters in Step 8. To avoid the unnecessary computation complexity, these L_{RT} deterministic paths only include those paths whose powers are higher than 25dB below the maximum deterministic path power, where the path power is denoted as $P_{l_{RT}}^{RT,real}$ and defined below);
- for each deterministic path (l_{RT} -th path sorted in ascending order of path delay):
 - the flag indicating whether the deterministic path is generated with scattering upon random small objects;
 - the normalized path delay $\tau_{l_{RT}}^{RT} = \tau_{l_{RT}} - \min(\tau_{l_{RT}}')$ and the first arrival absolute delay $\min(\tau_n')$ (with $\tau_{l_{RT}}$ to be the real absolute propagation delay of the path);
 - angles of arrival and departure [$\phi_{l_{RT},AOA}^{RT}$, $\theta_{l_{RT},ZOA}^{RT}$, $\phi_{l_{RT},AOD}^{RT}$, $\theta_{l_{RT},ZOD}^{RT}$];
 - the power $P_{l_{RT},k}^{RT,real}$ for k-th frequency bin, and the path power $P_{l_{RT}}^{RT,real} = \frac{1}{K_B} \sum_{k=1}^{K_B} P_{l_{RT},k}^{RT,real}$
 - the XPR $K_{l_{RT}}^{RT}$ of the path, where $K_{l_{RT}}^{RT} = \frac{1}{K_B} \sum_{k=1}^{K_B} K_{l_{RT},k}^{RT}$ with $K_{l_{RT},k}^{RT}$ being the XPR for k-th frequency bin.
 - to support for true motion, i.e. the case when a trajectory is specified for UT, a path ID is associated for each deterministic path. The same ID is associated for a path across a number of UT locations as far as 1) it has same interaction types in the same order and 2) its interactions occur in same walls or other surfaces.

The L_{RT} deterministic paths are sorted by normalized path delay ($\tau_{l_{RT}}^{RT}$) in ascending order. That is to say, $\tau_1^{RT} = 0$.

If $L_{RT}=0$ for a pair of link ends, the channel gain for this pair of link ends is assumed to be zero and the remaining steps are skipped with none of random cluster.

Step 4: Generate large scale parameters e.g. delay spread, angular spreads and Ricean K factor for random clusters.

The generation of large scale parameters takes into account cross correlation according to Table 7.5-6 and uses the procedure described in Subclause 3.3.1 of [14] with the square root matrix $\sqrt{C_{M \times M}(0)}$ being generated using the Cholesky decomposition and the following order of the large scale parameter vector: $\mathbf{s}_M = [s_K, s_{DS}, s_{ASD}, s_{ASA}, s_{ZSD}, s_{ZSA}]^T$. Limit random RMS azimuth arrival and azimuth departure spread values to 104 degrees, i.e., $ASA = \min(ASA, 104^\circ)$, $ASD = \min(ASD, 104^\circ)$. Limit random RMS zenith arrival and zenith departure spread values to 52 degrees, i.e., $ZSA = \min(ZSA, 52^\circ)$, $ZSD = \min(ZSD, 52^\circ)$. For the parameter selection from Table 7.5-6, the LOS/NLOS condition determined in Step 3 is applied.

Step 5: Generate delays (denoted as $\{\tau_n^{RC}\}$) for random clusters.

Delays are drawn randomly according to the exponential delay distribution

$$\tau_n' = -\mu_\tau^{RC} \ln(X_n) \quad (8.4-1)$$

where $\mu_\tau^{RC} = \max\left\{\mu_\tau, \frac{1}{L_{RT}} \sum_{l_{RT}=1}^{L_{RT}} \tau_{l_{RT}}^{RT}\right\}$, $X_n \sim \text{uniform}(0,1)$, and cluster index $n = 0, \dots, L_{RC}'$ with L_{RC}' to be configurable. A recommended value for L_{RC}' is the number of clusters given in Table 7.5-6.

$\mu_\tau = r_\tau DS + \frac{L_{RT}}{L_{RC}' + 1} \left(r_\tau DS - \frac{1}{L_{RT}} \sum_{l_{RT}=1}^{L_{RT}} \tau_{l_{RT}}^{RT} \right)$, where r_τ is the delay distribution proportionality factor given in Table 7.5-6.

Normalise the delays by subtracting the minimum delay and sort the normalised delays to ascending order:

$$\tau_n = \text{sort}\left(\tau_n' - \min(\tau_n')\right) / C_\tau \quad (8.4-2)$$

where C_τ is the additional scaling of delays to compensate for the effect of LOS peak addition to the delay spread, and is depending on the heuristically determined Ricean K-factor [dB] as generated in Step 4:

$$C_\tau = \begin{cases} 0.7705 - 0.0433 K + 0.0002 K^2 + 0.000017 K^3 & \text{LOS condition} \\ 1 & \text{NLOS condition} \end{cases} \quad (8.4-3)$$

For the delay used in cluster power generation in Step 6, the scaling factor C_τ is always 1.

The n -th random cluster is removed if $n=0$ or $|\tau_n - \tau_{l_{RT}}^{RT}| > \tau_{th}$ for any of $1 \leq l_{RT} \leq L_{RT}$, where τ_{th} is given by

$\tau_{th} = \frac{1}{2 \cdot L_{RC}'} \sqrt{\sum_{n=1}^{L_{RC}'} (\tau_n - \tau_{n-1})^2}$, and p_0 is the configurable probability for cluster inter-arrival interval to be less than τ_{th} . For example, set $p_0 = 0.2$ to obtain $\tau_{th} = 0.223 \mu_\tau^{RC}$.

Denote τ_n^{RC} for $1 \leq n \leq L_{RC}$ as the delays of the L_{RC} random clusters that remain after the cluster removal.

As an add-on feature, the absolute time of arrival of a cluster is derived as:

- $\tau_{l_{RT}}^{RT}$, if the cluster is the l_{RT} -th deterministic path obtained in Step 3 for $1 \leq l_{RT} \leq L_{RT}$;
- $\min(\tau_n') + \tau_n^{RC}$, if the cluster is the n -th random cluster for $1 \leq n \leq L_{RC}$.

Step 6: Generate powers (denoted as $P_i^{RC,real}$ for $1 \leq i \leq L_{RC}$) for random clusters.

Cluster powers for the random clusters are calculated assuming a single slope exponential power delay profile.

First, the virtual powers (denoted as $P_i^{RC,virtual}$ for $1 \leq i \leq L_{RC}$) of random clusters and virtual powers (denoted as $P_j^{RT,virtual}$ for $1 \leq j \leq L_{RT}$) of deterministic clusters are calculated as following.

Denote:

$$V_i^{RC} = \exp\left(-\tau_i^{RC} \frac{r_\tau - 1}{r_\tau DS}\right) \cdot 10^{\frac{-Z_{i,RC}}{10}} \quad (8.4-4)$$

$$V_j^{RT} = \exp\left(-\tau_j^{RT} \frac{r_\tau - 1}{r_\tau DS}\right) \cdot 10^{\frac{-Z_{j,RT}}{10}} \quad (8.4-5)$$

where $Z_{i,RC}$ and $Z_{j,RT}$ are the per cluster shadowing terms in [dB] and meet distribution of $N(0, \zeta^2)$. Then,

$$P_i^{RC,virtual} = \frac{1}{A+1} \frac{V_i^{RC}}{\sum_{i=1}^{L_{RC}} V_i^{RC} + \sum_{j=1}^{L_{RT}} V_j^{RT}} \quad (8.4-6)$$

$$P_j^{RT,virtual} = \frac{1}{A+1} \cdot \frac{V_j^{RT}}{\sum_{i=1}^{L_{RC}} V_i^{RC} + \sum_{j=1}^{L_{RT}} V_j^{RT}} + \frac{A}{A+1} \cdot \delta(j-1) \quad (8.4-7)$$

In the case of LOS condition, $A=K_R$ with K_R being the Ricean K -factor obtained in Step 4 and converted to linear scale; otherwise, $A=0$. The real power (including effects of pathloss) per random cluster in k -th frequency bin is given by

$$P_{i,k}^{RC,real} = \frac{\sum_{j=1}^{L_{RT}} P_{j,k}^{RT,real}}{\sum_{j=1}^{L_{RT}} P_j^{RT,virtual}} \cdot P_i^{RC,virtual} \quad (8.4-8)$$

for $1 \leq i \leq L_{RC}$ and $1 \leq k \leq K_B$. Similar to path power of deterministic cluster, the path power of i -th random cluster is calculated as

$$P_i^{RC,real} = \frac{1}{K_B} \sum_{k=1}^{K_B} P_{i,k}^{RC,real} \quad (8.4-9)$$

Step 7: Generate arrival angles and departure angles for both azimuth and elevation, for each random cluster.

For azimuth angles of the n -th random cluster:

The composite PAS in azimuth of all random clusters is modelled as wrapped Gaussian (see Table 7.5-6). The

AOAs are determined by applying the inverse Gaussian function with input parameters $P_n^{RC,real}$ and RMS angle spread ASA

$$\phi'_{n, AOA} = \frac{2(ASA/1.4) \sqrt{-\ln \left(P_n^{RC, real} / \max_{i,j} (P_i^{RC, real}, P_j^{RT, real}) \right)}}{C_\phi} \quad (8.4-10)$$

with constant C_ϕ defined as

$$C_\phi = \begin{cases} C_\phi^{NLOS} \cdot (1.1035 - 0.028K - 0.002K^2 + 0.0001K^3) & , \text{for LOS} \\ C_\phi^{NLOS} & , \text{for NLOS} \end{cases} \quad (8.4-11)$$

where C_ϕ^{NLOS} is defined as a scaling factor related to the total number of clusters and is given in Table 7.5-2.

In the LOS case, constant C_ϕ also depends on the Ricean K-factor K in [dB], as generated in Step 4. Additional scaling of the angles is required to compensate for the effect of LOS peak addition to the angle spread.

Assign positive or negative sign to the angles by multiplying with a random variable X_n with uniform distribution to the discrete set of $\{1, -1\}$, and add component $Y_n \sim N(0, (ASA/7)^2)$ to introduce random variation

$$\phi_{n, AOA} = X_n \phi'_{n, AOA} + Y_n + \phi_{center, AOA} \quad (8.4-12)$$

where $\phi_{center, AOA}$ is calculated as

$$\phi_{center, AOA} = \arg \left(\sum_{l=1}^{L_{RT}} P_l^{RT, real} \cdot \exp(j\phi_{l, AOA}^{RT}) \right) \quad (8.4-13)$$

Note that $\phi_{l, AOA}^{RT}$ shall be given in radians here.

The generation of AOD ($\phi_{n, AOD}$) follows a procedure similar to AOA as described above.

For zenith angles of the n-th random cluster:

The generation of ZOA assumes that the composite PAS in the zenith dimension of all random clusters is Laplacian (see Table 7.5-6). The ZOAs are determined by applying the inverse Laplacian function with input parameters $P_n^{RC, real}$ and RMS angle spread ZSA

$$\theta'_{n, ZOA} = - \frac{ZSA \ln \left(P_n^{RC, real} / \max_{i,j} (P_i^{RC, real}, P_j^{RT, real}) \right)}{C_\theta} \quad (8.4-14)$$

with C_θ defined as

$$C_\theta = \begin{cases} C_\theta^{NLOS} \cdot (1.3086 + 0.0339K - 0.0077K^2 + 0.0002K^3) & , \text{for LOS} \\ C_\theta^{NLOS} & , \text{for NLOS} \end{cases} \quad (8.4-15)$$

where C_θ^{NLOS} is a scaling factor related to the total number of clusters and is given in Table 7.5-4.

In the LOS case, constant C_θ also depends on the Ricean K-factor K in [dB], as generated in Step 4. Additional scaling of the angles is required to compensate for the effect of LOS peak addition to the angle spread.

Assign positive or negative sign to the angles by multiplying with a random variable X_n with uniform distribution to the discrete set of $\{1, -1\}$, and add component $Y_n \sim N(0, (ZSA/7)^2)$ to introduce random variation

$$\theta_{n,ZOA} = X_n \theta'_{n,ZOA} + Y_n + \bar{\theta}_{ZOA} \quad (8.4-16)$$

where $\bar{\theta}_{ZOA} = 90^\circ$ if the UT is located indoors and $\bar{\theta}_{ZOA} = \theta_{center,ZOA}$ if the UT is located outdoors, where $\theta_{center,ZOA}$ is calculated as

$$\theta_{center,ZOA} = \arg \left(\sum_{l=1}^{L_{RT}} P_l^{RT,real} \cdot \exp(j\theta_{l,ZOA}^{RT}) \right) \quad (8.4-17)$$

Note that $\theta_{l,ZOA}^{RT}$ shall be given in radians here.

The generation of ZOD follows the same procedure as ZOA described above except equation (8.4-16) is replaced by

$$\theta_{n,ZOD} = X_n \theta'_{n,ZOD} + Y_n + \theta_{center,ZOD} + \mu_{offset,ZOD} \quad (8.4-18)$$

where variable X_n is with uniform distribution to the discrete set of $\{1, -1\}$, $Y_n \sim N(0, (ZSD/7)^2)$, $\mu_{offset,ZOD}$ is given in Tables 7.5-7 to 7.5-11.

Step 8: Merge deterministic clusters and random clusters.

First, remove any deterministic or random cluster with less than -25 dB power compared to $\max\{P_j^{RT,real}, P_i^{RC,real}\}$ for all $1 \leq j \leq L_{RT}$ and $1 \leq i \leq L_{RC}$. Then, simply put the remaining deterministic clusters and random clusters into single set of clusters, and meanwhile maintain an attribute for each cluster to indicate whether the cluster is a deterministic cluster or a random cluster.

Step 9: Generate ray delays and ray angle offsets inside each cluster, where the cluster can be either random or deterministic.

Denote M as the number of rays per cluster, where $M=1$ if the cluster corresponds to $n=1$ in the LOS case, otherwise the value of M is given in Table 7.5-6.

When $K_B=1$:

The relative delay of m -th ray within n -th cluster is given by $\tau'_{n,m} = 0$ for $m = 1, \dots, M$.

The azimuth angle of arrival (AOA) for the m -th ray in n -th cluster is given by

$$\varphi_{n,m,AOA} = \varphi_{n,AOA} + C_{ASA} \alpha_m \quad (8.4-19)$$

where C_{ASA} is the cluster-wise rms azimuth spread of arrival angles (cluster ASA) in Table 7.5-6, and offset angle α_m is given in Table 7.5-3. $\varphi_{n,AOA}$ equals to the AOA angle output from Step 3 if n -th cluster is deterministic cluster, and equals to the AOA angle (8.4-12) in Step 7 if n -th cluster is random cluster.

The generation of AOD ($\phi_{n,m,AOD}$) follows a procedure similar to AOA as described above.

The zenith angle of arrival (ZOA) for the m -th ray in n -th cluster is given by

$$\theta_{n,m,ZOA} = \theta_{n,ZOA} + c_{ZSA} \alpha_m \quad (8.4-20)$$

where c_{ZSA} is the cluster-wise rms spread of ZOA (cluster ZOA) in Table 7.5-6, and offset angle α_m is given in Table 7.5-3. Assuming that $\theta_{n,m,ZOA}$ is wrapped within $[0, 360^\circ]$, if $\theta_{n,m,ZOA} \in [180^\circ, 360^\circ]$, then $\theta_{n,m,ZOA}$ is set to $(360^\circ - \theta_{n,m,ZOA})$. $\theta_{n,ZOA}$ equals to the ZOA angle output from Step 3 if n -th cluster is deterministic cluster, and equals to the ZOA angle (8.4-16) in Step 7 if n -th cluster is random cluster.

The zenith angle of departure (ZOD) for the m -th ray in n -th cluster is given by

$$\theta_{n,m,ZOD} = \theta_{n,ZOD} + (3/8)(10^{\mu_{lgZSD}}) \alpha_m \quad (8.4-21)$$

where μ_{lgZSD} is the mean of the ZSD log-normal distribution. $\theta_{n,ZOD}$ equals to the ZOD angle output from Step 3 if n -th cluster is deterministic cluster, and equals to the ZOD angle (8.4-18) in Step 7 if n -th cluster is random cluster.

When $K_B > 1$:

The relative delay of m -th ray within n -th cluster is given by $\tau'_{n,m} = \text{sort}\left(\tau''_{n,m} - \min_{1 \leq m \leq M} \{\tau''_{n,m}\}\right)$ that are sorted in ascending order, where $\tau''_{n,m} \sim \text{unif}(0, 2c_{DS})$, with the cluster delay spread as given in Table 7.5-6.

$\text{unif}(a, b)$ denotes the continuous uniform distribution on the interval $[a, b]$. Note that $\tau''_{n,m}$ shall be the independently generated.

The azimuth angles (AOA and AOD) and zenith angles (ZOA and ZOD) for the m -th ray in n -th cluster in each frequency bin is given by

$$\begin{aligned} \phi_{n,m,AOA} &= \phi_{n,AOA} + \phi'_{n,m,AOA} \\ \phi_{n,m,AOD} &= \phi_{n,AOD} + \phi'_{n,m,AOD} \\ \theta_{n,m,ZOA} &= \theta_{n,ZOA} + \theta'_{n,m,ZOA} \\ \theta_{n,m,ZOD} &= \theta_{n,ZOD} + \theta'_{n,m,ZOD} \end{aligned} \quad (8.4-22)$$

for $m = 1, \dots, M$, where $\phi_{n,[AOA|AOD]}$ and $\theta_{n,[ZOA|ZOD]}$ equal to the {AOA,AOD} and {ZOA, ZOD} angle outputs from Step 3 if n -th cluster is deterministic cluster, and equal to the {AOA,AOD} and {ZOA, ZOD} angle in Step 7 if n -th cluster is random cluster; and

$$\begin{aligned} \phi'_{n,m,AOA} &\sim 2c_{ASA} \text{unif}(-1, 1) \\ \phi'_{n,m,AOD} &\sim 2c_{ASD} \text{unif}(-1, 1) \\ \theta'_{n,m,ZOA} &\sim 2c_{ZSA} \text{unif}(-1, 1) \\ \theta'_{n,m,ZOD} &\sim 2c_{ZSD} \text{unif}(-1, 1) \end{aligned} \quad (8.4-23)$$

with the respective cluster angular spreads as given in Tables 7.5-6 to 7.5-11.

Assuming that $\theta_{n,m,ZOA}$ is wrapped within $[0, 360^\circ]$, if $\theta_{n,m,ZOA} \in [180^\circ, 360^\circ]$, then $\theta_{n,m,ZOA}$ is set to $(360^\circ - \theta_{n,m,ZOA})$.

Step 10: Generate power of rays in each cluster, where coupling of rays within a cluster for both azimuth and elevation could be needed.

Given $P_{n,k}$ as the real power in k -th frequency bin for the n -th cluster (either deterministic or random) obtained from Step 8,

When $K_B = 1$:

Couple randomly AOD angles $\phi_{n,m,AOD}$ to AOA angles $\phi_{n,m,AOA}$ within a cluster n . Couple randomly ZOD angles $\theta_{n,m,ZOD}$ with ZOA angles $\theta_{n,m,ZOA}$ using the same procedure. Couple randomly AOD angles $\phi_{n,m,AOD}$ with ZOD angles $\theta_{n,m,ZOD}$ within a cluster n .

The power of m -th ray in n -th cluster and in k -th frequency bin is given by $P_{n,m,k} = P_{n,k} / M$ for $m = 1, \dots, M$.

When $K_B > 1$:

$$P_{n,m,k} = P_{n,k} \cdot \frac{P'_{n,m}}{\sum_{m=1}^M P'_{n,m}} \quad \text{for}$$

The power of m -th ray in n -th cluster and in k -th frequency bin is given by $m = 1, \dots, M$, where

$$P'_{n,m} = \exp\left(-\frac{\tau'_{n,m}}{c_{DS}}\right) \exp\left(-\frac{\sqrt{2}|\phi'_{n,m,AOA}|}{c_{ASA}}\right) \exp\left(-\frac{\sqrt{2}|\phi'_{n,m,AOD}|}{c_{ASD}}\right) \exp\left(-\frac{\sqrt{2}|\theta'_{n,m,ZOA}|}{c_{ZSA}}\right) \exp\left(-\frac{\sqrt{2}|\theta'_{n,m,ZOD}|}{c_{ZSD}}\right) \quad (8.4-24)$$

and c_{DS} , c_{ASA} , c_{ASD} , and c_{ZSA} are respectively the intra-cluster delay spread and the corresponding intra-cluster angular spreads that are given in Table 7.5-6. The cluster zenith spread of departure is given by

$$c_{ZSD} = \frac{3}{8} 10^{\mu_{lgZSD}} \quad (8.4-25)$$

with μ_{lgZSD} being defined in Tables 7.5-7, 7.5-8, 7.5-9, 7.5-10 and 7.5-11.

Step 11: Generate XPRs

Generate the cross polarization power ratios (XPR) κ for each ray m of each cluster n . XPR is log-Normal distributed. Draw XPR values as

$$\kappa_{n,m} = 10^{X_{n,m}/10} \quad (8.4-26)$$

where $X_{n,m} \sim N(\mu_{\text{XPR}}, \sigma_{\text{XPR}}^2)$ is Gaussian distributed with σ_{XPR} given from Table 7.5-6. If n -th cluster is a deterministic cluster, $\mu = 10 \log_{10} \kappa_{l_{\text{RT}}}^{\text{RT}}$; otherwise, $\mu = \mu_{\text{XPR}}$ is given in Table 7.5-6.

Note: $X_{n,m}$ is independently drawn for each ray and each cluster.

Step 12: Draw initial random phases

Draw random initial phase $\left[\Phi_{n,m}^{\theta\theta}, \Phi_{n,m}^{\theta\phi}, \Phi_{n,m}^{\phi\theta}, \Phi_{n,m}^{\phi\phi} \right]$ for each ray m of each cluster n and for four different polarisation combinations $(\theta\theta, \theta\phi, \phi\theta, \phi\phi)$. The distribution for initial phases is uniform within $(-\pi, \pi)$.

In the LOS case, calculate an initial phase $\Phi_{\text{LOS}} = -2\pi d_{3D}/\lambda_0$ for both $\theta\theta$ and $\phi\phi$ polarisations, where d_{3D} is the 3D distance between transmitter and receiver and $\lambda_0 = c/f_c$ is the wavelength of the modelled propagation link.

Step 13: Generate channel coefficients for each cluster n and each receiver and transmitter element pair u, s .

In case of NLOS, the channel coefficients of ray m in cluster n for a link between Rx antenna u and Tx antenna s at time t in k -th frequency bin can be calculated as

$$H_{u,s,n,m,k}(t) = \begin{bmatrix} F_{rx,u,\theta}(\theta_{n,m,ZOA}, \varphi_{n,m,AOA}) \\ F_{rx,u,\phi}(\theta_{n,m,ZOA}, \varphi_{n,m,AOA}) \end{bmatrix}^T \begin{bmatrix} \exp(j\Phi_{n,m}^{\theta\theta}) & \sqrt{\kappa_{n,m}^{-1}} \exp(j\Phi_{n,m}^{\theta\phi}) \\ \sqrt{\kappa_{n,m}^{-1}} \exp(j\Phi_{n,m}^{\phi\theta}) & \exp(j\Phi_{n,m}^{\phi\phi}) \end{bmatrix} \\ \cdot \begin{bmatrix} F_{tx,s,\theta}(\theta_{n,m,ZOD}, \varphi_{n,m,AOD}) \\ F_{tx,s,\phi}(\theta_{n,m,ZOD}, \varphi_{n,m,AOD}) \end{bmatrix} \cdot \exp\left(j2\pi \frac{f_k}{c} (\hat{r}_{rx,n,m}^T \cdot \bar{d}_{rx,u} + \hat{r}_{tx,n,m}^T \cdot \bar{d}_{tx,s})\right) \\ \cdot \left(\frac{-|OL_{n,m}(f_k) + BL_{n,m}(f_k, t)|}{\sqrt{P_{n,m,k}} \cdot 10^{20}} \right) \exp\left(j2\pi \frac{f_k}{c} \hat{r}_{rx,n,m}^T \cdot \bar{v} t\right) \quad (8.4-27)$$

where $F_{rx,u,\theta}$ and $F_{rx,u,\phi}$ are the receive antenna element u field patterns in the direction of the spherical basis vectors, $\hat{\theta}$ and $\hat{\phi}$ respectively, $F_{tx,s,\theta}$ and $F_{tx,s,\phi}$ are the transmit antenna element s field patterns in the direction of the spherical basis vectors, $\hat{\theta}$ and $\hat{\phi}$ respectively. The delay (TOA) for ray m in cluster n for a link between Rx antenna u and Tx antenna s is given by:

$$\tau_{u,s,n,m} = \tau_n + \tau'_{n,m} - \frac{1}{c} \hat{r}_{rx,n,m}^T \cdot \bar{d}_{rx,u} - \frac{1}{c} \hat{r}_{tx,n,m}^T \cdot \bar{d}_{tx,s} \quad (8.4-28)$$

For the m -th ray within n -th cluster, $\hat{r}_{rx,n,m}$ is the spherical unit vector with azimuth arrival angle $\varphi_{n,m,AOA}$ and elevation arrival angle $\theta_{n,m,ZOA}$, given by

$$\hat{r}_{rx,n,m} = \begin{bmatrix} \sin \theta_{n,m,ZOA} \cos \varphi_{n,m,AOA} \\ \sin \theta_{n,m,ZOA} \sin \varphi_{n,m,AOA} \\ \cos \theta_{n,m,ZOA} \end{bmatrix} \quad (8.4-29)$$

$\hat{r}_{tx,n,m}$ is the spherical unit vector with azimuth departure angle $\varphi_{n,m,AOD}$ and elevation departure angle $\theta_{n,m,ZOD}$, given by

$$\hat{r}_{tx,n,m} = \begin{bmatrix} \sin \theta_{n,m,ZOD} \cos \varphi_{n,m,AOD} \\ \sin \theta_{n,m,ZOD} \sin \varphi_{n,m,AOD} \\ \cos \theta_{n,m,ZOD} \end{bmatrix} \quad (8.4-30)$$

Also, $\bar{d}_{rx,u}$ is the location vector of receive antenna element u and $\bar{d}_{tx,s}$ is the location vector of transmit antenna element s , $\kappa_{n,m}$ is the cross polarisation power ratio in linear scale. If polarisation is not considered, the 2x2 polarisation matrix can be replaced by the scalar $\exp(j\Phi_{n,m})$ and only vertically polarised field patterns are applied.

The Doppler frequency component is calculated from the arrival angles (AOA, ZOA), and the UT velocity vector \bar{v} with speed v , travel azimuth angle ϕ_v , elevation angle θ_v and is given by

$$\bar{v} = v \cdot [\sin \theta_v \cos \phi_v \quad \sin \theta_v \sin \phi_v \quad \cos \theta_v]^T, \quad (8.4-31)$$

In case of LOS, the channel coefficient is calculated in the same way as in (8.4-27) except for $n=1$:

$$H_{u,s,n=1,k}(t) = \begin{bmatrix} F_{rx,u,\theta}(\theta_{LOS,ZOA}, \phi_{LOS,AOA}) \\ F_{rx,u,\phi}(\theta_{LOS,ZOA}, \phi_{LOS,AOA}) \end{bmatrix}^T \begin{bmatrix} \exp(j\Phi_{LOS}) & 0 \\ 0 & -\exp(j\Phi_{LOS}) \end{bmatrix} \begin{bmatrix} F_{tx,s,\theta}(\theta_{LOS,ZOD}, \phi_{LOS,AOD}) \\ F_{tx,s,\phi}(\theta_{LOS,ZOD}, \phi_{LOS,AOD}) \end{bmatrix} \\ \cdot \exp\left(j2\pi \frac{f_k}{c} (\hat{r}_{rx,LOS}^T \cdot \bar{d}_{rx,u} + \hat{r}_{tx,LOS}^T \cdot \bar{d}_{tx,s})\right) \cdot \left(\sqrt{P_{1,k}} \cdot 10^{\frac{-(OL_{n,m=1}(f_k) + BL_{n,m=1}(f_k, t))}{20}} \right) \exp\left(j2\pi \frac{f_k}{c} \hat{r}_{rx,LOS}^T \cdot \bar{v} t\right) \quad (8.4-32)$$

where the corresponding delay (TOA) for cluster $n=1$ for a link between Rx antenna u and Tx antenna s is

$$\tau_{u,s,n=1} = \tau_n - \frac{1}{c} \hat{r}_{rx,LOS}^T \cdot \bar{d}_{rx,u} - \frac{1}{c} \hat{r}_{tx,LOS}^T \cdot \bar{d}_{tx,s}.$$

In (8.4-27) and (8.4-32), the oxygen absorption loss, $OL_{n,m}(f)$, for each ray m in cluster n at carrier frequency f is modelled as

$$OL_{n,m}(f) = \alpha(f)/1000 \cdot c \cdot \left[\tau_n + \tau'_{n,m} + \min\left(\tau'_{l_{RT}}\right) \right] \quad [\text{dB}] \quad (8.4-33)$$

where:

- $\alpha(f)$ is the frequency dependent oxygen loss per distance (dB/km) characterized in Subclause 7.6.1;
- c is speed of light (m/s); and
- τ_n is the delay (s) obtained from Step 3 for deterministic clusters and from Step 5 for random clusters.
 $\min(\tau'_n)$ is from the output of Step 3.

In (8.4-27) and (8.4-32), blockage modelling is an add-on feature. If the blockage model is applied, the blockage loss, $BL_{n,m}(f,t)$ in unit of dB, for each ray m in cluster n at carrier frequency f and time t is modelled in the same way as given in Subclause 7.6.4; otherwise $BL_{n,m}(f,t)=0$ dB for all f and t .

Annex A: Further parameter definitions

A.1 Calculation of angular spread

Based on the circular standard deviation in directional statistics, the following expression for the angular spread AS in radians is proposed

$$AS = \sqrt{-2 \ln \frac{\sum_{n=1}^N \sum_{m=1}^M \exp(j\phi_{n,m}) P_{n,m}}{\sum_{n=1}^N \sum_{m=1}^M P_{n,m}}} \quad (A-1)$$

where $P_{n,m}$ is the power for the m th subpath of the n th path and $\phi_{n,m}$ is the subpaths angle (either AOA, AOD, ZOA, ZOD) given in radians.

A.2 Calculation of mean angle

The power weighted mean angle is given by

$$\mu_{\phi} = \arg \left\{ \sum_{n=1}^N \sum_{m=1}^M \exp(j\phi_{n,m}) P_{n,m} \right\} \quad (A-2)$$

where $P_{n,m}$ is the power for the m th subpath of the n th path and $\phi_{n,m}$ is the subpaths angle (either AOA, AOD, ZOA, ZOD) given in radians.

Annex B: Change history

Change history							
Date	Meeting	TDoc	CR	Rev	Cat	Subject/Comment	New version
2017-02	RAN1#88	R1-1703641				Skeleton TR based on TR 38.900 v14.2.0, adding new changes (from R1-1701231, R1-1701406, R1-1701410, R1-1701411, R1-1701412, R1-1701413, R1-1701414, R1-1701416, R1-1701417 and R1-1701425) to have a TR applicable for the frequency range 0.5 to 100 GHz	0.0.1
2017-02	RAN1#88	R1-1704145				Adding new agreements (from R1-1702701, R1-1703635, R1-1703873, R1-1703358, R1-1702703, R1-1703637, R1-1703354, R1-1703458, R1-1703647, R1-1701936) and reflecting comments from RAN1 e-mail discussions [88-17].	0.1.0
2017-02	RAN#75	RP-170394				Submitted to RAN for information	1.0.0
2017-03	RAN#75	RP-170737				Add TR number further to the approval of revised SID in RP-170379. Submitted to RAN for one step approval	1.0.1
2017-03	RAN#75					MCC clean-up – Further to RAN#75 decision, TR goes under change control as Rel-14	14.0.0
2017-06	RAN#76	RP-171208	0001	-	F	Correction on site specific effective height for TR38.901	14.1.0
2017-06	RAN#76	RP-171208	0003	-	F	Correction for LOS probability	14.1.0
2017-06	RAN#76	RP-171208	0004	-	F	Correction for scaling factor for ZOD generation	14.1.0
2017-06	RAN#76	RP-171208	0005	-	F	Correction for modelling of intra-cluster angular and delay spreads	14.1.0
2017-06	RAN#76	RP-171208	0007	-	F	TR38.901 CR LCS Radiation Field Notation	14.1.0
2017-06	RAN#76	RP-171208	0008	-	F	TR38.901 CR Mean angle definition	14.1.0
2017-06	RAN#76	RP-171208	0009	-	F	TR38.901 CR O2I penetration loss	14.1.0
2017-06	RAN#76	RP-171208	0010	1	F	TR38.901 CR Correction on Rural LSP	14.1.0
2017-06	RAN#76	RP-171208	0011	1	F	Clarification for spatial consistency procedure	14.1.0
2017-06	RAN#76	RP-171208	0013	-	F	TR38.901 CR Scenarios in Simulation Assumptions	14.1.0
2017-06	RAN#76	RP-171208	0014	-	F	TR38.901 CR TDL Spatial Filter	14.1.0
2017-06	RAN#76	RP-171208	0015	-	F	Correction of spatial-consistency UE mobility modelling Procedure A	14.1.0
2017-07						MCC: UMa LOS probability in Table 7.4-2 is made fully visible	14.1.1
2017-09	RAN#77	RP-171648	0016	-	F	Correction on the formula of Annex A	14.2.0
2017-09	RAN#77	RP-171648	0018	2	F	Correction on cross polarization power ratios in TR 38.901	14.2.0
2017-09	RAN#77	RP-171648	0019	1	F	TR38.901 CR Spatially-consistent UT modelling	14.2.0
2017-09	RAN#77	RP-171648	0020	1	F	TR38.901 CR Calibraton Results	14.2.0
2017-12	RAN#78	RP-172687	0022	-	F	Correction on 3D-InH channel model in TR 38.901	14.3.0
2018-06	SA#80	-	-	-	-	Update to Rel-15 version (MCC)	15.0.0
2019-09	RAN#85	RP-191944	0023	-	B	Addition of indoor industrial channel model – version created in error – withdrawn	15.1.0
2019-10	RAN#85	RP-191944	0023	-	B	Addition of indoor industrial channel model – creation of rel-16 report	16.0.0